DNA 13.018

Technical Report

R 771

NAVAL CIVIL ENGINEERING LABORATORY

Port Hueneme, California 93043

Sponsored by

DEFENSE NUCLEAR AGENCY

July 1972

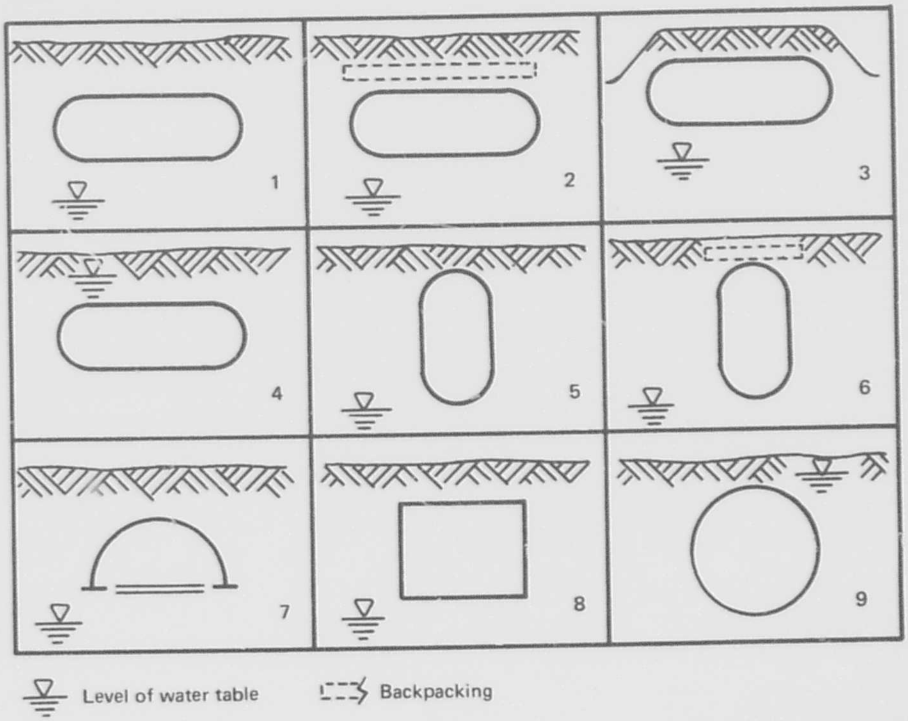

SUMMARY OF SOIL–STRUCTURE INTERACTION

Approved for public release; distribution unlimited.

179R

SUMMARY OF SOIL–STRUCTURE INTERACTION

Technical Report R-771

Y-F008-08-02-108, DNA 13.018

by

J. R. Allgood

ABSTRACT

This report summarizes currently available knowledge of soil–structure interaction as it pertains to facilities that provide protection from nuclear weapons effects. The major subdivisions of the subject are discussed in sufficient detail to convey a general understanding of the subject and to provide key references.

The recommended design methodology is illustrated for the horizontally oriented buried cylinder. A parallel approach is suggested for buried structures of other configurations. It is suggested that analysis of resulting designs be accomplished by the finite element method. Illustrations of two-dimensional and three-dimensional solutions by this method are given.

Information on peripheral subjects, such as ground motions, stress wave fracturing, and system optimization, is included to the minimum extent necessary to convey an appreciation of the overall soil–structure interaction problem. Particular emphasis is given to methods for transferring load away from a buried structure to the soil, thereby, permitting economic design and a large increase in resistance.

The summary represents work performed under DNA (formerly DASA) sponsorship over the past 10 years.

CONTENTS

Unclassified

Security Classification

DOCUMENT CONTROL DATA - R & D

(Security classification of title, body of abstract and indexing annotation must be entered when the overall report is classified)

1. ORIGINATING ACTIVITY (Corporate author) Naval Civil Engineering Laboratory Port Hueneme, California 93043	2a. REPORT SECURITY CLASSIFICATION Unclassified 2b. GROUP

3. REPORT TITLE

SUMMARY OF SOIL–STRUCTURE INTERACTION

4. DESCRIPTIVE NOTES (Type of report and inclusive dates)

Final; July 1970 – December 1971

5. AUTHOR(S) (First name, middle initial, last name)

J. R. Allgood

6. REPORT DATE	7a. TOTAL NO. OF PAGES	7b. NO. OF REFS
July 1972	161	173

8a. CONTRACT OR GRANT NO. b. PROJECT NO. DNA 13.018 Y-F008-08-02-108 c. d.	9a. ORIGINATOR'S REPORT NUMBER(S) TR-771 9b. OTHER REPORT NO(S) (Any other numbers that may be assigned this report)

10. DISTRIBUTION STATEMENT

Approved for public release; distribution unlimited.

11. SUPPLEMENTARY NOTES	12. SPONSORING MILITARY ACTIVITY Defense Nuclear Agency Washington, D. C. 20360

13. ABSTRACT

This report summarizes currently available knowledge of soil–structure interaction as it pertains to facilities that provide protection from nuclear weapons effects. The major subdivisions of the subject are discussed in sufficient detail to convey a general understanding of the subject and to provide key references.

The recommended design methodology is illustrated for the horizontally oriented buried cylinder. A parallel approach is suggested for buried structures of other configurations. It is suggested that analysis of resulting designs be accomplished by the finite element method. Illustrations of two-dimensional and three-dimensional solutions by this method are given.

Information on peripheral subjects, such as ground motions, stress wave fracturing, and system optimization, is included to the minimum extent necessary to convey an appreciation of the overall soil–structure interaction problem. Particular emphasis is given to methods for transferring load away from a buried structure to the soil, thereby, permitting economic design and a large increase in resistance.

The summary represents work performed under DNA (formerly DASA) sponsorship over the past 15 years.

Unclassified

Security Classification

14. KEY WORDS	LINK A		LINK B		LINK C	
	ROLE	WT	ROLE	WT	ROLE	WT
Soil—structure interaction						
Buried structures						
Protective structures						
Blast shelters						
Inclusions in soil						

DD FORM 1 NOV 65 1473 (BACK)
(PAGE 2)

Unclassified

Security Classification

1.0 INTRODUCTION

1.1 OBJECTIVES

From about 1962 through 1968 extensive research was accomplished in an attempt to gain an understanding of soil–structure interaction phenomenology. Most of this work was sponsored by the Defense Nuclear Agency (DNA). Subsequently, work was continued at a lesser level-of-effort but with more attention given to synthesizing the knowledge gained. This document summarizes the principal aspects of what has been learned about soil–structure interaction under the DNA program.

1.2 ANALYSIS OF THE PROBLEM

Understanding soil–structure interaction is necessary to effect adequate designs for buried structures that resist large static or blast loads. In the past, accurate design relations or special procedures were not needed because most of the applications were for culverts under low highway fills—or similar applications where the loads were nominal. This is evinced by the fact that practically all culvert failures were attributable to lack of control in soil placement or to unexpected causes such as undermining from water infiltration or exfiltration.[1.1]

The high fills of today's highways and railroads, the need for protective facilities to resist blast loads, and the rapidly developing need for underground urban development require improved design procedures and much better construction controls than has been common in the past.

1.3 BACKGROUND

DNA-sponsored work in the area of soil–structure interaction has been directed toward providing a means for designing, analyzing, and understanding the behavior of protective systems subjected to blast loading. To solve the blast response problem, it was first necessary to gain a better understanding of the static problem.

Considerable work on the static problem, mostly on culverts, was accomplished prior to the DNA-sponsored research. Notable among culvert investigations were those of Marston[1.2] and Spangler,[1.3] which included development of a theory of behavior founded on an assumed load distribution. Design methods based on seam strength, limiting ring compression, and minimum flexibility also have been proposed. None of these methods are adequate to achieve efficient designs by themselves, principally because they do not properly account for arching and do not consider all possible modes of failure.

The state of the art of pipe culvert technology through 1970, including an extensive bibliography, is given in Reference 1.1.

Unfortunately, very few of the soil—structure interaction experiments performed to date include adequate measurements of soil properties and soil behavior. Part of the reason for this is that good soil strain and stress instrumentation has only become available in recent years. Also, until recently, adequate theories were not available to guide experimentalists in good experiment designs.

The theory of elasticity solutions[1.4, 1.5] constituted the first major theoretical advance since the Marston theory. This was followed by a series of successively improved finite element computer programs[1.6] that permit static or dynamic, linear or nonlinear solutions of two-dimensional systems (plain stress or plain strain). Programs for three-dimensional linear systems are also available.[1.7] While not completely adequate, these analytical tools have vastly improved knowledge and capabilities in the area of soil—structure interaction.

Extensive experimentation has been accomplished in an attempt to gain an understanding of static- and blast-loaded soil—structure systems. References 1.8 through 1.12 provide pertinent bibliographical information. Key references to recent work are cited in subsequent sections of this document.

1.4 SCOPE AND APPROACH

The plan of this report is to present general information on soil properties, loading, and ground motions followed by a more detailed treatment of the various aspects of soil—structure interaction. Thereafter, approximate procedures for designing specific configurations are given and, finally, soil—structure systems analysis is discussed.

1.5 REFERENCES

1.1. Highway Research Board. National Cooperative Highway Research Program Report 116: Structural analysis and design of pipe culverts, by R. J. Krizek, et al., Washington, D. C., 1971.

1.2. A. Marston. "The theory of external loads on closed conduits in the light of the latest experiments," Highway Research Board, Proceedings, vol. 9, 1929, pp. 138-170.

1.3. Iowa State College. Engineering Experiment Station. Bulletin No. 153: The structural design of flexible-pipe culverts, by M. G. Spangler. Ames, Iowa, Dec. 1941.

1.4. J. O. Burns. An analysis of circular cylindrical shells embedded in elastic media, Ph.D. thesis, University of Arizona. Tucson, Ariz., 1965.

1.5. Air Force Weapons Laboratory. Technical Report No. AFWL-TR-65-98: Pressure distribution on underground structural cylinders, by K. Höeg. Kirtland Air Force Base, N. M., Apr. 1966. (Contract AF 29(601)-6368) (AD 631671)

1.6. Naval Civil Engineering Laboratory. Contract Report CR 69.019: Dynamic response analysis of two-dimensional structures with initial stresses and non-homogeneous damping, by I. Farhoomand, E. Rukos, and E. L. Wilson. Berkeley, Calif., University of California, Jan. 1970. (Contract N62399-69-C-0016) (AD 874628L)

1.7. University of California. Structural Engineering Laboratory. Report No. SESM 70-20: SAP; a general structural analysis program, by E. L. Wilson. Berkeley, Calif., Sept. 1970. (Contract DACW 68-67-C-004)

1.8. Iowa State University. Engineering Experiment Station. Final Report on Contract DA-49-146-ZX-085: A study of loads on underground structures, pt. 1. An annotated bibliography, by D. A. Van Horn. Ames, Iowa, Jan. 1963. (DASA 1406)

1.9. Defence Research Board. Report DR-170: Bibliography of soil dynamics and soil-structure interaction during dynamic or similar loadings, compiled by G. T. Hughes, et al. Ottawa, Canada, Mar. 1965.

1.10. Air Force Weapons Laboratory. Technical Report No. AFWL-TR-67-145: An annotated bibliography of protective structures research, by M. J. C. Garcia. Kirtland Air Force Base, N. M., Feb. 1968. (See also AFWL-TR-69-179, Feb. 1970)

1.11. Highway Research Board. Subcommittee SGF-B5C1: Stress and displacement bulletin: Solutions to boundary value problems in stresses and displacements of earth masses and layered systems, by D. Hampton, B. B. Schimming, and E. L. Skok. Washington, D. C., Jan. 1966.

1.12. University of Southampton. Department of Civil Engineering. Report no. 1: The dynamic response of a cylinder shell embedded in an elastic half-space using the finite element method of analysis, by C. S. Duns. Southampton, England, Feb. 1966. (Research Contract no. A/70/GEN/9658)

2.0 MEDIA

2.1 INTRODUCTION

This chapter provides background information on material properties essential to soil—structure system design. The material included is limited to the minimum considered essential to convey an appreciation of the soil properties, test, and relations needed for design and analysis of buried structures. Sources of detailed background information are cited for those who wish to pursue the subject in greater depth.

Unless otherwise stated, the discussion pertains to soils that are principally granular as clays are not usually suitable for soil—structure systems that must sustain high loads. There are exceptions, such as a clay layer to attenuate stress pulses or to create a water barrier; however, the higher moduli and shear strength of granular soils and their relative insusceptibility to plastic flow are preferable to the corresponding characteristics of clays. A desirable soil for protective construction is a granular soil with sufficient fines and moisture to have a significant cohesive strength.

Approximate designs can often be achieved based upon one or more key soil parameters. For example, a reasonably good approximation of the peak vertical displacement of a homogeneous semi-infinite granular soil field subjected to a uniform surface load can be achieved with elastic theory by using the secant confined compression modulus corresponding to the applied pressure. This assumes that in the determination of the modulus in the laboratory, the initial density and other influential factors are the same as in the field.

As is commonly known, the soil stress—strain curve corresponding to the initial loading is usually of principal interest in static applications. For blast loads, the entire load—unload—reload characteristics are of interest, especially for loads that are short with respect to the natural period of the soil—structure system. Complete characteristics, including the geology of the soil field, are absolutely essential in defining late-time motions. One reason for this is that, when the loading is dynamic, portions of the field may be unloading while others are being reloaded. Thus, to adequately define behavior, relations are needed which determine the soil state at any phase of possible loadings. Such relations are called constitutive equations; more will be said about them in a later section. Constitutive equations embody soil properties familiar to the soils engineer; principal properties from among these are reviewed in subsequent sections.

2.2 BACKGROUND

Whitman has summarized and assessed knowledge of the behavior of soils to dynamic loading, and has given information on testing methods for determining needed soil properties.[2.1] Elasticity relations corresponding to standard soil tests are given in the Appendix. Analysis of laboratory data to derive soil constitutive properties has been discussed by Jackson.[2.2] A variety of equations of state have been formulated for use in various computer programs including those by DiMaggio,[2.3] Isenberg and Lee,[2.4] and Nelson.[2.5, 2.6] Further research and development is needed to enhance understanding of the behavior of earth materials and to achieve an adequate analytical description; nonetheless, representations are sufficiently good that reasonable near-surface ground motion predictions are possible.[2.7-2.16]

This treatise is predicated on the assumption that near-surface ground motions can be predicted sufficiently well for design purposes by one of the approximate methods or by one of the major codes, and that the resulting data will serve as input for a soil–structure analysis utilizing the methods of subsequent chapters. Thus, the principal interest for present purposes is in constitutive properties for the soil in the vicinity of structures buried near the surface. In most cases the indicated limitation of scope simplifies matters as the necessity of considering the thermo-dynamic properties is precluded.

2.3 SOIL PROPERTIES

Soil generally behaves as an anisotropic medium in that the application of hydrostatic stress does not produce equal strains in all directions. For most applications, however, it is sufficient to assume that soil is isotropic under pure compression. Naturally, soil properties are very sensitive to boundary conditions and to the nature of the deposit and the loading. This fact must be kept in mind when defining soil properties and relating laboratory measurements to corresponding field conditions.

Commonly employed properties of granular materials are itemized and categorized in Table 2.1. Some of the parameters might logically be placed in other categories; however, the groupings given are convenient for discussion purposes.

Table 2.1. Soil Properties[a]

Symbol	Parameter	Index or Equation
	Natural Properties	
–	angularity	–
–	grain size distribution	$e_{max} - e_{min}$
ρ	mass density	–
e_w	water content	$e_w = 100\, W_w/W_s$
$\bar{e}$	void ratio	$\bar{e} = V_v/(V - V_v)$
	Placed Properties	
d_r	relative density	$d_r = (e_{max} - \bar{e})/(e_{max} - e_{min})$
K_o	at-rest coefficient of lateral earth pressure	$K_o \approx 0.95 - \sin\bar{\phi}$
K_p	passive coefficient of lateral earth pressure	$K_p = \tan^2(45^o + \phi/2)$
K_a	active coefficient of lateral earth pressure	$K_a = \tan^2(45^o - \phi/2)$
ν	Poisson's ratio	$\nu = (M_s - 2G)/2(M_s - G) = K_o/(1 + K_o)$
k	bulk modulus	$k = 3\Delta V/\sigma_{kk}$
	Intrinsic Properties	
$\bar{c}$	cohesion	–
$\bar{\phi}$	angle of friction	–
u	pore pressure	$u = u_i + \Delta u_{cw} + \Delta u_{dis}$
	Static Load Properties	
M_s	confined compression modulus from $\sigma_{11} - \epsilon_{11}$ diagram	–
M_u	unloading modulus	–
s	shear strength	–
G	shear modulus	–
	Dynamic Load Properties	
C_d	dilatation wave velocity	–
C_s	shear wave velocity	–
ξ	damping	–

[a] Note: See List of Symbols for definition of terms.

2.3.1 Natural Properties

Inherent properties of a soil mass include particle angularity, grain size distribution, mass density, water content, and void ratio. These properties influence other properties that are used in design but are of only indirect interest otherwise. Fortunately, the designer has the option of modifying the natural properties or even of using an imported soil in the vicinity of a buried structure. As a consequence, the backfill soil and its placement are subject to control.

2.3.2 Placed Properties

"Placed" properties means those properties that are most influenced by the manner in which the soil is placed in the neighborhood of a buried structure. They include the relative density (or some other measure of density), the at-rest coefficient of lateral earth pressure, Poisson's ratio, and the bulk modulus. Relative density is undoubtedly the most important of these for most applications as it is one of the principal determinants of stiffness and shear strength.

In many field installations, particularly those with free-draining cohesionless soils, density, or some index of density, is the sole parameter employed in governing the degree of compaction. Density is principally dependent upon the soil type, the compaction effort employed during placement, and the water content. The influence of soil type and relative density on the angle of friction, is indicated in Figure 2.1.[2.17] Initial void ratio also influences the angle of friction.

Soils compact on loading from a given initial density after the manner indicated in Figure 2.2. Degree of compaction is conveniently expressed in terms of the void ratio or the relative density as indicated in Table 2.1. Two expected characteristics are evident in Figure 2.2: first, for high initial densities, the relative density does not change much with load, and second, the curves for all initial densities converge toward a common value above 100 psi.

Curves giving the variation of density with water content for a given compactive effort for granular and cohesive soils are contrasted in Figure 2.3. Many basically granular soils contain fines and moisture that given them some cohesion which would result in compaction curves intermediate to those shown in Figure 2.3.[2.18] Compactive effort, of course, is a major determinant of placed density. Detailed discussions of density and methods for determining density are given in References 2.1 and 2.19 through 2.27. AASHO and other test specifications are summarized in Reference 2.19. The influence of density on soil moduli and other parameters is discussed in subsequent sections.

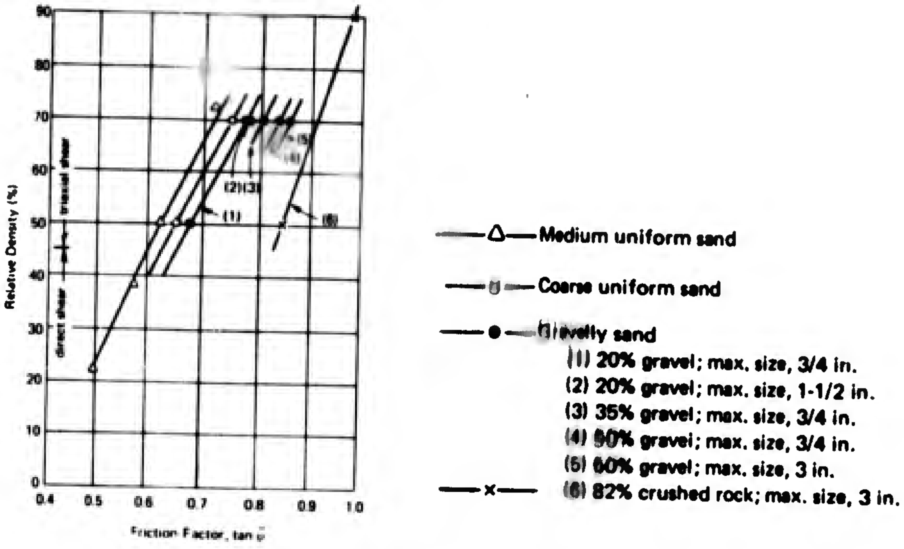

Figure 2.1. Effect of relative density on the friction factor for coarse-grained soils. (From Reference 2.17)

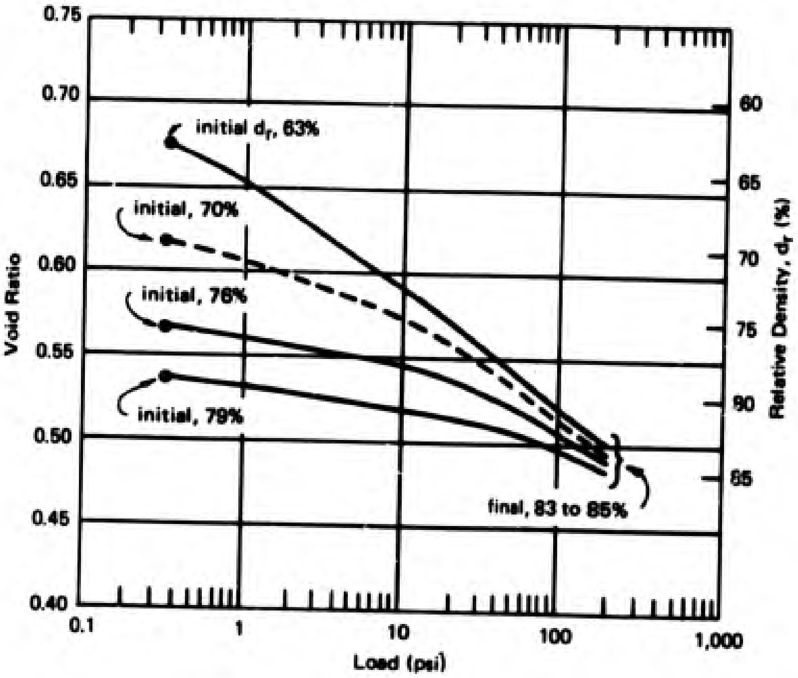

Figure 2.2. Compressibility characteristics of a fine, uniform sand in relation to placement relative density. (From Reference 2.17).

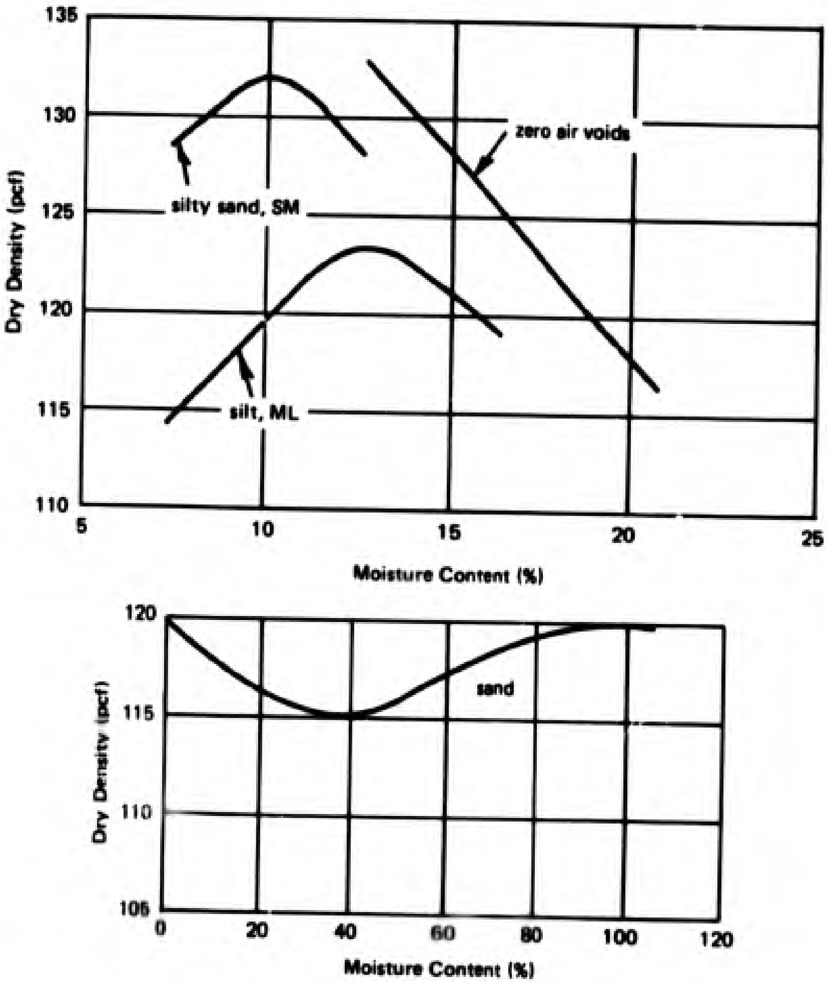

Figure 2.3. Modified AASHO compaction curves.

Hendron[2.28] and others have shown that, above about 10 psi, the at-rest coefficient of lateral earth pressure, K_o (the ratio of horizontal to vertical stress), does not vary much on loading. As may be deduced from Figure 2.4, however, it progressively increases on unloading to over twice its value when loaded. Tests have shown that the at-rest coefficient of lateral earth pressure is not greatly different for similarly placed subangular and subrounded dry sands.[2.29] Clearly, K_o depends primarily on the process by which a soil is placed or deposited.

According to Terzaghi,[2.30] K_o varies from about 0.3 for loose sand to 0.5 for dense sand. Below the water table, K_o will be nearly 1.0. Tamping the soil in layers may increase the value of K_o to 0.8; or alternately, for mounded installations or embankments where lateral expansion is possible, the effective value of K_o may be 0.2 or less. Where the sand-drop method is used, K_o is usually about 0.45. In a homogeneous soil field subjected to a uniform surface load, the magnitude of K_o may be estimated from the relationship[2.31]

$$\left.\begin{aligned} K_o &= 1 - \sin\bar{\phi} \quad \text{(sand)} \\ K_o &= 0.95 - \sin\bar{\phi} \quad \text{(clay)} \end{aligned}\right\} \tag{2.1}$$

where $\bar{\phi}$ = angle of internal friction under drained conditions (or under undrained conditions with effective stresses considered). Equation 2.1 applies both to noncohesive and cohesive soils provided effective stresses are considered. The precision of the equation is within about ±0.15.

Poisson's ratio (the ratio of horizontal strain to vertical strain) is the strain counterpart of K_o. Strictly speaking, Poisson's ratio, ν, has different values in each of the coordinate directions and varies with load; however, a unique value may be employed in design by defining it in terms of the secant moduli corresponding to a given applied stress. The resulting relation is given in the right column of Table 2.1. (A relation for ν in terms of the at-rest coefficient of lateral earth pressure, K_o, also is given in Table 2.1. Values of Poisson's ratio for various soils determined from a number of different investigators are summarized in Reference 2.32.) As with K_o, Poisson's ratio will be influenced by the placement method.

Placement method will also affect the bulk modulus, k, which is defined as the ratio of the mean principal stress to the volumetric strain. It is often chosen as an independent variable in constitutive relations[2.2]; consequently, it is one of the more important soil parameters. The range of variation of k is about the same as for the confined compression modulus which will be discussed after a review of the intrinsic soil properties.

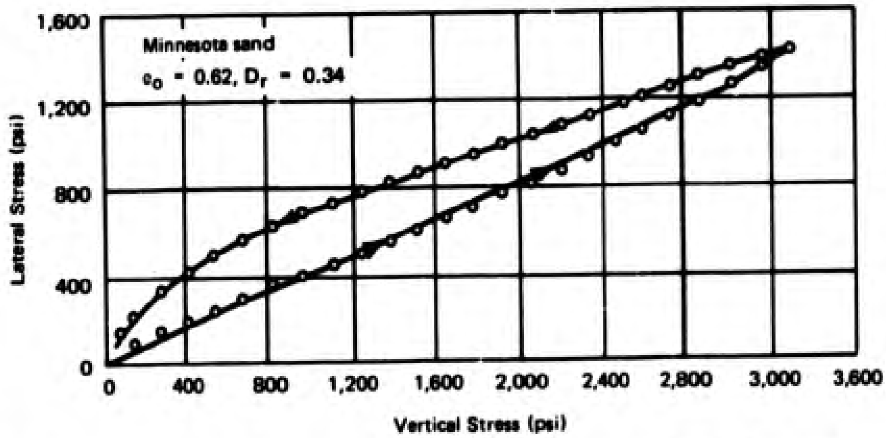

Figure 2.4. Lateral stress during one-dimensional compression. (From Reference 2.28)

2.3.3 Intrinsic Properties

Intrinsic soil properties, as defined by Whitman,[2.1] are those properties which are independent of the overall size of the soil mass or of the boundary conditions imposed upon the mass. They govern the shear strength of a soil. As indicated in Table 2.1, the intrinsic soil parameters are the cohesion, the angle of friction, and the excess pore pressure developed during shear at a constant water content. For most granular soils, the cohesion is expected to be less than 25 psi; the angle of friction varies from about 30 degrees to 45 degrees depending on the angularity of the particles.

Pore pressure changes can occur even in a dense, dry sand; however, such changes are not significant below a few feet from the surface and above the water table, except in the unusual circumstance that the minor principal stress is very small compared to the major principal stress.[2.1]

2.3.4 Load Properties

The remaining prime design parameters are termed load properties—those resistance characteristics exhibited under load, usually in some type of laboratory or field test. These properties include the confined compression modulus, M_s, the unloading modulus, M_u, the shear modulus, G, and the shear strength. In soil–structure interaction designs, one must be concerned with preventing failure of both the soil and the structure. Usually, the principle soil parameters affecting resistance are the soil moduli and the shear strength.

Compressibility moduli commonly used in soil–structure interaction theory include:

E_s = Young's modulus of elasticity

M_s = secant confined (constrained) compression modulus

M_t = tangent modulus

M_ℓ = loading modulus, usually M_s or M_t

M_u = unloading modulus

M_r = reloading modulus

G = shear modulus

k = bulk modulus

These moduli are usually determined from confined compression, null, triaxial, or proportional loading tests. A typical test data sheet is shown in Figure 2.5. Certain soil moduli are selected to correspond to applied pressures, as indicated in Figure 2.5, and some are taken as variable moduli.

In addition to the above list, there are various moduli associated with specific soil–structure configurations, such as the foundation modulus for footings and the modulus of elastic support for buried cylinders. The latter moduli are defined in the discussion of particular geometric configurations, Chapters 4 and 5. The moduli itemized above are defined and discussed next.

2.3.5 Compression Moduli

The term compression moduli, as used here, is intended to include the group M_s, E, and M_t. The confined compression modulus is the secant to the stress–strain diagram corresponding to the applied stress in a confined compression test. Approximate solutions for nonlinear systems are often achievable with the elastic theory where Young's modulus is obtained from the relation

$$E = \frac{(1+\nu_s)(1-2\nu_s)}{1-\nu_s} M_s = \eta M_s \qquad (2.2)$$

where M_s is the confined compression modulus corresponding to the applied pressure, and ν_s is Poisson's ratio.

As the name implies, the tangent modulus is the tangent to the stress–strain diagram—usually at a mean stress in the load increment of interest. Secant and tangent moduli are shown in the laboratory data sheet, Figure 2.5.

During initial loading in a uniaxial strain test of a granular material, (for $0 < \sigma \leq 100$ psi) there is often an initial phase characterized by a concave downward portion of the stress–strain diagram. As loading progresses, a second phase begins as the voids close resulting in a concave upward portion of the stress–strain diagram. Only when the particles begin to break does the stress–strain diagram reverse curvature and become concave downward again.

The variation of M_s for a given sand and initial density is indicated in Figure 2.6a. In this plot the limits of variation of stress–strain measurements are shown for NCEL sand placed by the sand-drop technique in a 5-foot soil tank composed of 1/2-inch-thick steel rings. The at-rest coefficient of lateral earth pressure for the tests was 0.45. As may be observed, the variation of the data for a given type of test is quite large, even under the well-controlled conditions of these tests.

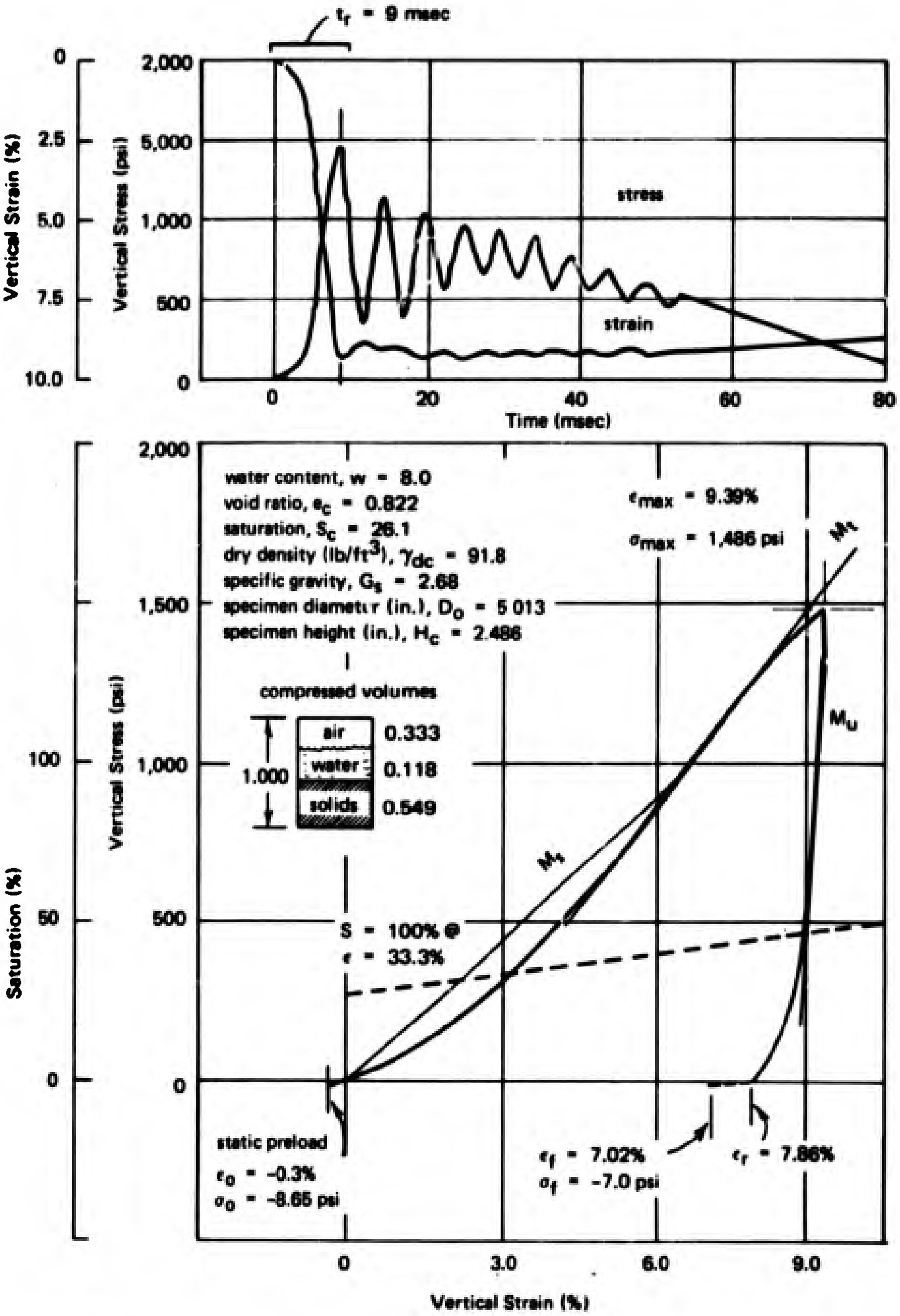

Classification: gray silty, clayey sand (SM-SC)

Remarks: LL = 21, PL = 14, PI = 7, e_o = 0.828, S_o = 25.9%

Project: DISTANT PLAIN Event 6
NCEL Project 3.11

Area: Watching Hill site, DRES, Canada

Boring No.: NCEL 1 Sample No.: 3

Depth: 6.2
El: 2,157.8 Date: 10-9-67

Figure 2.5. Uniaxial strain test results—dynamic test No. NCEL 1.3.2. (From Reference 2.33)

An indication of the variation of M_s with initial density, as determined from the cited tests, may be observed from Figure 2.6b.[2.29] The two curves shown correspond to the maximum and minimum densities achievable by the sand-drop method. The most important observation to be made from Figure 2.6b is that there is a large (factor of 3 at 25 psi) difference in $M_{s_{eff}}$ at low pressures and that this difference becomes larger with increasing pressure up to some maximum difference that is not determinable from the test result shown.

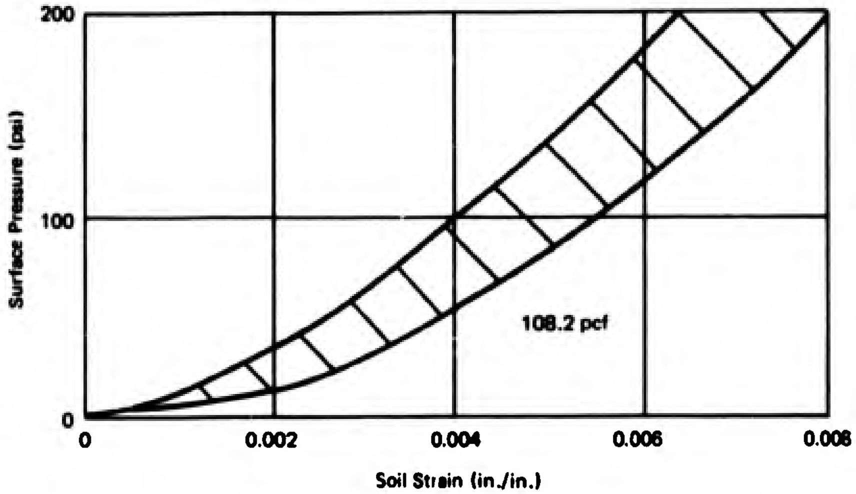

(a) Variation for a given initial density.

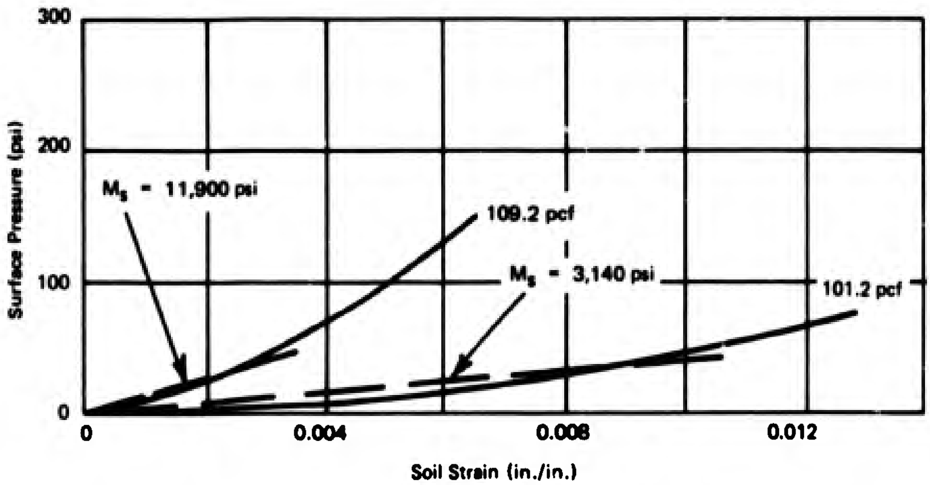

(b) Variation with density.

Figure 2.6. Variation in soil stress–strain properties. (Confined compression of NCEL sand in soil tank.)

Variation of M_s for a given initial density has not been thoroughly documented. In one set of experiments, under well-controlled conditions, the variation was found to be ±20%[2.34]; under field conditions, the variation would be expected to be greater than those limits.

Caution must be exercised in attempting to determine M_s from a consolidometer test. Results from consolidometer tests are seldom reliable unless the load is applied pneumatically or hydrostatically through a flexible diaphragm. If test results using such loading are not readily achievable, M_s may be estimated for unsaturated, medium sand compacted to 95% AASHO T99-49 density from the relation

$$M_s \approx 1{,}000\, p_s^{0.8} \tag{2.3}$$

where p_s is the stress at which M_s is required. M_s decreases rapidly from the value given by Equation 2.3 as the percentage of fines greater than about 200 mm increases. Equation 2.3 was proposed by Luscher.[2.35]

In multilinear analysis, the tangent modulus is normally used instead of the secant modulus. Naturally, the above discussion relative to the secant modulus also pertains to the tangent modulus. The unloading modulus is also normally taken as a tangent modulus.

2.3.6 Unload and Reload Characteristics

For blast-loaded fields, the unloading modulus, M_u, may be even more important than M_s because most of the time elapses during the unloading phase of the motion. Unload characteristics of a silty sand are shown in Figure 2.5. The salient features of unload–reload behavior are:

1. The unload–reload curves are much steeper than the initial loading.
2. There is a permanent residual strain remaining after unloading.
3. A hysteresis occurs with accompanying energy loss.

For a virgin sand the energy loss during the initial load–unload cycle is of the order of 50%. On subsequent loadings, the energy loss per cycle decreases.[2.1]

2.3.7 Shear Strength

Shear strength, s, means the stress at which shear failure occurs. Typical shear stress–strain and volume change curves are indicated in Figure 2.7. As may be noted the curves are concave downward, and

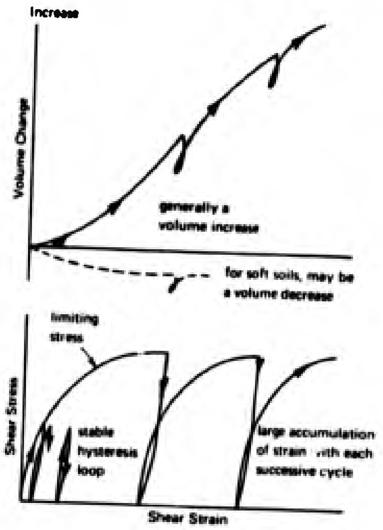

Figure 2.7. Typical stress–strain and volume change curves in shear. (From Reference 2.1)

successive load–unload cycles produce similar curves. For shear stress levels less than about one-half of the limiting stress, a relatively stable hysteresis loop is developed after many cycles of loading. Except for very soft soils there is usually an increase in volume with increase in shear load because the grains move apart in attempting to slide over each other.

Shear strength is readily determined from triaxial shear tests; however, in the absence of such data, one may use the Mohr-Coulomb hypothesis as modified by Terzaghi to include pore pressure effects as follows:

$$s = \bar{c} + (\sigma - u)\tan\bar{\phi} \qquad (2.4)$$

where s = shear strength

$\bar{c}$ = cohesion

σ = total stress normal to the plane

u = $u_i + \Delta u_{cw} - \Delta u_{dis}$

u_i = initial pore pressure

Δu_{cw} = the excess pore pressure developed during shear at a constant water content

Δu_{dis} = the excess pore water pressure negated by consolidation during loading

$\bar{\phi}$ = friction angle

Admittedly, the Mohr-Coulomb equation is an oversimplification of the actual strength behavior of soils; however, it provides a sufficiently accurate approximation for many applications and serves to indicate the dominant parameters involved. More sophisticated descriptions of strength are discussed in Section 2.5.

Although Equation 2.4 contains no lineamental parameters, shear strength is dependent upon the shape, mass, and manner of loading. These factors influence σ and u.

2.3.8 Shear and Bulk Moduli

The shear modulus, G, is the slope of the shear stress–strain envelope at the extant state of strain. Concomitantly, the shear failure envelope is dependent on system geometry and will, in consequence, be dependent on the system stress invariants. This is tantamount to stating that the initial shear modulus can be determined from a triaxial shear test but that the shear modular function cannot.

Various analytical representations of the shear modulus have been formulated, including those of Farhoomand[2.36] and Nelson.[2.5, 2.6] These formulations show that the shear modulus is highly dependent on the geometry and the state of stress in the media. The shear modulus or the bulk modulus are not necessarily expressed as explicit functions in constitutive models.

The bulk modulus is defined as the ratio of the mean stress to the volumetric strain.[2.37] It is, by definition, a function of the stress invariants. Dependence of the shear and bulk moduli, and of the shear strength on inertia and strain rate effects is not completely known. Analytical relations between the various soil moduli are given in Chapter 4.

2.4 DYNAMIC EFFECTS

Dynamic effects may be thought of as those associated with phenomena at or near the front of stress waves and as those characteristic of the mass action. Phenomena related to the wave front other than the pressure–density discontinuity include reflections, refractions, strain-rate effects, and energy attenuation. Wave propagation in solids is an extensive field of study that is beyond the scope of this discussion; it will be discussed in a later section to the minimum extent necessary to achieve the goals of this report.

The effect of strain rate on the compressional properties of dry granular materials is generally negligible. There may, however, be a 10 to 15% change in $\bar{\phi}$ that can lead to large changes in bearing capacity. Just how and why the friction angle is affected by strain rate is not known.

For moist sands the excess pore water pressure from consolidation (and, hence, the shear strength) is affected by the rate of straining; nonetheless, limit shear resistance has only a weak dependence on strain rate. With saturated sands physical properties may be two or more times the static values due to differences in excess pore pressure generated at higher strain rates. Strain rate effects in cohesive soils also appear to be almost solely due to changes in the excess pore water pressure, Δu_{cw}.

Mass-action phenomena are roughly analogous to the characteristics of the single-degree-of-freedom spring-mass system, viz:

1. Load duration will not influence peak deflection, if the ratio of load duration to fundamental natural period is greater than about 6.

2. Soil mass will not influence peak deflection, if the ratio of load duration to the fundamental natural period is greater than about 6.

3. The loading will, in effect, be static, if the ratio of the rise time to the fundamental natural period is greater than about 6.

The fundamental compression mode frequency (normal to the surface of a uniform soil field) may be approximated by the relation

$$\omega = \sqrt{\frac{3\hat{k}g}{\gamma L}} \tag{2.5}$$

where $\hat{k}$ = M_t/L = stiffness of the soil field (lb/ft^2/ft)

g = acceleration of gravity (ft/sec^2)

γ = density of soil (pcf)

L = depth to water table or to bedrock (feet)

M_t = initial tangent modulus from a confined compression test

For a soil with an initial tangent modulus of 5,000 psi and the water table at a depth of 10 feet, the natural period will be about 12 msec. Then the approximate time which distinguishes long- from short-duration loads is about 72 msec.

Soil is a dissipative medium; hence, short-duration loads decay rapidly with depth, as is well known from high-explosive field tests. For example, in 500-ton shots in Canada where the top 5 feet is a highly compressible silty-clay, it has been found that air-blast pulses of the order of 500-psi peak pressure and 15-msec duration dissipate to 1/5th of their surface magnitude in a depth of 5 feet.[2.38]

As movement occurs in a soil mass because of volume expansion or other causes, inertia forces are generated. These inertia forces are usually more important than strain-rate effects.

2.5 CONSTITUTIVE RELATIONS

For isotropic elastic materials, stress and strain are related by the equation

$$\sigma_{ij} = \lambda e_{kk} \delta_{ij} + 2\mu \epsilon_{ij} \tag{2.6}$$

where σ_{ij} = tensor representing the six independent components of stress

ϵ_{ij} = tensor representing the corresponding six components of strain

e_{kk} = the change of volume per unit volume

δ_{ij} = Kronecker delta (1 if $i = j$; 0 if $i \neq j$)

λ, μ = Lamé's constants

Equation 2.6 shows that only Lamé's constants, λ and μ, are necessary; however, the four parameters—Young's modulus of elasticity, E; Poisson's ratio, ν; the shear modulus, G; and the bulk modulus, k—are often used as they are measurable.

Yield conditions for engineering materials are commonly expressed in the form

$$f(J_1, \sqrt{J_2'}) = 0 \tag{2.7}$$

where $J_2' = 1/2\, \sigma_{ij}' \sigma_{ij}$ = second invariant of the Cauchy deviatoric stress tensor

$J_1 = \sigma_{kk}$ = 3 times mean normal stress = $3p$

$\sigma_{ij}' = \sigma_{ij} - p\,\delta_{ij}$ = deviator stress tensor

For example, the Prager-Drucker generalization of the three-dimensional Mohr-Coulomb yield criterion is

$$\sqrt{J_2'} = k_1 - \alpha p \tag{2.8}$$

where k_1, α = material constants

p = mean normal stress

Equation 2.8 is adaptable to nonlinear materials, such as soil, by using incremental stress–strain relations and by incorporating the soil coefficients as functions of the stress or strain invariants. DiMaggio and Sandler have proposed a model for predicting observed laboratory and field behavior which satisfies continuity, stability, and uniqueness requirements.[2.3] Jackson has demonstrated a method for obtaining a polynomial model that fits laboratory data.[2.2] Nelson and Baron have developed a variable modulus model that provides good agreement with measured ground motions,[2.39] and Nelson has improved upon the latter model.[2.5, 2.6]

Hadala has performed ground motion calculations which show that the initial peak vertical velocity and stress are relatively insensitive to the constitutive model used.[2.40] By contrast, the peak horizontal motions are strongly affected by the character of the constitutive model.

2.6 REFERENCES

2.1. Army Engineer Waterways Experiment Station. Contract Report No. 3-26: The response of soils to dynamic loadings, rept. 26. Final report, by R. V. Whitman. Vicksburg, Miss., May 1970.

2.2.———. Miscellaneous Paper No. S-69-16: Analysis of laboratory test data to derive soil constitutive properties, by J. G. Jackson. Vicksburg, Miss., Apr. 1969.

2.3. Paul Weidlinger, Consulting Engineer. Report on Contract DASA 01-69-C-0130: Material models for soils, by F. L. DiMaggio and I. Sandler. New York N. Y., Apr. 1970. (DASA 2521) (AD 710824)

2.4. Agbabian-Jacobsen Associates. Report AJA 6813-251: Material properties for ELK code, by J. Isenberg and L. C. Lee. Los Angeles, Calif., Oct. 1969. (Contract DASA 01-68-C-0081) (DASA 2344) (AD 860586L)

2.5. Army Engineer Waterways Experiment Station. Contract Report No. S-68-1: Investigation of ground shock effects in nonlinear media, rept. 1. Development of mathematical material models, by I. Nelson and M. L. Baron. Vicksburg, Miss., Mar. 1968. (Contract DACA 39-67-C-0048)

2.6. ———. Contract Report No. S-68-1: Investigation of ground shock effects in nonlinear media, rept. 2. Modeling the behavior of a real soil, by I. Nelson. Vicksburg, Miss., July 1970. (Contract DACA 39-67-C-0048)

2.7. P. A. Abbott. "Hand solution of one-dimensional inelastic wave-propagation problems," in Proceedings, International Symposium on Wave Propagation and Dynamic Properties of Earth Materials, Albuquerque, New Mexico, August 23-25, 1967. Albuquerque, N. M., University of New Mexico Press, 1968, pp. 371-392.

2.8. Classified reference.*

2.9. Classified reference.

2.10. Space and Missile Systems Organization. Technical Report No. SAMSO-TR-70-88-vol. 2: Free field ground motion for beneficial facility siting, vol. 2. Equations of state for geologic media (U), by S. H. Schuster and J. Isenberg. Los Angeles Air Force Station, Calif., June 1970. (Contract F04701-68-C-0192) (ATI-AJA-R-6819-776-2) (AD 871440)

2.11. Classified reference.

---

* Classified reference list available to qualified requestors.

2.12. Classified reference.

2.13. Paul Weidlinger, Consulting Engineer. Report on Contract DA-49-146-XZ-508: Air induced ground shock effects on alluvium-playa material, by J. P. Wright, M. L. Baron, and I. Nelson. New York, N. Y., July 1968. (DASA 2222) (AD 852704L)

2.14. Classified reference.

2.15. Classified reference.

2.16. Classified reference.

2.17. Bureau of Reclamation. Earth manual, 1st ed. rev. Denver, Colo., 1968.

2.18. E. J. Yoder. Principles of pavement design. New York, Wiley, 1959.

2.19. G. A. Leonards, ed. Foundation engineering. New York, McGraw-Hill, 1962.

2.20. Army Engineer Waterways Experiment Station. Technical Memorandum No. 3-271: Soil compaction investigation, rept. 1. Compaction studies on clayey sands. Vicksburg, Miss., Apr. 1949.

2.21.————. Technical Memorandum No. 3-271: Soil compaction investigation, rept. 2. Compaction studies on silty clay. Vicksburg, Miss., July 1949.

2.22.————. Technical Memorandum No. 3-271: Soil compaction investigation, rept. 3. Compaction studies on sand subgrades. Vicksburg, Miss., Oct. 1949.

2.23. ————. Technical Memorandum No. 3-271: Soil compaction investigation, rept. 4. Subgrade compaction studies. Vicksburg, Miss., Feb. 1950.

2.24.————. Technical Memorandum No. 3-271: Soil compaction investigation, rept. 5. Miscellaneous laboratory tests. Vicksburg, Miss., June 1950.

2.25.————. Technical Memorandum No. 3-271: Soil compaction investigation, rept. 6. Effect of size of feet on sheepsfoot roller. Vicksburg, Miss., June 1954.

2.26.————. Technical Memorandum No. 3-271: Soil compaction investigation, rept. 7. Effect on soil compaction of tire pressure and number of coverages of rubber-tired rollers and foot-contact pressure of sheepsfoot rollers. Vicksburg, Miss., June 1956.

2.27.————. Technical Memorandum No. 3-271: Soil compaction investigation, rept. 8. Effect of lift thickness and tire pressure. Vicksburg, Miss., Oct. 1957.

2.28. A. J. Hendron. The behavior of sand in one-dimensional compression, Ph.D. thesis, University of Illinois. Urbana, Ill., 1963.

2.29. Naval Civil Engineering Laboratory. Technical Report R-582: Influence of soil modulus on the behavior of cylinders buried in sand, by J. R. Allgood, J. B. Ciani, and T. K. Lew Port Hueneme, Calif., June 1968. (AD 670477)

2.30. K. Terzaghi and R. B. Peck. Soil mechanics in engineering practice, 2d ed. New York, Wiley, 1967.

2.31. E. W. Brooker. The influence of stress history on certain properties of remolded cohesive clays, Ph.D. thesis, University of Illinois. Urbana, Ill., 1964.

2.32. J. N. Kay and R. J. Krizek. "Adaptation of elastic theory to the design of circular conduits," Institution of Engineers, Australia, Civil Engineering Transactions, Apr. 1970, pp. 85-90.

2.33. Army Engineer Waterways Experiment Station. Preliminary report, Operation DISTANT PLAIN, Event 6. Soil property investigation for Project 3.10, soil sampling and testing, by J. G. Jackson and J. E. Windham. Vicksburg, Miss., Dec. 1967.

2.34. Naval Civil Engineering Laboratory. Technical Report R-606: Static behavior of buried reinforced-concrete model cylinders, by J. R. Allgood and H. G. Herrman. Port Hueneme, Calif., Jan. 1969. (AD 682929)

2.35. U. Luscher. "Buckling of soil-surrounded tubes," American Society of Civil Engineers, Proceedings, Journal of the Soil Mechanics and Foundations Division, vol. 92, no. SM6, Nov. 1966, pp. 211-228.

2.36. I. Farhoomand. Nonlinear dynamic analysis of two-dimensional solids, Ph.D. thesis, Department of Civil Engineering, University of California. Berkeley, Calif., Sept. 1970.

2.37. Y. C. Fung. Foundations of solid mechanics. Englewood Cliffs, N. J., Prentice-Hall, 1965.

2.38. Army Engineer Waterways Experiment Station. Miscellaneous Paper No. S-71-6: Free-field code predictions versus field measurements: A comparative analysis for the PRAIRIE FLAT event, by J. S. Zelasko and G. Y. Baladi. Vicksburg, Miss., Mar. 1971.

2.39. I. Nelson and M. L. Baron. "Application of variable moduli models to soil behavior," International Journal of Solids and Structures, vol. 7, no. 4, Apr. 1971, pp. 399-417.

2.40. Army Engineer Waterways Experiment Station. Technical Report No. S-71-4: Ground shock calculation parameter study, rept. 1. Effect of various nonlinear elastic-plastic model formulations, by G. Y. Baladi and P. F. Hadala. Vicksburg, Miss., Apr. 1971.

3.0 GENERAL ASPECTS OF LOADING AND SOIL–STRUCTURE SYSTEM BEHAVIOR

3.1 LOADING

A typical blast load consists of an instantaneous rise to the peak pressure, p_o, followed by an exponential decay of duration, τ, as indicated in Figure 3.1. The parameters, p_o and τ, depend on the characteristics of the weapon producing the pulse and on the height of burst. With these characteristics known, the blast parameters are readily determined from charts.[3.1] Under certain conditions, precursors and other irregularities in wave shape occur; however, worst-case loading consists of an instantaneous rise followed by the typical exponential decay. Such idealized blasts may be approximated by several analytical relations, one of which (for a surface burst) is[3.2]

$$p(x,t) = P(R_s)\left[0.4 + 0.6\left(\frac{x}{R_s}\right)\right]^{14} U(R_s - x) \qquad (3.1)$$

where $p(x,t)$ = overpressure at point x on the surface at time t after detonation of the weapon

x = distance from ground zero (feet)

t = time after detonation of the weapon (seconds)

U = unit step function

R_s = shock radius of blast at time t (feet)

$$= \left(\frac{A_1 W c_o^2}{\bar{p}_a}\right)^{1/5} t^{2/5}$$

$$P(R_s) = \frac{14 A_1 W}{75} R_s^{-3}$$

$\bar{p}_a$ = ambient air pressure (psf)

c_o = ambient sound velocity of air (fps)

A_1 = 3×10^{15} ft-lb per Mt, for a surface burst

W = weapon yield (Mt)

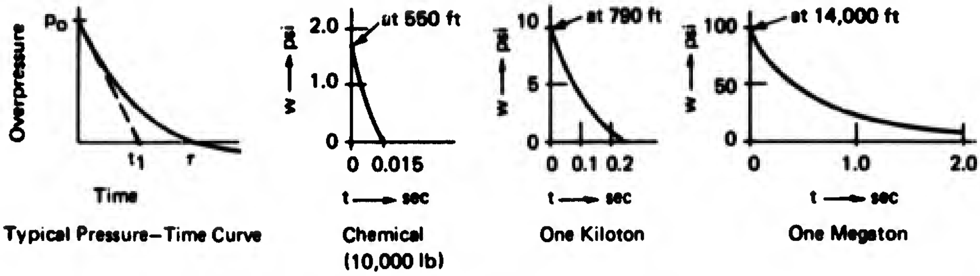

Figure 3.1. Pressure–time signatures of typical explosions.

For $p_o > 100$ psi, the peak surface overpressure may be determined from the relation[3.3]

$$p_o = 3{,}450\left(\frac{1{,}000}{R}\right)^3 W \qquad (3.1a)$$

where p_o = peak surface overpressure (psi)

W = weapon yield (Mt)

R = range (feet)

The intercept of the initial tangent of Equation 3.1 is a measure of the effective load duration, t_1, which is the duration of a triangularly shaped load that produces the same peak deflection of a system as the actual blast loading. Use of equivalent triangular loads materially aids computation.

Selection of a suitable equivalent triangular load, t_1, is accomplished by adhering to the guiding principle that *the area under the actual pressure–time curve should equal the area under the equivalent triangular load to the time of peak or limit deflection.* The term limit deflection means the maximum initial peak deflection that an element or structure is designed to sustain without incurring collapse. The above statement accounts for the fact that it is the total energy to the time of peak deflection and not the total energy under the positive phase of the pressure–time curve that is of dominant importance in design. The difficulty in applying the above principle is that the time to maximum deflection is not known initially; however, it usually may be approximated with sufficient accuracy for initial design. Charts for determining air-blast parameters, including the impulse and the durations of equivalent triangular loads, are given in Reference 3.1.

Within about three crater radii from ground zero, the air blast moves outward so rapidly that the air-blast loading on the surface is essentially a plane-wave loading. Further out, the induced stress wave tends to assume an angle β with the surface as indicated in Section 3.2.1. The angle β will, of course, depend on whether the location of interest is in the sub-seismic, the seismic, or the super-seismic region. The distinction between these regions is whether the velocity of the stress front in the ground is greater than, equal to, or less than the velocity of the air-blast front.

As the air-blast-induced stress wave propagates downward from the surface, it attenuates and changes shape. Usually, the peak stress decreases and the rise time increases with depth. The pressure attenuation is given by the relation[3.4]

$$p_z = \alpha_z p_o \tag{3.2}$$

where p_o = peak surface overpressure (psi)

p_z = peak stress at depth z (psi)

α_z = attenuation factor = $\dfrac{t_d/t_{50}}{1 + z/L_w}$

L_w = $3.7\,W^{1/3} C_d\, p_o^{-1/2}$

$$t_d/t_{50} = \begin{cases} 1 & \text{for } p_o < 1{,}000 \text{ psi} \\ 27.5/p_o^{0.48} & \text{for } p_o > 1{,}000 \text{ psi} \end{cases}$$

W = weapon yield (Mt)

t_d = effective duration of the applied overpressure (seconds)

t_{50} = intercept on the time axis of a straight line drawn from the peak pressure through the point on the overpressure curve at which the pressure is 50% of its maximum value (seconds)

C_d = velocity of stress front in the soil (fps)

z = depth to point of interest (feet)

Equation 3.2 is a twice modified equation for spatial dispersion.[3.5]

The rise time is approximately one-half of the transit time of the stress front from the ground surface to depth z.[3.6]

$$t_r = \frac{z \cos\beta}{2C_d} \quad (3.3)$$

where β = angle of stress front with the surface

C_d = velocity of the stress front

The stress wave may tend to produce a shock front in the first few feet near the surface in locking media. These shock fronts break down quickly at larger depths, however, because of the dissipative nature of unsaturated soils. Below the water table shocks may reappear.

Approximate relations for predicting absolute values of displacement, velocity, and acceleration may be found elsewhere.[3.1] Actually, absolute motions are of little interest in structural design and analysis except in the design of shock isolation systems; rather, concern is with stress and relative motions both of which result from passage of the wave front.

Below the water table, it appears that two distinct compressional waves are propagated: (1) a wave that is transmitted through the water–solid system without change in the pore volume, and (2) a slower wave that only progresses when change in the pore volume takes place.[3.7] Wave propagation is discussed more fully in the next section.

3.2 WAVE PROPAGATION

3.2.1 General Characteristics

The purpose of this section is to convey a general understanding of wave propagation as it relates to or influences body motions, shock transmission, and soil–structure interaction. Discussion is mostly limited to phenomenology governing survivability.

In the material to follow, it is assumed that:

1. The reader is familiar with the general aspects of nuclear and high-explosive detonations, air-blast propagation, and cratering.
2. The realm of interest corresponds to the higher overpressure region: 200 psi $< p_o <$ 3,000 psi, where p_o = peak surface side-on overpressure.

A rationale for the lower overpressure limit is that virtually any closed structure that will withstand the backfill stresses will resist 200-psi overpressure. Three thousand psi occurs near the lip of the crater for surface detonations and is, thus, a practical upper limit for most facilities in soil. Restricting attention to the 200-psi-to-3,000-psi region avoids, in most cases, the need for considering outrunning.

The concatenation of events experienced by a structure buried in soil following a near surface explosion depends primarily on the range from ground zero, the free-field profile and properties, the height or depth of burst, and the weapons characteristics. Detailed treatment of the phenomenology involved may be found in Reference 3.1. For present purposes it will suffice to give a general description of events in the higher overpressure regions and to discuss how they influence subsurface systems.

Characteristic transpirations within a few crater radii from ground zero for a surface burst on a uniform soil field are as follows: a few milliseconds after detonation the air blast arrives over a close-in structure inducing dilatation, P, and shear, S, waves that propagate downward at an angle with respect to the surface as indicated in Figure 3.2. For overpressures above a few hundred psi (depending on the type of weapon and the weapon yield), the gaseous detonation products spread very rapidly over the surface, producing what is essentially a plane-wave loading. Further from ground zero, the angle β increases to values that may exceed 90 degrees. The air-blast-induced stress wave causes downward and outward motions.

Simultaneously with propagation of the air blast, a direct-induced stress front moves outward from the crater. Close to ground zero, the direct-induced wave travels slower than the shock front in air; however, the wave traveling through the basement rock may reach distant locations and be fed up through the overburden in advance of the air blast, producing a condition known as outrunning.[3.1] Another characteristic of the direct-induced wave is that it attenuates rapidly with distance; consequently, stresses near the surface attributable to it are usually smaller than those from the air blast. The principal degrading effect of the direct-induced wave is the larger late-time motions that are initially upward and outward and then downward and inward as indicated by the particle paths shown in Figure 3.3. For short-duration loads and large bomb masses, as with high-explosive shots,[3.8] these motions are very large because of the large kinetic energy imparted to the soil, and because of the lack of confinement of the soil surface from the air blast while the direct-induced wave is acting.

Undoubtedly, the P- and S-waves and the late-time direct-induced waves are, from a structural design point-of-view, the principal causative effects at overpressures greater than about 200 psi, but they may not be the only ones. In non-ideal media, reflected waves from the water table, underlying strata, and basement interfaces; relief waves from the crater; and certain other waves[3.9] combine to produce complex late-time particle paths. Further from ground zero, Rayleigh and other waves combine to produce even more complex particle paths and the added obfuscation that the amplitude of the initial wave is likely to be less than the amplitude of subsequent waves.[3.10]

Fortunately, except for systems that are limited in the amount of rotation and other motions and for design of shock isolation systems, these motions do not greatly complicate design for the high overpressure region. The reason is that in nearly all cases, the maximum stresses result from the P-wave. The main effect of the direct-induced, late-time air-blast-induced, and extraneous waves is to move an inclusion with the free-field. Except for structures of extended lineament (for example, long tunnels), these motions are of little consequence. *It is the early-time air-blast-induced stress waves that are of principal importance in design.*

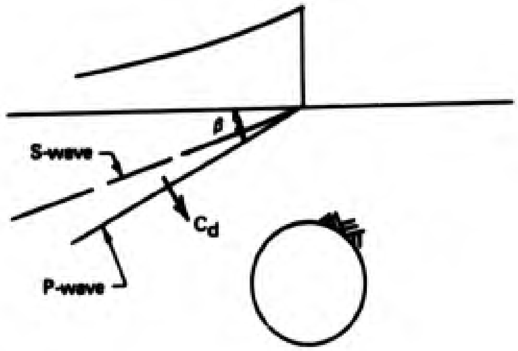

$$\beta = \begin{cases} \sin^{-1} \dfrac{C_d}{U} & \text{for } \dfrac{C_d}{U} < 1 \\ \dfrac{\pi}{2} & \text{for } \dfrac{C_d}{U} > 1 \end{cases}$$

Figure 3.2. Air-blast induced P and S waves.

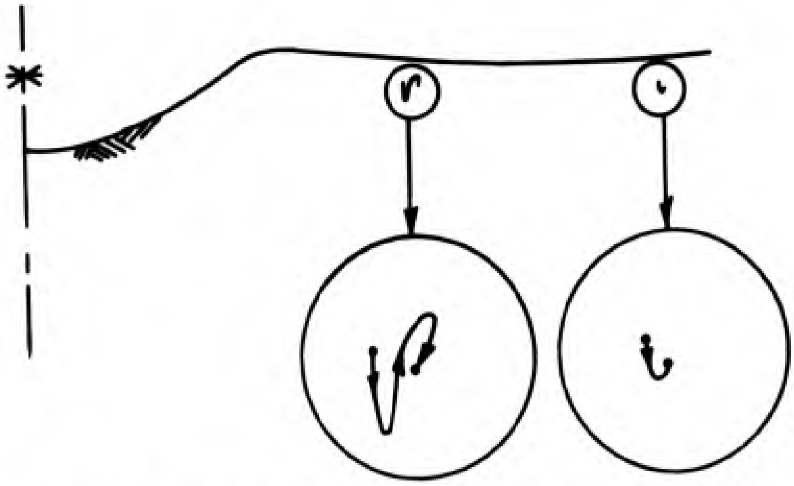

Figure 3.3. Particle paths from surface burst over homogeneous soil field.

Auspiciously, the analytics of air-induced stress waves are relatively tractable. Quite often one-dimensional elastic wave theory will suffice if one is careful to employ an appropriate effective soil modulus. For this reason it is worth reviewing the basic relations of elementary wave theory.

3.2.2 Basic Wave Theory

Consider one-dimensional wave propagation in an ideal media where the effects of lateral motion are negligible. For these conditions it is well known[3.9] that:

1. The velocity of a dilatational wave front is given by

$$C_d = \sqrt{\frac{E}{\rho}} \tag{3.4}$$

where E = Young's modulus of elasticity of the material

ρ = mass density of the media

2. Stress is determined by the ratio of particle and wave front velocities

$$\sigma = E\,\frac{v}{C_d} \quad \text{or} \quad \sigma = (\rho\, C_d)\,v$$

where v = particle velocity

$\rho\, C_d$ = acoustic impedance

3. A plane compression wave is reflected unchanged from a fixed-end or a rigid interface and as a tensile wave from a free-end or unconfined face.

4. Intersecting waves combine algebraically.

5. In the interior of an elastic solid compression (dilatation), waves and shear waves occur that are propagated with different velocities as follows:

$$\left.\begin{aligned} C_d &= \text{dilatational wave velocity} = [(\lambda + 2\mu)/\rho]^{1/2} \\ C_s &= \text{shear wave velocity} = (\mu/\rho)^{1/2} \end{aligned}\right\} \tag{3.6}$$

where λ = Lamé's first constant

μ = G = Lamé's second constant

6. Where the force is negligible, the one-dimensional wave equation is:

$$\frac{\partial^2 \delta}{\partial t^2} = C_d^2 \frac{\partial^2 \delta}{\partial \zeta^2} \tag{3.7}$$

where δ = deflection at a point of interest

t = time

ζ = coordinate of position

Solutions to this equation are of the form

$$\delta = f(\zeta + C t) + f_1(\zeta - C_1 t)$$

Generalized wave equations and solutions for a variety of boundary conditions may be found in References 3.9 and 3.11.

7. Closed form solutions to the wave equations are not available for most "real world" situations; hence, one must resort to graphical[3.12] or computer solutions.[3.13]

8. In bounded solids, so-called Rayleigh and Love waves occur that are attributable to different E and ρ near the surface. Theoretically, these waves travel without change in form, and, consequently, they tend to dominate the motions at low overpressure, that is, at great distances from ground zero.

3.2.3 Reflection and Refraction

When an elastic wave impinges upon a slip-free interface, four waves result: refracted P and S waves and reflected P and S waves. The influence of soil nonlinearities on this process is not completely clear. These phenomena, the change in seismic impedance with depth, the occurrence of waves along stratum, and the development of relief waves, all tend to further complicate the ground motions from P, S, Rayleigh, and direct-induced waves.[3.9] It is indeed fortunate that, in most instances, only the shock isolation system design and not the structural design is influenced by the late-time ground motions.

Situations where reflected or refracted waves might be important in structural design include configurations where the water table or a rock interface is close to the inclusion or where the structure extends beneath the water table. These situations require special analysis.

In the next section, factors affecting structural behavior and design (but not the design of shock isolation systems) are discussed, followed by specific relations and procedures for treating particular configurations.

3.2.4 Approximations to Ground Motions

Beyond the region of influence of the direct-induced wave and out to about the range corresponding to a 200-psi overpressure (depending on the weapon yield), the peak vertical downward deflection of a point near the surface will be

$$\delta_m = \epsilon_s C_d t_1 \qquad (3.8)$$

where ϵ_s = average unit strain over the loaded depth, Figure 3.4

C_d = velocity of propagation of the stress front

t_1 = equivalent triangular duration of the load

DLF = dynamic load factor

Recognizing that $\epsilon_s \approx$ DLF $p_o/2 E_s$, $\rho C_d^2 = E$, and that the impulse of the load is $I = p_o t/2$, Equation 3.8 may be written as

$$\delta_m \approx \text{DLF} \frac{I}{\rho C_d} \qquad (3.9)$$

and the other terms are as previously defined. Where basement rock is within a few hundred feet of the surface, a better approach is to integrate over the depth of the upper layer to determine the average stress, then to calculate the total strain as the average stress divided by the effective soil modulus times the depth to bedrock.

For dry soil fields, the product DLF in Equation 3.9 may be taken as 2. For nonhomogeneous soil fields, ρC_1 must be an effective value determined from a seismic survey or from known values of M_s of the various

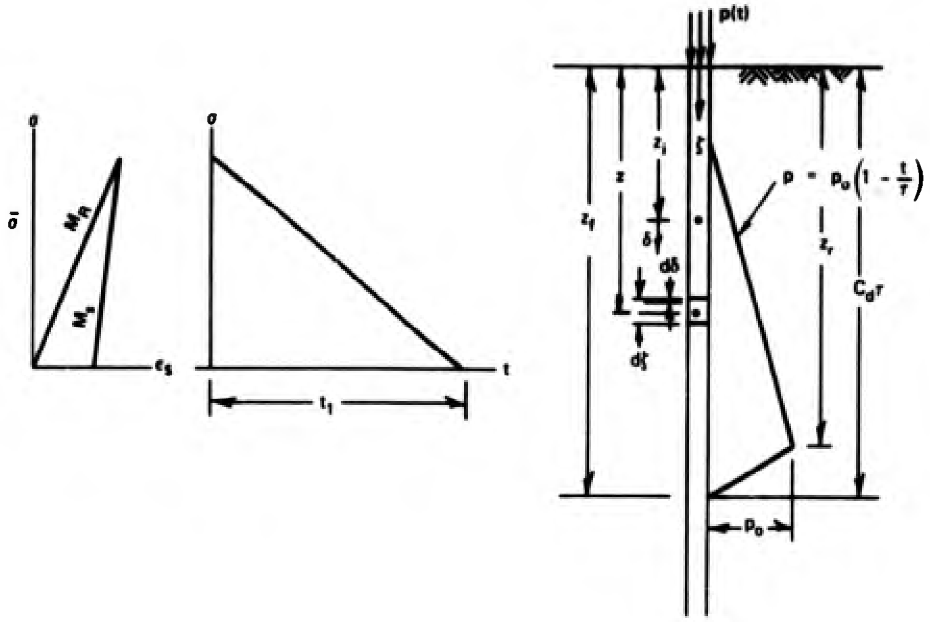

Figure 3.4. Stress–depth relationships.

layers. Motions for saturated soil fields obviously will be different than for dry fields. One of the principal differences is that the horizontal motions will be much larger. In the region under consideration (200 psi $< p_o <$ 3,000 psi), the horizontal displacement for dry soil fields may be taken as one-half of the vertical displacement.

It should be recognized that the peak displacements from Equation 3.9 are the initial maximum displacements and that, in some circumstances, there will be late-time motions (attributable to energy being fed into a given station from locations closer to ground zero) that have larger amplitudes. Fortunately, the late-time motions have low velocities and, hence, generally do not govern the survivability of protective structures.

The horizontally outward and vertically upward peak magnitudes of the direct-induced wave are nearly equal and may be approximated by the relation

$$\delta_r = 5{,}000 \frac{W_e}{(\rho C_d) R} \qquad (3.10)$$

where δ_r = peak amplitude of direct-induced displacement (inches)

W_e = equivalent yield (Kt)[3.1]

ρ = mass density of soil ($lb\text{-}sec^2/ft^4$)

R = range from ground zero (kft)

C_d = velocity of the stress front (kft/sec)

Superimposing the peak displacements from the air-blast and direct-induced waves gives a reasonable approximation of the total displacement. Again the reader is reminded that the amplitude of the late-time deflections may far exceed the values given by Equations 3.9 and 3.10. Only classified information is available on late-time motions at present (April 1972), and even that information is of questionable validity.[3.14]

Relations for velocities and accelerations may be found in Reference 3.15.

3.3 INTERACTION

3.3.1 Relative Displacement

As a soil stress wave envelops an inclusion a stress wave is propagated through the walls to the underlying soil. If the velocity of the stress wave through the inclusion is different from that in the soil, then the stress front will be distorted immediately below the inclusion.

Test results indicate that for inclusions in soil subjected to stress waves:[3.16, 3.17]

1. Shape of the inclusion has little influence on the peak acceleration and velocity induced.
2. Mass has only a slight influence at overpressures less than 600 psi. (In one test, increasing the mass by a factor of 13 halved the peak acceleration and left the peak velocity unchanged.)
3. At loads less than 600 psi, the differential displacement between an inclusion and the surrounding soil is principally due to distortion of the stress front resulting from differences in stiffness.
4. At higher overpressures there is evidence that inertial effects may be important; however, no test data exist to check this.

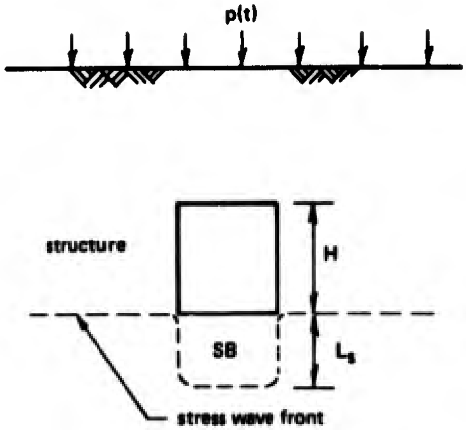

Figure 3.5. Distortion of stress front below a stiff structure.

The influence of distortion of the stress front, Figure 3.5, may be estimated by noting that the difference in transit time over the height, H, is:

$$\Delta t = \left(\frac{1}{C_d} - \frac{1}{C_f}\right)H$$

where C_d = velocity of the stress front in the soil

C_f = velocity of the stress front in the inclusion

Thus, the length of the soil block, L, immediately below the inclusion that is strained by the transmitted stress is:

$$L_s = C_d \Delta t = \left(1 - \frac{C_d}{C_f}\right)H$$

The total strain over this length is approximately equal to the peak relative displacement attributable to the stress wave:

$$\xi_s = \epsilon L_s = \frac{\overline{\eta}\alpha_z p}{E_s}\left(1 - \frac{C_d}{C_f}\right)H \qquad (3.10)$$

where ϵ = average unit strain in the soil block, SB, Figure 3.5

p = peak surface overpressure

α_z = stress attenuation to the depth of the midheight of the inclusion

$\overline{\eta}$ = stress concentration factor

E_s = soil modulus corresponding to the stress $\alpha_z p$

Equation 3.10 agrees well with experimental results[3.8] at the lower overpressures.

An approximation of the relative deflection attributable to the inertia of a rock inclusion is obtained from an unpublished development by R. J. Odello of the NCEL staff. First, the inertia force on the rock is determined from the relation

$$F_I = (a_r - a_s) m_r \tag{3.11}$$

where m_r = mass of the rock (lb mass)

a_r = acceleration of the rock (g's)

a_s = acceleration of the soil at the elevation of the rock (g's)

Using Newton's second law, the equations of motion for the rock and the displaced soil, each acting alone, are

$$\sigma_r A_r = a_r m_r \tag{3.12}$$

$$\sigma_s A_r = a_s m_s \tag{3.13}$$

where m_s = mass of the soil displaced by the rock

σ_r = stress on the rock

σ_s = stress in the soil

A_r = projected area of the rock in the direction of the stress front

Dividing Equation 3.12 by Equation 3.13 gives

$$\frac{\sigma_r}{\sigma_s} = \frac{a_r m_r}{a_s m_s} \tag{3.14}$$

From the theory of rigid inclusions by Coutinho[3.3] it is known that the stress concentration factor for a rigid inclusion in a soil field is 2; thus

$$a_r = 2 \frac{m_s}{m_r} a_s \tag{3.15}$$

Substituting Equation 3.15 into Equation 3.11 gives

$$F_I = (2m_s - m_r)a_s \tag{3.16}$$

Newmark gives an empirical dimensional equation for free-field soil acceleration as[3.1]

$$a_s = 1{,}500\,\frac{p\alpha_z}{C_d} \tag{3.17}$$

where p = peak surface overpressure (psi)

α_z = stress attenuation to depth z (dimensionless)

C_d = velocity of the dilatational wave (fps)

Equation 3.17 substituted into Equation 3.16 gives

$$F_I = 1{,}500(2m_s - m_r)\,\frac{p\alpha_z}{C_d} \tag{3.18}$$

Assuming that the static and dynamic soil reaction are equal, the foundation reaction on the rock in terms of the relative deflection can be determined from a relation by Allgood and Carter[3.18] that is based upon experimental results by White.[3.19]

$$\sigma_b = 125\,\xi_I^{0.625} \tag{3.19}$$

where ξ_I = relative displacement between the rock and the soil (inches)

σ_b = foundation reaction stress (psi)

Dividing the inertia force, Equation 3.18, by the projected area of the rock gives the foundation stress which, when set equal to Equation 3.19, gives

$$\xi_I = \left[12(2m_s - m_r)\,\frac{p\alpha_z}{C_d\,a_r}\right]^{1.6} \tag{3.20}$$

where ξ_I = relative displacement due to inertia (inches)

m_r = mass of rock (lb mass)

m_s = mass of displaced soil (lb mass)

p = peak overpressure (psi)

α_z = attenuation factor at the depth of the rock (dimensionless)

C_d = velocity of the dilatational stress front (fps)

a_r = projected area of rock (in.^{2})

The total relative displacement is

$$\Delta = \xi_s + \xi_I \tag{3.21}$$

Neglecting the interface shear, as was done in the above development, results in smaller relative displacements than is indicated by Equation 3.20. Estimates of relative displacement using Equation 3.20 indicate that, at the higher overpressures, the relative displacement attributable to the direct loading from the stress wave is larger than that due to the stress front distortion. Actually, it remains to obtain an experimental check on Equation 3.20.

3.3.2 Interface Pressure

Assuming that there is no significant reflection at the interface, the peak interface pressure from an air blast which reaches an inclusion may be expressed as

$$p_i = (p + \gamma d_o)(1 - A)\alpha_z \tag{3.22}$$

where p_i = equivalent uniform surface live load

γ = density of the soil

d_o = depth of burial of crown below surface

A = arching = $1 - p_i/p_v$ = that portion of the applied load that is transferred to or away from the structure

p_v = $\alpha_z p_o$ = peak load in free field at elevation of crown

α_z = attenuation factor for dynamic loads from Equation 3.22

Determination of arching is discussed in a later section.

3.3.3 Interface Reflections

One might expect wave reflections from a structure interface; however, they are not usually indicated in measurements except where flat tops of structures are close to the surface. The probable reason that reflections have not evinced themselves in field tests is that relatively small structures have been used wherein the duration of any reflected wave would be small. (Deviation of the reflected wave, if any, would depend on the time it takes a relief wave to reach the edges of the inclusion.) Such short-duration reflected pulses are damped out almost immediately by the soil which is highly dissipative. Diminution of reflected waves might also be enhanced by the tendency of structures to move away from the soil at the loaded interface. Reflections would also be minimized by structures that are less stiff than the enveloping soil.

Structures with curved surfaces should be used in the high over-pressure regions to gain sufficient resistance. Curved surfaces tend to minimize the effect of reflected pressure, since the stress front impinges at different positions at different times. For these reasons, reflected pressure effects are usually neglected in determining the interface load.

In those instances where a flat root is relatively close to the surface, or where saturated soil conditions exist, and a regular reflection normal to the surface occurs, the peak pressure will be

$$p_{ir} = \eta_1 p_i = \left[1 + \frac{(\rho C)_2 - (\rho C)_1}{(\rho C)_1 + (\rho C)_2}\right] p_i \qquad (\rho C)_2 > (\rho C)_1 \qquad (3.23)$$

where $(\rho C)_1$ = acoustic impedance of soil

$(\rho C)_2$ = acoustic impedance of inclusion

In Equation 3.23 note that $(\rho C)_2 < (\rho C)_1$ would indicate reflection of a tensile wave. Because soils can resist little tension, such reflections would not be expected to occur, although temporary relief of compression in the vicinity of the inclusion would be possible.

3.3.4 Stress Concentration and Dynamic Load Factors

Two stress related parameters that are often important in design are the stress concentration factor and the dynamic load factor. The stress concentration factor, as in classical elasticity,[3.20] is the ratio of the peak stress at the interface to the stress which would exist at the same point in the field without the inclusion. Of course, the stress concentration factor is highly dependent on inclusion geometry and stiffness.

Mow has shown that for cylinders and spheres in linearly elastic fields, the dynamic stress concentration factor is within 10% of corresponding static values.[3.21] One would expect the difference to be even less in the case of a soil field because of the dissipative effects on rapid changes in stress. Thus, in practical situations, the stress concentration in the free field under blast loading is not expected to be significantly different from that for the corresponding static loading.

In elementary vibration theory the dynamic load factor is defined for a simple spring-mass system as that factor which when multiplied by the peak applied load gives the peak spring reaction.[3.22] Dynamic load factors corresponding to each mode of response are also defined for multi-degree-of-freedom systems. Thus, there is a natural and useful carryover to buried structures.

To exemplify: from tests on thin 24-inch-diameter cylinders in dry sand with $d_o/D = 0.375$, the arching was zero and the dynamic load factor for the first compression mode, as indicated by the thrust at the springline, was 1.2.[3.23] By contrast, in vertical capsule tests the dynamic load factor for the first compression mode in the longitudinal direction was 2.[3.24] These and other data indicate that for stiff cylinders the dynamic load factor for the fundamental mode will be 2, but that lesser values might occur for very flexible cylinders.

3.3.5 Stress Wave Fracturing

Stress waves transmitted to structures travel through the walls and are reflected and refracted at discontinuities or boundaries. These reflected and refracted waves can cause catastrophic failures. One example of this is the model expansion chamber, Figure 3.6, shown after testing.[3.25] Reflected tensile stress waves caused failure at every welded joint. The author has also seen control mechanisms fractured from the unexposed side of a blast valve by a reflected stress wave. Obviously, the designer must be aware of the potentialities of stress wave fracturing if he is to avoid unexpected failures.

An appreciation of the problem is gained by considering one-dimensional wave propagation through a concrete slab or other element of essentially uniform section normal to the direction of wave propagation.

Referring to the stress wave diagram of Figure 3.7 and assuming a triangular load pulse with an instantaneous rise to a pressure p_o and a duration τ, the stress after the first reflection from the bottom face can be expressed as

$$\sigma_z = p_o\left(1 - \frac{t - \frac{z}{C_d}}{\tau}\right) - p_o\left(1 - \frac{t - \frac{2h - z}{C_d}}{\tau}\right) \qquad (3.24)$$

for $\frac{h}{C_d} < t < \frac{2h}{C_d}$; $h < z < 2h$; $\sigma_z < p_o$

where σ_z = tensile stress after the first reflection of the shock wave from the bottom face of the element

p_o = initial peak pressure

t = time

z = total distance $h + d''$

C = velocity of stress front

h = total depth of the element

τ = duration of load pulse

d'' = distance from bottom face to the reflected wave front

The first term on the right side of this equation gives the stress before it reaches the underside, and the second term gives the stress after reflection. It should be noted that *the tensile stress produced by the reflection is equal to the decay in the pressure pulse to the time of interest.* Equation 3.24 may be reduced to

$$\sigma_z = \frac{2p_o}{C_d\tau}(z - h) \qquad (3.25)$$

for $h < z < 2h$; $\sigma_z < p_o$; $d'' < C_d\tau$

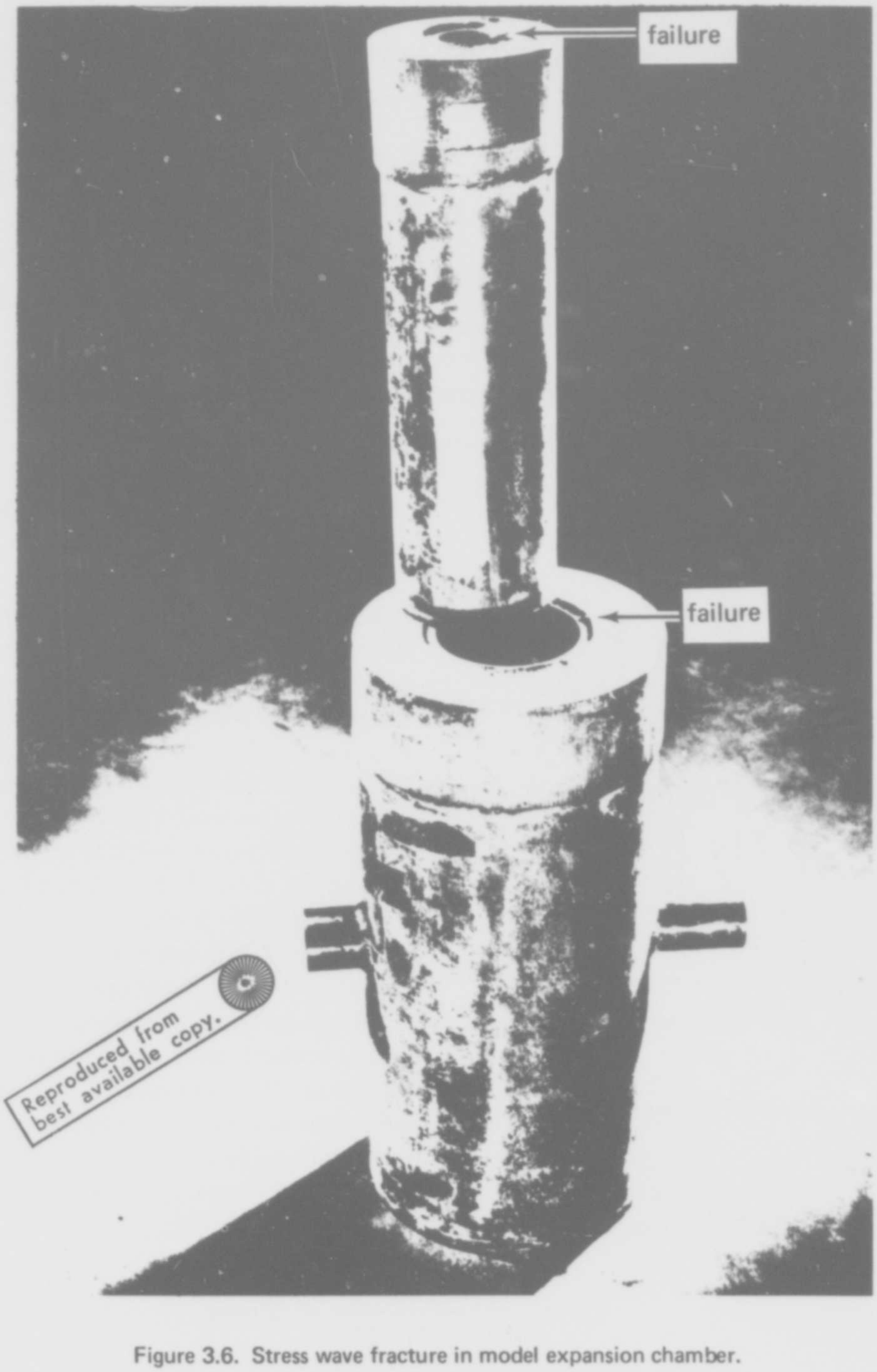

Figure 3.6. Stress wave fracture in model expansion chamber.

The duration corresponding to a given peak pressure that will result in the failure stress $\sigma_z = f_t'$ being produced at a distance d'' from the bottom of the element (z = h + d'') is, then,

$$\tau_{cr} = \frac{2 p_o d''}{C_d f_t'} \tag{3.26}$$

and

$$\sigma_{z_{max}} = \frac{2 p_o}{C_d \tau} C_d \tau = 2 p_o \tag{3.27}$$

where d'' = distance from bottom of slab

f_t' = static tensile strength of concrete

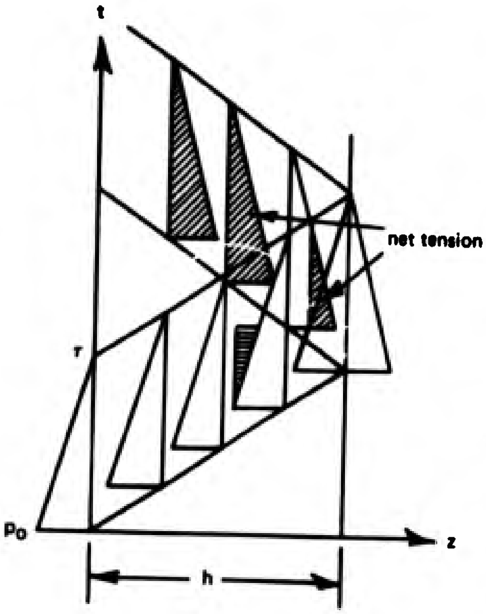

Figure 3.7. Stress wave diagram.

The static tensile strength of concrete varies from about 1/8 to 1/30 of the compressive strength. Information from water-shock load tests on walls[3.26] indicates that the strain rate associated with a reflected tensile stress wave in concrete is of the order of 2 in./in./sec. Extrapolating slightly Cowell's curves[3.27] for increase in tensile strength of plain concrete versus strain rate indicates an increase in tensile strength from dynamic straining of about 100%. With this information Equation 3.26 can be employed to find the effective load duration corresponding to a given overpressure which would result in spalling. The value obtained can be compared with the actual effective load durations to determine whether or not spalling might be a problem.

As an example, let p_o = 10,000 psi, d'' = 6 inches, f_t' = 500 psi, and C = 12 x 10^4 in./sec. Then

$$\tau_{cr} = \frac{(2)(10{,}000)(6)}{(12 \times 10^4)(500)} = 2 \text{ msec} \tag{3.28}$$

In this case any weapon yield less than about 2.5 Mt would have a duration sufficiently short to produce spalling. From this calculation it appears that spalling will be a problem for high overpressures and small weapon yields.

The principal danger of stress wave fracturing is for structures or components exposed to the air blast. This includes silos and air entrainment systems. Sharp-fronted short-duration shocks are not so apt to be transmitted to fully buried structures above the water table because of the tendency of soil to dissipate high frequency transients.

3.3.6 Reducing Interface Pressure—Arching

Arching is a convenient artifice defined as the percentage of load directly over a structure that is transmitted to or away from it. As is evident from the equations given below, the amount of load transferred to or away from a buried inclusion is primarily dependent upon its relative stiffness with respect to the surrounding media. Fortunately, the stiffness of the inclusion can be adjusted by the use of a low modulus, low strength material such as a polyurethane foam. Such a material used in the vicinity of a buried structure is commonly referred to as backpacking. The following sections give arching and backpacking relations. As presented here, the relations are only applicable to structures under deep fills or high surface overpressures.

The methodology given below is based on an empirical equation for arching developed by Gill.[3.28] He found that all available arching data for plates and cylinders in granular soil, when plotted as a function of a geometry-stiffness factor, w, could be fitted by the relation

$$A = A_o(1 - e^{-n\omega}) \qquad (3.29)$$

where A = $1 - (p_i/p_v)$ = arching

p_i = interface pressure at crown

p_v = uniform pressure in free field

e = Naperian constant

A_o, n = experimentally determined constants (A_o = 0.87 and n = 0.135 for a sharp-grained sandblaster's sand.)

ω = $A_g(M_s/p_i)\,\xi$

A_g = geometry factor to be further defined

M_s = secant modulus from a confined compression test

ξ = relative deflection between structure and free field

For convenience, let $\omega = \Omega/(1 - A)$. Then Equation 1 may be rewritten as

$$\left(1 - \frac{A}{A_o}\right)^{1-A} = e^{-n\Omega} \tag{3.30}$$

where

$$\Omega = A_g \frac{E_s}{p_v} \zeta \tag{3.30a}$$

A nomograph for obtaining solutions from Equation 3.30a is given in Figure 3.8.

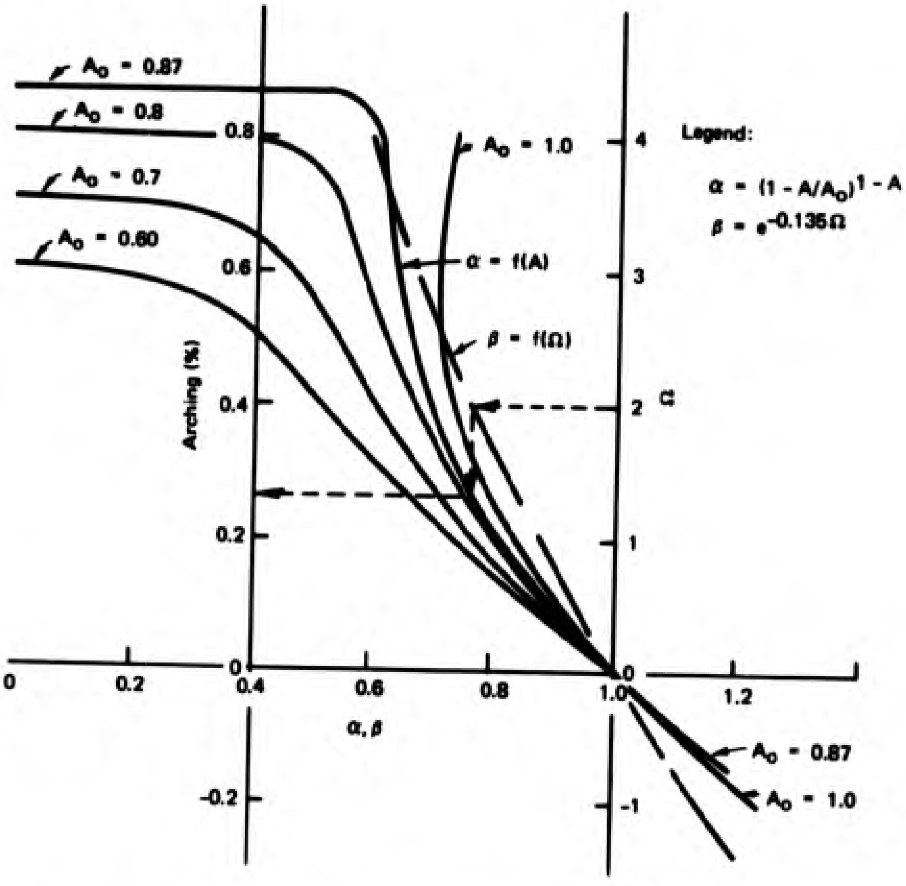

Figure 3.8. Plot for determining the arching over structures in granular soils.

For any inclusion in a soil field, the relative deflection may be expressed as

$$\xi = (\epsilon_c - \epsilon_s)H \tag{3.31}$$

where ϵ_c = average strain over height of inclusion

ϵ_s = average strain in free field over height of inclusion

H = height of inclusion

Assuming that ϵ_s is adequately approximated by

$$\epsilon_s \approx \frac{p_v}{E_s} \tag{3.32}$$

Equations 3.31 and 3.32 substituted into Equation 3.30a give

$$\Omega = A_g\left(\frac{\epsilon_c}{\epsilon_s} - 1\right)H \tag{3.33}$$

where $$A_g = \text{geometry factor} = \frac{S\,d_o}{A_s\,D} \tag{3.33a}$$

and S = perimeter of structure

A_s = plan area of structure

and d_o and D are as defined in Figure 3.9.

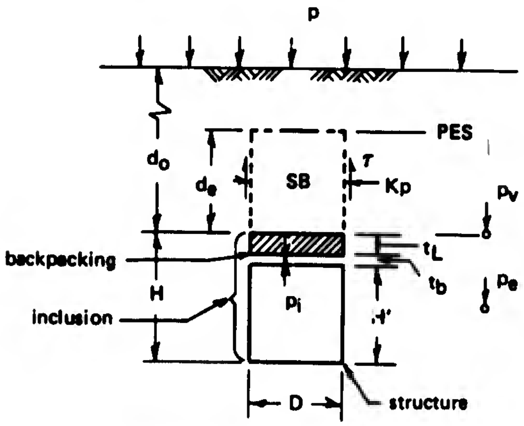

Figure 3.9. Inclusion in soil field.

When specialized to a particular geometry, Equation 3.33 with Equation 3.30 permits one to determine the amount of arching that will be developed in the soil—provided the depth to the plane of equal settlement is known.

3.3.7 Plane of Equal Settlement

The plane of equal settlement is a horizontal plane above an inclusion at which the settlement is the same as in the adjacent soil field. It is the limit beyond which an inclusion does not influence the free-field stresses and deflections. The plane of equal settlement is identified by the letters PES in Figure 3.9. The location of the PES is estimated by writing the limit equilibrium equation of soil block SB. For an infinitely long inclusion

$$|(p - p_i)D| = 2\tau d_e \tag{3.34}$$

where τ = the limit shear on the sides of SB

D = width of the inclusion

d_e = depth from top of inclusion to the PES

Using the approximation $p_v \approx p$ and the Coulomb expression for shear[3.29]

$$\tau = c + p_v K_o \tan\phi_o \tag{3.35}$$

where c = cohesion

K_o = at-rest coefficient of lateral earth pressure

ϕ_o = angle of friction of the soil

together with the definition of arching in Equation 3.34 gives

$$\frac{d_e}{D} = \left| \frac{A}{2\frac{c}{p_v} + K\tan\phi_o} \right| \qquad A > 0 \tag{3.36}$$

The corresponding value of d_e for a vertical cylinder is one-half of that given by Equation 3.36.

Experimental evidence indicates that the maximum arching which can be developed by a dry, granular soil is $A_o \approx \tan\phi_o$; hence, for that case,

$$\frac{d_e}{D} = \frac{1}{2K}$$

The range of K for granular soils is usually about 0.3 to 0.5; consequently, the distance above an inclusion to the plane of equal settlement will be 1.0 to 1.6 diameters. It is important to notice that maximum arching cannot be developed if the soil surface is below the plane of equal settlement. If the soil surface is appreciably above the plane of equal settlement, it may be possible to develop nearly 100% arching.

With d_e defined, it is possible to evaluate the geometry factor for structures of interest.

3.3.8 Arching in Soils With Cohesion

Among the meager data on structures in cohesive soils are the horizontal cylinder tests of Dorris[3.14] and the vertical spring-cylinder tests of Jester.[3.30] All of these data were for buckshot clay which has a cohesive strength of about 15 psi at 26% water content, and a zero angle of friction. Dorris' data show that arching decreases with increase in load. Jester's results show that:

1. Active and passive arching can be developed in a cohesive soil.
2. There are two basically different ranges of behavior. In the first range, behavior is governed principally by the relative stiffness of the inclusion with respect to the stiffness of the soil. In the second range, the limiting load that a structure will attract is controlled by the bearing capacity of the soil below the structure.
3. The majority of the arching action takes place within one diameter above an inclusion.
4. For structure stiffnesses greater than that of the soil, the stiffness of the soil beneath the device dominates the behavior.
5. The amount of active arching decreases when creep occurs; however, cohesive soils appear to have the capability of sustaining arching for long periods of time.

The subject of creep in cohesive soils requires further investigation.

For a soil with both intergranular friction and cohesion, a hypothesis regarding behavior can be deduced from what is known about the behavior of granular and cohesive soils and from available theory. As with purely cohesive soils, it should be expected that there will be at least two different modes of behavior: one at loads less than the cohesive resistance, and the other at greater loads. Research is presently underway to determine the variation of A_o with load, relative stiffness, and depth of cover. Once this is established, arching will be determinable from Equation 3.30. Thereafter, the interface pressure can be calculated, and a suitable design can be evolved.

3.3.9 Backpacking

From experiments and fundamental considerations, it has been deduced that for backpacking to be effective:

1. The depth-of-cover-to-diameter ratio must be large enough to permit formation of a soil arch over the inclusion.
2. Unless it is inordinately thick, the backpacking must yield to transfer a large percentage of the applied load to the soil arch.
3. A certain minimum stress must exist under the soil arch to maintain its integrity.
4. If conditions 1 through 3 are met, the peak pressure on the structure will be the yield stress of the backpacking.

In addition to these conditions, the soil over the top of a structure (t_b in Figure 3.9) must be sufficient to keep the buckling resistance greater than the yield stress of the backpacking.

The objective in design is to proportion and place the backpacking to meet the above conditions and to minimize the load to the structure or the cost of the system.

By Equation 3.33 with $\Omega = \Omega_m$ for maximum arching

$$\frac{\epsilon_c}{\epsilon_s} = \frac{\Omega_m}{A_g H} + 1 \tag{3.37}$$

Assume that all of the strain in the inclusion is from deformation of the backpacking. Then, at strain hardening of the backpacking,

$$\frac{\epsilon_c}{\epsilon_s} = \frac{\epsilon_{hL}}{\epsilon_s}\left(\frac{t_L}{H}\right) \tag{3.38}$$

where ϵ_{hL} = hardening strain of the backpacking

t_L = thickness of the backpacking

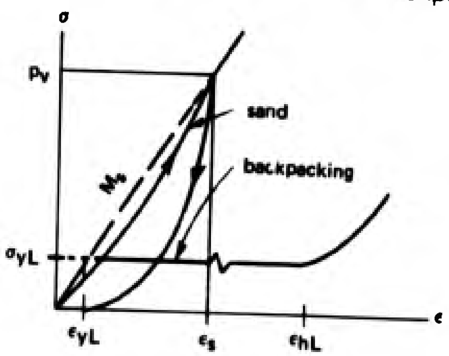

Figure 3.10. **Stress—strain diagrams.**

Combining Equations 3.37 and 3.38 gives the required thickness of the backpacking as

$$\frac{t_L}{H} = \frac{\epsilon_s}{\epsilon_{hL}}\left(\frac{\Omega_m}{A_g H} + 1\right) \tag{3.39}$$

The minimum yield stress of the backpacking that will permit development of maximum arching in a granular soil is

$$\frac{\sigma_{yL}}{p_v} = \frac{p_o}{p_v} = 1 - A_o \approx 1 - \tan\phi_o \qquad (3.40)$$

This stress will be sufficient to maintain the integrity of the soil arch when $d_o = d_e$. It may be desirable to use a $(\sigma_{yL}/p_v) < 1 - \tan\phi_o$ if $d_o > d_e$.

Arching and interface stress for $p_v < p_i(1 - A)$ may be determined from Equation 3.30.

3.4 SOIL LIQUEFACTION

The possible occurrence of liquefaction should be considered for any facility in soil where water is present. This is particularly true of structures in granular soils which are saturated or may become saturated on initial loading. Liquefaction is manifested by an increase in pore pressure and subsequent loss or reduction of shear strength.[3.31]

Liquefaction has developed during earthquakes, but has been considered an unlikely occurrence in nuclear blasts. More recent evaluation views liquefaction as a potentially significant problem because of: (1) increase in pore pressure caused by compression from blast loading, and (2) the likelihood of multiple attack. Reportedly, loss of shear strength has occurred in field tests.[3.32] Further, the increased pore pressure responsible for the loss of shear strength has evinced itself in the form of geysers in many field tests.

A few test structures in high-explosive tests have extended below the water table; however, no enhanced relative displacement has been noted that could be attributed to liquefaction. This may have been due to the short duration and rapid attenuation of the load. Although there is no known instance of failure of structural systems in blast tests from liquefaction, it has been established that marked changes in soil properties occur and that these changes persist for days or even weeks after a blast.[3.32] Thus, a system which resisted an attack of a given magnitude might fail under an identical subsequent attack.

It is clear that: (1) the possibility of liquefaction should be a matter of serious concern to the system designer, and (2) further investigation of liquefaction is warranted.

3.5 REFERENCES

3.1. Air Force Systems Command. Manual AFSCM 500-8: Systems applications of nuclear technology: Effects of air blast, ground shock, and cratering on hardened structures. Washington, D. C., Mar. 1967.

3.2. L. E. Fugelso, R. K. Waddick, and G. L. Neidhardt. "Elastic free-field motion due to nuclear air blast," American Society of Civil Engineers, Proceedings, Journal of the Engineering Mechanics Division, vol. 94, no. EM6, Dec. 1968, pp. 1337-1364.

3.3. The Rand Corporation Technical Report R-425-PR: A review of nuclear explosion phenomena pertinent to protective construction, by H. L. Brode, Santa Monica, California, May 1964.

3.4. Classified reference.*

3.5. A. J. Hendron and H. E. Auld. "The effect of soil properties on the attenuation of airblast-induced ground motions," in Proceedings, International Symposium on Wave Propagation and Dynamic Properties of Earth Materials, Albuquerque, New Mexico, August 23-25, 1967. Albuquerque, N. M., University of New Mexico Press, 1968, pp. 29-47.

3.6. University of Illinois. Department of Civil Engineering. Report on Contract NBy-32279: Attachments and connections to buried structures, by J. D. Haltiwanger, et al. Urbana, Ill., Oct. 1965. (AD 475427)

3.7. K. Ishihara. "Propagation of compressional waves in a saturated soil," in Proceedings, International Symposium on Wave Propgation and Dynamic Properties of Earth Materials, Albuquerque, New Mexico, August 23-25, 1967. Albuquerque, N. M., University of New Mexico Press, 1968, pp. 451-467.

3.8. Naval Civil Engineering Laboratory. Technical Report R-668: Response of buried capsules in the high-overpressure region, by R. J. Odello and J. R. Allgood. Port Hueneme, Calif., Apr. 1970. (AD 705990)

3.9. H. Kolsky. Stress waves in solids. New York, Dover, 1963.

3.10. Defense Atomic Support Agency. Report DASA 1285(IV): Nuclear geoplosics, a sourcebook of underground phenomena and effects of nuclear explosions, pt. 4. Empirical analysis of ground motion and cratering, by F. M. Sauer, et al. Washington, D. C., May 1964. (Contracts DA-49-146-XZ-030 and DA-49-146-XZ-121)

---

* Classified reference list available to qualified requestors.

3.11. Y. C. Fung. Foundations of solid mechanics. Englewood Cliffs, N. J., Prentice-Hall, 1965.

3.12. P. A. Abbott. "Hand solution of one-dimensional inelastic wave-propagation problems," in Proceedings, International Symposium on Wave Propagation and Dynamic Properties of Earth Materials, Albuquerque, New Mexico, August 23-25, 1967. Albuquerque, N. M., University of New Mexico Press, 1968, pp. 371-392.

3.13. Paul Weidlinger, Consulting Engineer. Report on Contract DA-49-146-XZ-508: Air induced ground shock effects on alluvium-playa material, by J. P. Wright, M. L. Baron, and I. Nelson. New York, N. Y., July 1968. (DASA 2222) (AD 852704L)

3.14. Army Engineer Waterways Experiment Station. Technical Report No. 1-682: Response of horizontally oriented buried cylinders to static and dynamic loading, by A. F. Dorris. Vicksburg, Miss., July 1965.

3.15. Classified reference.

3.16. Naval Civil Engineering Laboratory. Technical Report R-483: Motion of subsurface soil inclusions subjected to surface blast loading—results of series II tests, by L. W. Heller. Port Hueneme, Calif., Oct. 1966. (AD 640440)

3.17.————. Technical Report R-508: Motion of subsurface soil inclusions subjected to surface blast loading—results of series III tests, by C. R. White. Port Hueneme, Calif., Jan. 1967. (AD 645179)

3.18.————. Technical Report R-539: Predicting blast-induced body motions of a buried structure with footings, by J. R. Allgood and W. O. Carter. Port Hueneme, Calif., Aug. 1967. (AD 657839)

3.19.————. Technical Report R-536: Static and dynamic bearing tests on a strip footing in saturated sand, by C. R. White. Port Hueneme, Calif., June 1967. (AD 654712)

3.20. S. Timoshenko and J. N. Goodier. Theory of elasticity, 2d ed. New York, McGraw-Hill, 1951.

3.21. RAND Corporation. Memorandum RM-3962-PR: Dynamic response of lined and unlined underground openings, by C. C. Mow. Santa Barbara, Calif., Mar. 1964. (AD 602456)

3.22. J. M. Frankland. "Effects of impact on simple elastic structures," Society of Experimental Stress Analysis, Proceedings, vol. 6, no. 2, 1948, pp. 7-27.

3.23. Naval Civil Engineering Laboratory. Technical Report R-332: Static and blast loading of small buried cylinders, by J. R. Allgood and H. L. Gill. Port Hueneme, Calif., Nov. 1964. (AD 452683)

3.24.———. Technical Report R-728: Static and dynamic tests of model pressurized underground fuel storage containers, by W. F. Gates and S. K. Takahashi. Port Hueneme, Calif., May 1971. (AD 726160)

3.25.———. Contract Report CR 69.025: Evaluation of high-pressure airblast attenuation effectiveness of air entrainment subsystems, by S. P. Gill, et al. San Leandro, Calif., Physics International Company, Apr. 1970. (Contract N62399-70-C-0003) (AD 875425L)

3.26. Y. C. Kim and R. C. Binder. "Response of models to water-shock loading," American Society of Civil Engineers, Proceedings, Journal of the Engineering Mechanics Division, vol. 91, no. EM6, Dec. 1965, pp. 67-89.

3.27. Naval Civil Engineering Laboratory. Technical Report R-447: Dynamic properties of plain portland cement concrete, by W. L. Cowell. Port Hueneme, Calif., June 1966. (AD 635055)

3.28.———. Technical Report R-541: Active arching of sand during dynamic loading; results of an experimental program and development of an analytical procedure, by H. L. Gill. Port Hueneme, Calif., Sept. 1967. (AD 658502)

3.29. K. Terzaghi and R. B. Peck. Soil mechanics in engineering practice. New York, Wiley, 1948, p. 82.

3.30. Army Engineer Waterways Experimental Station. Technical Report No. N-70-7: An experimental investigation of soil-structure interaction in a cohesive soil, by G. E. Jester. Vicksburg, Miss., Mar. 1970. 2 vols. (AD 706210, vol. 1; AD 706211, vol. 2)

3.31. W. D. L. Finn, D. J. Pickering, and P. L. Bransby. "Sand liquefaction in triaxial and simple shear tests," American Society of Civil Engineers, Proceedings, Journal of the Soil Mechanics and Foundations Division, vol. 97, no. SM4, Apr. 1971, pp. 639-659.

3.32. C. R. Smith. "Project LN323: Soil pore pressure and shear strength experiment," in Event DIAL PACK preliminary report, vol. 1, pt. 2. Defense Atomic Support Agency, Information and Analysis Center, Special Report DASIAC-SR-115, Santa Barbara, Calif., May 1971, pp. 595-644. (DASA 2606-I-pt. 2) (AD 884880L)

4.0 BASICS OF SOIL–STRUCTURE INTERACTION

4.1 INTRODUCTION

The purpose of this chapter is to summarize what is known about the behavior, design, and analysis of the soil–structure configurations of principal interest in protective construction. To understand their behavior one should consider buried facilities primarily as soil–structures. Often the only purpose of the structure per se is to provide confinement so that the soil can carry the load.

Normally the best configuration is a system designed so that the soil carries most of the load. Since the soil is the principal component, it follows that the soil properties must be known. Further, the bedding, backfill, and overburden must be properly constructed.*

Conditions which constitute proper bedding, backfill, and overburden are generally the same as for culverts,[4.1] although there will be departures depending on the individual system geometry as indicated in later sections.

Before launching on a disquisition of specific systems, it is advisable to examine general parameters common to essentially all soil–structure entities. This is readily accomplished through a dimensional analysis.

4.2 DIMENSIONAL ANALYSIS

Assume a blast loading with an instantaneous rise to the peak overpressure and a linear decay that forms a triangular pulse acting uniformly over the surface above a closed, fully buried structure that is long with respect to its maximum lateral dimension. Assume further that gravity and other body forces are of negligible magnitude compared to the applied load. A dimensional analysis for this general class of systems is given in Table 4.1. Usually one is interested in determining the deflection, y, or stress, σ, at some critical location. Here, deflection is used as the independent variable.

In Table 4.1, the number of nondimensional pi terms is 14 (the number of parameters minus the number of dimensions). It may be noted that τ, M_s, ρ_s, and H are used as nondimensionalizing parameters.

* Here, the terms bedding, backfill, and overburden refer, respectively, to the material below, at the sides of, and above a buried structure.

Table 4.1. Dimensional Analysis of Fully Buried Two-Dimensional Structure

Parameter No.	Component	Symbol	Parameter Description	Dimension	Pi Terms $\pi_1 = f(\pi_2 \ldots \pi_{15})$
1	load	p	surface pressure	$F L^{-2}$	$\pi_1 = \frac{y}{H}$
2		α_z	attenuation	–	$\pi_2 = \frac{p}{M_s}$
3		t	any time	T	
4		τ	duration of load	T	$\pi_3 = \alpha_z$
5	soil	M_s	soil strain or modulus	$F L^{-2}$	$\pi_4 = \frac{t}{\tau}$
6		K	measure of lateral strain	–	$\pi_5 = K$
7		$\bar{c}$	cohesion	$F L^{-2}$	$\pi_6 = \frac{\bar{c}}{M_s}$
8		ϕ_o	angle of friction	–	
9		u	porosity	$F L^{-2}$	$\pi_7 = \phi_o$
10		ρ_s	mass density of soil	$M L^{-3}$	$\pi_8 = \frac{u}{M_s}$
11		C_d	velocity of stress wave	$L T^{-1}$	$\pi_9 = \frac{C_d \tau}{H}$
12	structure	H	depth of inclusion	L	
13		D or	width of inclusion	L	$\pi_{10} = \frac{L}{H}$
14		L	any dimension	L	$\pi_{11} = \frac{M_s}{EA/H}$
15		EA	compressional stiffness	F	
16		EI	bending stiffness	$F L^2$	$\pi_{12} = \frac{M_s}{EI/H^3}$
17		C_f	velocity of stress wave	$L T^{-1}$	$\pi_{13} = \frac{C_f \tau}{H}$
18		ρ_I	effective mass density of inclusion	$M L^{-3}$	
19	system	d_o	depth of cover	L	$\pi_{14} = \frac{\rho_I}{\rho_s}$
20	dependent variable	y or σ	displacement or stress	L or $F L^{-2}$	$\pi_{15} = \frac{d_o}{H}$

For static loading, π_3, π_4, π_9, π_{13}, and π_{14} drop out leaving 10 terms. With unsaturated granular soils, π_5, π_6, π_7, and π_8 are negligible. Also, in many buried structures π_{11} is negligible. Hence, for most statically loaded systems with granular soil

$$\pi_1 = f(\pi_2, \pi_{10}, \pi_{12}, \pi_{15})$$

or

$$\frac{y}{H} = f\left(\frac{p}{M_s}, \frac{L}{H}, \frac{M_s}{E\,I/H^3}, \frac{d_o}{H}\right) \tag{4.1}$$

The dimensional analysis of Table 4.1 is readily modified for structures with footings, backpacking, mounds, or other characteristics different from those assumed. In any case, the pi terms in Equation 4.1 will usually constitute the dominant parameters; they are used repeatedly in the following sections.

4.3 UNLINED TUNNELS

Unlined underground openings are possible in most unsaturated soils possessing reasonable cohesive strength. Sokolovkii has derived relations for the shape of stable underground openings;[4.2] a typical stable opening is indicated in Figure 4.1. Such openings have a region on either side, indicated by the shaded area in the figure, where slip occurs. Theoretically, stable openings in soil with an angle of friction of 45 degrees can resist static loads of up to five times the cohesive strength of the soil. Since cohesive strengths of 15 psi are not uncommon, it is evident that unlined tunnels in such soils should be capable of resisting static loads on the order of 75 psi.

Unlined openings are susceptible to spalling and even collapse if they are subjected to stress waves or ground motions; consequently, liners should be used in protective facilities that are expected to survive an attack. Even so, the consideration of unlined tunnels is important to the designer of protective facilities because it permits him to gain an appreciation of the shape and resistance of stable arch forms. A properly installed liner that supports the underside of the arch would provide the confinement necessary to reduce the slip and would permit the soil to carry much more load. Horizontal circular cylinders fit well into the stable arch void and, therefore, are efficient buried structures.

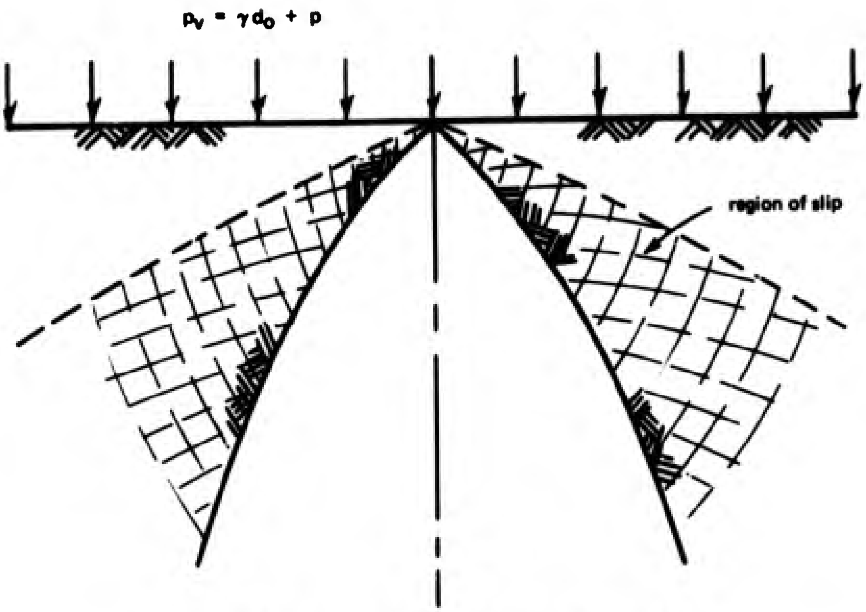

Figure 4.1. Typical stable arch form in cohesive soils.

4.4 HORIZONTAL CYLINDER

If a horizontal cylinder, Figure 4.2, is placed so that the strength of the soil is properly mobilized, the resulting system has a truly fantastic load-carrying capacity. For example, 1-foot-diameter and 2-foot-diameter models a few thousandths of an inch thick have survived blast loads of 250 psi to 800 psi in field tests.[4.3] Indeed, near surface cylindrical shelters can be designed to resist blast loads of several thousand psi if shock isolation and other requirements can be met.

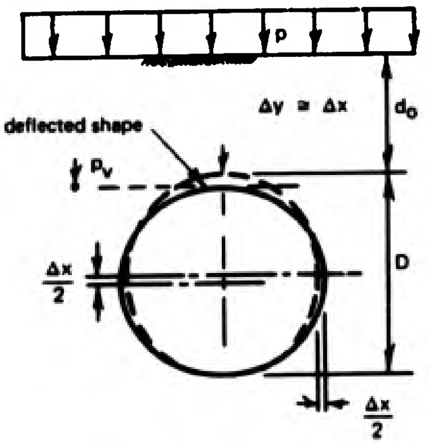

Figure 4.2. Deflected shape of horizontal cylinder.

Early research on soil–structure interaction was centered around the conduit. This resulted in the Iowa Formula[4.4] and various other[4.5] largely empirical methodologies, plus a significant body of experience. The need to design protective facilities arose after the advent of nuclear weapons. The latter period resulted in approximate design relations,[4.6] elastic theory solutions,[4.7] and finite element programs.[4.5] Also, during the latter period, good instrumentation was developed to permit meaningful validation of system behavior and analytical methods. Virtually all of this analytical and measurement capability was achieved under DASA (now the Defense Nuclear Agency) sponsorship. Fortunately, the knowledge and capability gained in studying cylindrical shelters carries over to culverts and pipes as used in civil construction.[4.1, 4.8]

Possible modes of failure of horizontal cylinders include:

1. Excessive flattening or increase in horizontal diameter
2. Compressive yielding of the walls
3. Buckling of the walls consisting of either caving of the top or a local transitional crimp at some location on the perimeter; the buckling may be elastic or plastic
4. Seam or joint failure
5. Longitudinal bending or joint separation

In addition, failure may occur at or near end walls (in the case of shelters). Also, uncontrolled water or any other occurrence that undermines or otherwise degrades the bedding or backfill may result in failure or possibly collapse of the system.

The performance of a buried cylinder depends on its relative stiffness with respect to the stiffness of the enveloping soil. Thus, it is useful to establish quantitative boundaries to distinguish systems of fundamentally different characteristics. Convenient boundaries are:

Flexible . . . . $10^4 < \dfrac{M_s}{E\,I/D^3}$

Intermediate . . . . $10^1 < \dfrac{M_s}{E\,I/D^3} < 10^4$

Stiff . . . . $\dfrac{M_s}{E\,I/D^3} < 10^1$

Flexible cylinders are those whose wall stiffness has little effect on their vertical diametral deflection (usually less than 10%). Stiff cylinders are those for which the average strain over the depth of the cylinder is less than or equal to the free-field soil strain ($\epsilon_c \leq \epsilon_s$).

An adequate definition of failure is difficult to formulate for buried cylinders. Part of the reason is that there is a variety of modes of failure; the main difficulty, however, is that even if compressive or flexural yielding, buckling, or some other potential mode of failure is initiated, collapse rarely ensues.[4.9] Instead, the load is transferred to the soil, and the system continues carrying load. To circumvent the difficulty in defining failure, Watkins[4.9] proposes the use of the performance limit defined as that deformation beyond which the cylinder would continue to deflect and collapse if the loads were not relieved by soil arching.

For present purposes, failure will connote: the occurrence of visible distress as indicated by wall crushing or excessive cracking; buckling; plastic deformation (other than local); separation or rupture of seams and joints; or excessive deflection which impairs the functional performance of the installation. Clearly, designs should be evaluated in terms of both their failure and their collapse loads.

4.4.1 Theory

Burns[4.7] developed the theory for an elastic circular cylinder in an isotropic linearly elastic field loaded by a uniform static surface pressure. Hoëg introduced simplifying modifications and changes;*[4.10] Kay and Krizek[4.11] among others have plotted the equations. Allgood reduced certain of the elastic theory equations to a simple form and pointed out that these equations can be used for design if the proper effective soil modulus is used.[4.6, 4.8] Useful simplified elastic theory relations and plots are given below.

4.4.1.1 Deflection. For a Poisson's ratio of 1/3, an at-rest coefficient of lateral earth pressure of 1/2, and no interface shear (full slippage), the elastic theory solution for deflection under static loading reduces to

$$\frac{\Delta y/D}{p_v/E_s} = \frac{14F + 1}{3(2F + 3)} \tag{4.2}$$

where Δy = diametral deflection at crown

D = mean diameter of cylinder

E_s = elastic modulus of the soil

$$F = \frac{1}{96(1 - \nu_c^2)}\left(\frac{E_s}{EI/D^3}\right)$$

---

* Burn's and Hoëg's developments differ.

ν_c = Poisson's ratio of cylinder material

EI = stiffness of cylinder

p_v = effective free-field stress at the elevation of the crown

Equation 4.2 is based on the condition that the compressibility of the cylinder does not influence the deflection; this is virtually always the case in practical applications. For most fully buried cylinders the horizontal expansion, Δx, will be within a few percent of the vertical contraction, Δy. For flexible cylinders where $F \gg 1$, the right side of Equation 4.2 reduces to 2.33. Experimental results show that actual deflections lie between the theoretical values for conditions of full slippage and those of no slippage, in which case, the constant reduces to 2.0. Thus, for flexible cylinders

$$\frac{\Delta y}{D} = 2\frac{P_v}{M_s} \tag{4.3}$$

P_v/M_s is proportional to the vertical soil strain. Equation 4.3 shows that the deflection of a flexible buried cylinder is solely dependent on the diameter and the vertical soil strain. Hence, to keep the deflections small, the soil must be well compacted.

Equation 4.2, adjusted for average interface conditions, is plotted in Figure 4.3. The plot is for a Poisson's ratio of 0.33; however, less than a ±5% error results for *cylinder* materials with a Poisson's ratio between 0.2 and 0.4. Also, an error of less than 9% will occur for a Poisson's ratio of the *soil* larger or smaller than 0.33. These errors are small when compared to the possible variation in M_s; therefore, they are of secondary concern in the design of most buried cylinders.

Figure 4.3 is convenient for estimating the diametral deflection if EI and M_s are known. EI is usually easily found from the design method given later, except for cylinders of concrete or other brittle materials. With concrete cylinders EI varies around the cylinder and changes with load due to cracking.[4.12] Conservative estimates of deflection may be made based on the EI of the cracked section at the haunch at the design load.

The ratio $\Delta y/D$ in Equation 4.3 may be considered as the average vertical strain of the cylinder, ϵ_c. Since $\Delta y \simeq \Delta x$ for flexible cylinders, the average horizontal strain over the width is also equal to ϵ_c. In the free field, however, the lateral strain under a uniform surface load is zero. Thus, the net effect of the presence of the cylinder is to produce a lateral strain to educe a vertical strain concentration factor of 2.

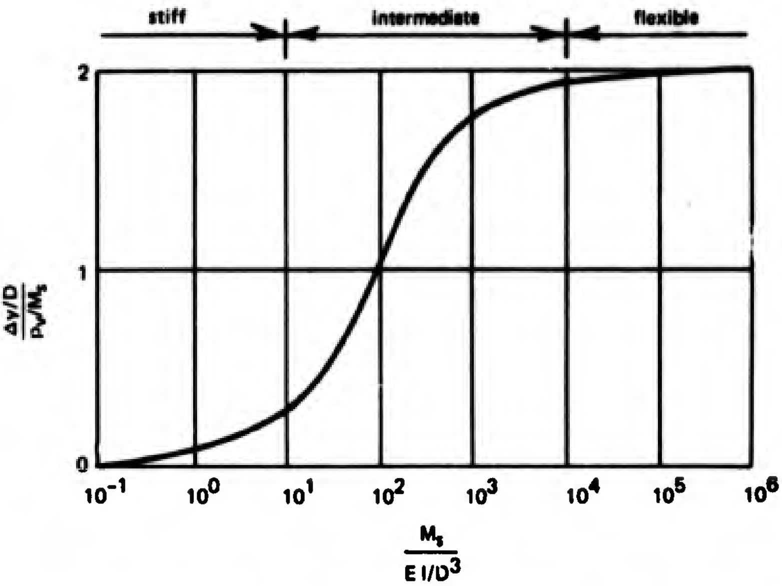

Figure 4.3. Vertical diametral deflection of a cylinder under static loading.

4.4.1.2 Arching. The ratio of the strains ϵ_c and ϵ_s largely controls the amount of arching that occurs as may be observed on examining Equations 3.30 and 3.33. Substituting $H = D$ and the geometry factor

$$A_g = 2\frac{d_o}{D^2}\left(1 + \frac{D}{L}\right) \tag{4.4}$$

into Equation 3.33 with $L/D > 1$, gives

$$\Omega = 2\frac{d_o}{D}\left(\frac{\epsilon_c}{\epsilon_s} - 1\right); \quad d_o < d_e \tag{4.4a}$$

Using values of Ω from this equation permits determination of the arching from Figure 3.8.

For most practical horizontal cylinder–soil systems, $1 < \epsilon_c/\epsilon_s < 2$; hence, $0 < \Omega < 2(d_o/D)$. Thus, for fully buried cylinders where $0 < d_o < 1.4\,D$, $0 < A \leq 35\%$. As indicated in Section 3.0, arching can be greatly increased by decreasing the effective stiffness of the inclusion. The results of finite element computer calculations which demonstrate this effect are given in a later section.

In design, where EI is not known initially, a reasonable estimate of arching can be obtained from the relations[4.13]

$$A = 0.2 - 0.2\left(1 - \frac{d_o}{D}\right)^2 \quad \text{for } \frac{d_o}{D} < 1.0$$

$$A = 0.2 \quad \text{for } \frac{d_o}{D} > 1.0$$

These relations approximate the envelope of available test data of cylinders in granular fields.

From the above it is clear that for horizontal cylinders in uniform soil fields, the magnitude of the deflection (in terms of the average vertical cylinder strain) relative to the soil strain determines the magnitude of the arching. Arching will act whether the loading is static or dynamic. Rebound of the soil has been known to occur in certain circumstances which bulks the backfill, breaks down the intergranular locking, and debilitates ability to resist subsequent loadings by arching. This may occur with soils that are relatively elastic under short-duration loads, especially where the water table is close to the surface.

4.4.1.3 Soil Moduli. M_s is dependent upon media characteristics, as discussed in Section 2.3.4, and upon system geometry (boundary conditions) and loading. For full burial and a uniform surface loading, as shown in Figure 4.2, M_s may be taken as the secant confined compression modulus (from a uniaxial compression test) corresponding to the peak applied pressure. Dependence of the effective soil modulus on depth of cover is given by the relation

$$M_{s_{eff}} = (1 + \nu_s)\tilde{B} M_s \tag{4.5}$$

where

$$\tilde{B} = \frac{1 - (R/r)^2}{(1 + \nu_s)[1 + (1 - 2\nu_s)(R/r)^2]} \tag{4.5a}$$

and R = cylinder radius

r = $R + d_o$

ν_s = Poisson's ratio of the soil

d_o = depth of cover

Equation 4.5a was developed by Luscher;[4.14] it is plotted in Figure 4.4.

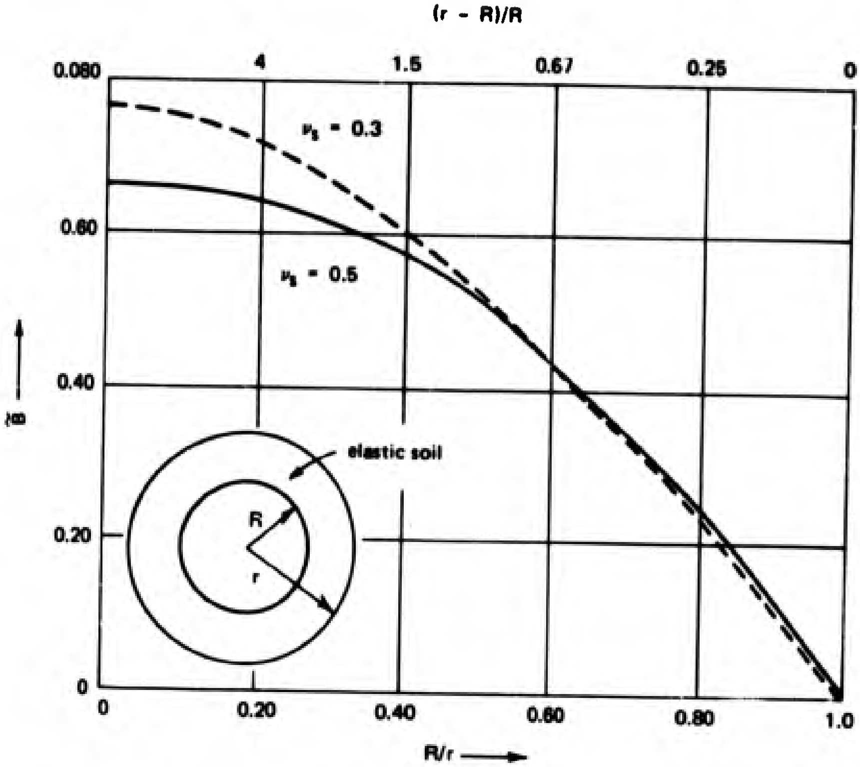

Figure 4.4. Modulus of soil support for elastic ring. (From Reference 4.14)

Full burial may be defined from Equation 4.5 as that depth of burial for which $M_{s_{eff}} = \eta M_s$, where η is arbitrarily close to 1.0. Full burial might also be defined in terms of the depth to the plane of equal settlement from Equation 3.36, that is, $d_o > d_e$. Usually, however, a structure is regarded as fully buried if the depth of cover over the crown is one diameter or more and if, in the case of a mounded structure, the side slopes are 14 degrees or less.[4.15] The latter usage is predicated on the fact that roof caving (first bending mode buckling) does not usually occur at depths of cover of one diameter or greater.

Where the slopes of mounds are greater than 14 degrees, in embankment situations, or where the load is not uniform, determination of the effective soil modulus may be more difficult. In these circumstances, the effective modulus should be taken as the secant modulus of the triaxial stress–strain curve corresponding to the extant vertical and lateral stress condition. Discussion of the state of stress in embankment and deep fills is beyond the scope of this document.

A related subject which warrants discussion here is the interrelation of the various soil moduli and coefficients that are used in the soil–cylinder interaction literature. They are related to the confined compression modulus as follows:

- Modulus of elasticity (from the elastic theory),

$$E_s = \left[\frac{(1-2\nu)(1+\nu)}{1-\nu}\right] M_s = \tilde{C} M_s \qquad (4.6)$$

- Modulus of elastic support (from a theoretical development by Luscher[4.14]),

$$k_s = \tilde{B} E_s = \tilde{B}\tilde{C} M_s \qquad (4.7)$$

where $\tilde{B}$ is given by Equation 4.5a and Figure 4.4.

- Coefficient of soil reaction (from various buckling theory developments[4.16]),

$$k_z = \frac{k_s}{R} = \frac{\tilde{B}\tilde{C}}{R} M_s \qquad (4.8)$$

- Modulus of passive pressure of the sidefill material (from the Iowa formula[4.4]),

$$E' = 16.4\left(\frac{D_L \bar{K} W_c}{\Delta x} - \frac{EI}{R^3}\right) \qquad (4.9)$$

where Δx = horizontal expansion of cylinder

W_c = load on pipe per unit of length

EI = pipe wall stiffness

R = pipe radius

E' = eR = modulus of passive resistance

e = modulus of passive pressure of the sidefill material (FL - 2/L)

$\bar{K}$ = bedding coefficient

D_L = deflection lag factor

Equation 4.9 is fundamentally an empirical equation that was developed to predict the deflection of culverts. For flexible conduits, where $EI/R^3 <$ 0.061 E' and assuming a typical bedding coefficient of 0.1 and a deflection lag factor of 2, Equation 4.9 becomes

$$E' = 1.64 \frac{p_v}{\Delta y/D} \qquad (4.10)$$

By letting EI/D^3 go to zero in Equation 4.2 and using Equation 4.9 it may be shown that $M_s \approx 1.0$ to $2.0\ E'$. For a bedding coefficient of 0.075, $M_s = 1.22\ E'$. Substituting this relation in Equation 4.10 gives $\Delta y/D = 2p/M_s$, which agrees with Equation 4.3.

There has been a lot of confusion created by the variety of soil moduli and coefficients that have been used in soil–cylinder developments. It is suggested that M_s or $M_{s_{eff}}$ be used hereafter for approximate calculations. M_s is convenient to use, because it is directly determinable from standard laboratory tests. As pointed out previously, in many approximate static calculations the effective secant modulus, M_s, is the only soil parameter needed as variations attributable to Poisson's ratio and other parameters are less than those from uncertainties in M_s.

Use of the constrained (one-dimensional compression) modulus is advantageous, because (a) it is relatable to dry density, vane shear strength, and certain other useful indices of field soil conditions, and (b) it is a standard, widely used laboratory test. The confined compression test cannot be expected to give correct results consistently unless the load is applied pneumatically or hydrostatically through a flexible membrane.

In some instances, particularly for noncohesive soils, one may use density, vane shear, CBR (California Bearing Ratio), or other tests as an index of M_s.[4.14,4.17] Incidentally, for field installations of flexible culverts $[M_s/(EI/D^3) > 10^4]$, M_s may be back-calculated using Equation 4.3. This serves as a good check on laboratory or other determinations presuming, of course, that Δy is measured as the fill above the crown is placed. If this is done, care should be taken to obtain a calibration for M_s, against the index for the soil being used, that is truly representative of the boundary condition and loading in the actual installation. Fortunately, good static soil strain and stress gages are now available which permit complete definition of the state of stress and strain (and, consequently, the soil modulus) at a point.

4.4.1.4 Thrust. By the elastic theory, the minimum thrust possible at the spring line in any culvert is equal to pr; but it is well known from numerous experiments (References 4.18 through 4.22) that the thrust is usually considerably less than pr. Thrust, as calculated from the arching theory, is compared with experimental values and with the elastic theory in Figure 4.4. Values of thrust were computed by determining ϵ_c/ϵ_s from Figure 4.3 for selected values of $M_s/(EI/D^3)$. The values of ϵ_c/ϵ_s were then substituted into Equation 4.5 to find corresponding values of Ω, which permitted entering Figure 3.8 to find the arching. Lastly, the thrust at the springline under static loading was calculated from the relation $N_{sp} = (1 - A)pR$. As may be observed, there is reasonable agreement between the calculated curve and the experimental data. Both of these differ markedly from the slip and no-slip cases calculated by the elastic theory.

Referring to the experimental data in Figure 4.5, the single points represent the average of several tests. The point representing Marino's tests[4.21] probably indicates a higher thrust than the other data because the test cylinders had spherical end caps. Because end caps stiffen the cylinder, they would be expected to attract load, some of which would be "dumped" into the cylinder. Available data indicate that the thrust determined from the arching is a reasonable upper bound for long cylinders. For capsules with small values of L/D, the design thrust should be increased as indicated by Marino's data.

The thrust at the crown may be determined from the relation

$$\frac{N_{cr}}{p_v R} = 1 - \frac{N_{sp}}{p_v R} \tag{4.11}$$

For blast load conditions, the thrust may be determined from the relation

$$\bar{N}_{sp} = \alpha_z \, DLF (1 - A) p R \tag{4.12}$$

where α_z = attenuation factor as given by Equation 3.2

DLF = dynamic load factor

The variation of the thrust around the perimeter of a buried cylinder under static loading is approximately

$$N(\theta) = N_{sp} + (p_v R - 2N_{sp}) \sin\theta \tag{4.13}$$

where θ is the angle measured counter clockwise from a horizontal diameter. Equation 4.13 also holds for the quasi-static state after envelopment of a shelter by the blast wave.

Under a blast loading, the thrust at a point increases to a peak value in a few milliseconds, slightly overshoots the value corresponding to a static load of the same magnitude, and then decreases in a quasi-static manner as the load decays. Maximum variation from the static thrust occurs at the crown where bending mode amplification occurs.

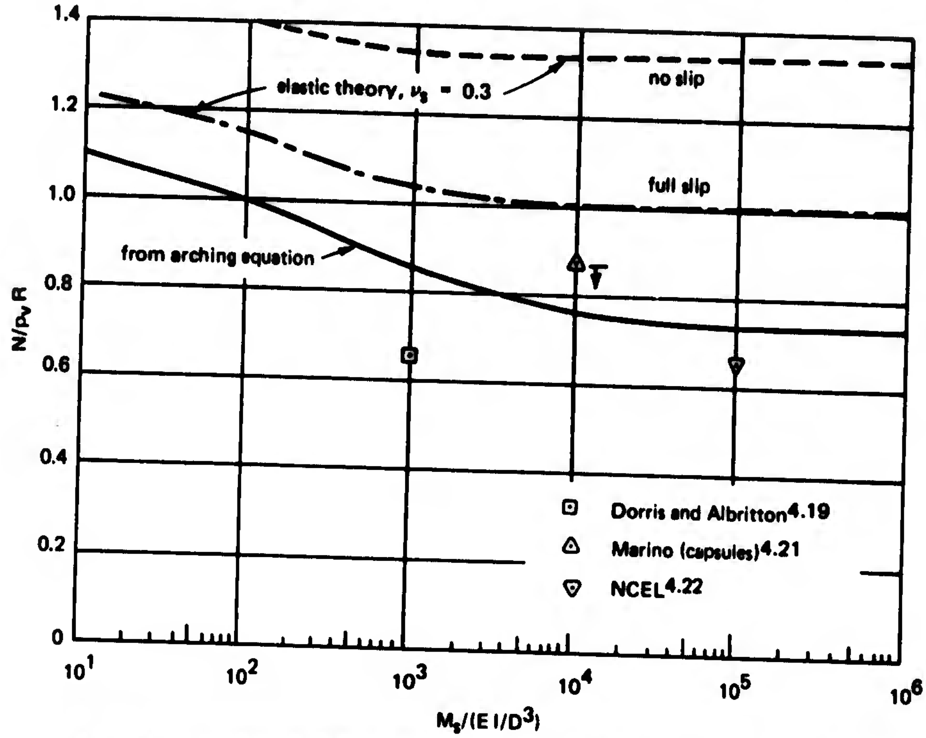

Figure 4.5. Comparative determination of thrust at springline under static loading.

4.4.1.5 Moment. As with thrust, elastic theory gives moments which are large compared to experimentally determined values as is indicated in Figure 4.6. As may be observed from Figure 4.5, the elastic theory and the experimental data are closer together for stiff cylinders than for flexible ones. Also note that there is a considerable spread in the moment data for the stiffer cylinders even when, as in the plotted points, the data are by the same experimenter.

Flexible cylinders in granular soils tend to develop circumferential waves at the higher loads. Outward deflecting lobes of these waves apparently develop local shear stresses that limit moments, especially under high loads.

Under blast loading, the peak moments are about the same as under static loading except in the vicinity of the crown. Experimental data show that although there is little or no dynamic amplification of thrust or moment in most of the circumference, a factor of about two amplification of moment occurs in the vicinity of the crown. The resulting localized enhancement of bending is not as serious as it might seem on initial thought, as the buckling load in the excited bending mode (wave frequency) would be greater than the transitional buckling load. Yielding, however, will occur at a lower load than under a static load of the same magnitude. If this is taken into account, the experimental curve of Figure 4.6 may be used as a design curve for either type of loading. Crown moments increase rapidly as the depth of burial decreases below one diameter; thus, facilities that provide protection against nuclear weapons effects should nearly always be buried at least one diameter.

4.4.1.6. Buckling. Buckling of buried cylinders may develop in any one of several different mo[illegible] the so[illegible]n the depth of cover, the cylinder geometry, the wall stiff[illegible] and transitional[illegible]lus. Possible buckling modes include caving of the c[illegible] of the [illegible]p-through) buckling. These are actually different [illegible]e type of buckling, but they are usually diff[illegible] [illegible]mingly different physical characteristics. Tra[illegible]nal [illegible]ay [illegible] when the strains are in either the elastic or [illegible]lastic [illegible]endin[illegible] the magnitude of the governing parameters.

Transitional buc[illegible]om reversal of one of the circumferential waves that typically [illegible]round the perimeter of relatively flexible cylinders at high loads. A relation defining elastic buckling has been developed and validated by comparison with test data.[4.6,4.16] A plot of the theory is given in Figure 4.7. For long cylinders, or short cylinders where $M_s D^3/EI < 10^6$, the caving and transitional buckling load is approximated by the asymptotic solution

$$p_{i(cr)} = \overline{C}\sqrt{E_s\left(\frac{EI}{D^3}\right)} \tag{4.14}$$

where $\overline{C} = 6\sqrt{\widetilde{B}\widetilde{C}}$ (4.15)

$p_{i(cr)} = (1 - A)p_{cr}$ = critical interface pressure producing buckling (4.16)

and $\widetilde{B}$ and $\widetilde{C}$ are as defined in Equation 4.5a and Equation 4.6. Clearly the critical interface pressure is highly dependent upon the soil modulus and the arching.

The solution of Figure 4.4 and Equation 4.5a is based on uniform elastic support around the perimeter, but it gives reasonable results if the effective soil modulus corresponding to the buckling load is used for M_s. Since the buckling load is not known initially for use in determining M_s, iteration may be required. Normally not more than one or two cycles of iteration is warranted because of the wide variation in actual buckling loads.

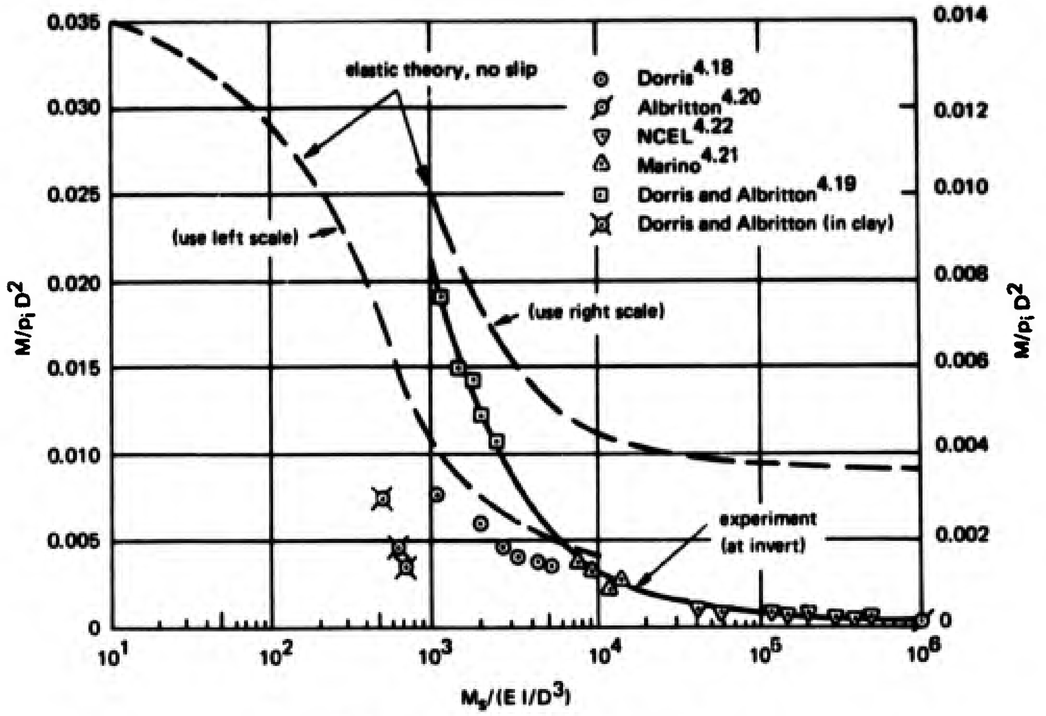

Figure 4.6. Moments in buried cylinders.

Buckling is inherently a phenomenon of wide variability because of its sensitivity to initial shape, boundary conditions, locked in stresses, and stress concentrations. As a consequence, the load factor or other factor of safety against buckling should be higher than for other potential modes of failure.

One helpful effect results from a tendency for the soil to compact in the vicinity of a cylinder during loading more than it does in the free field. This local compaction is particularly pronounced near highly flexible cylinders in soil fields with low initial densities, thereby increasing their buckling loads.

Solutions for the inelastic buckling of confined cylinders have been developed,[4.23] however, they are difficult to apply, and they have not been checked against experimental data. This is not critical since normally it is desirable to design for elastic behavior, especially when employing backpacking.

4.4.1.7 Backpacking. Interface pressures on horizontally buried cylinders may be reduced by factors of up to 10 by proper use of backpacking to permit transfer of the load through the soil in arching. The general Equations 3.30, 3.33, and 3.39 for arching and backpacking thickness are readily specialized to the horizontal cylinder by use of the proper geometry factor. On substituting the appropriate parameters in Equation 3.33a, the geometry factor for horizontal cylinders is found to be

$$A_{gh} = 2\frac{d_o}{D^2}\left(1 + \frac{D}{L}\right) \qquad d_o \leq d_e \tag{4.17}$$

where L = length of cylinder

d_e = depth to the plane of equal settlement

With A_{gh} known, the arching can be calculated from Equations 3.30 and 3.33 provided ϵ_c/ϵ_s can be determined.

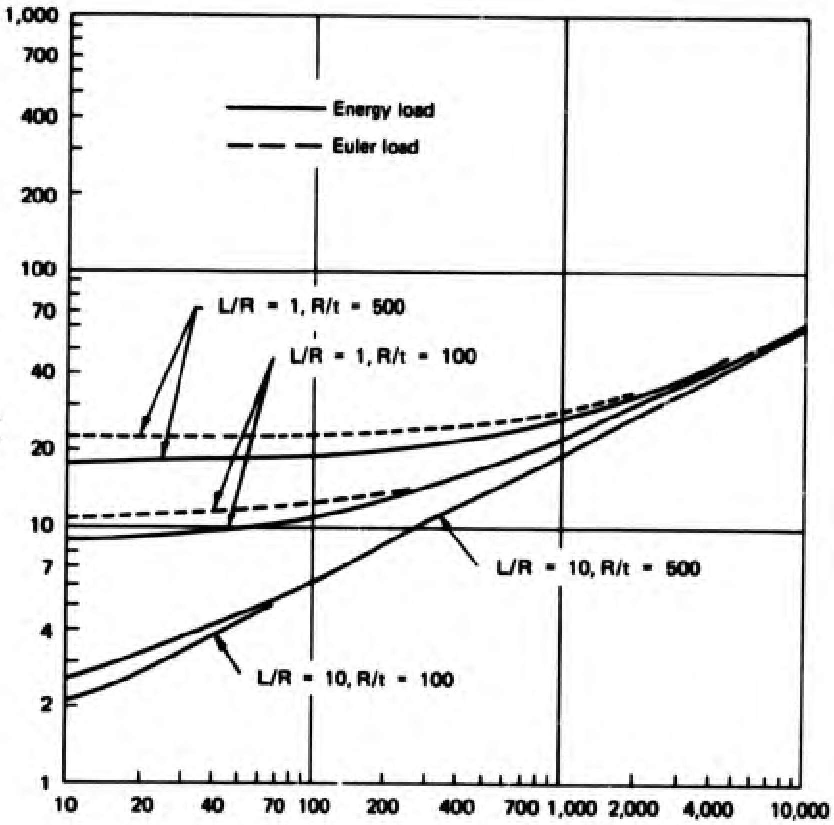

$$\frac{p_{cr}}{E\left(\frac{t}{R}\right)^3} = \frac{1}{12}\left(\frac{p_{cr}R^3}{EI}\right)$$

$$\frac{k_z R}{E\left(\frac{t}{r_i}\right)^3} = \frac{\tilde{B}\tilde{C}}{96}\left(\frac{E_s}{EI/D^3}\right)$$

Figure 4.7. Critical pressures for cylinders with elastic support.

For very flexible horizontal cylinders in dry sand, $\epsilon_c/\epsilon_s = 2$. Hence, in those instances where $d_o = d_s$ and $K = 0.35$, $\Omega = 2/K = 5.7$ and $A = A_o$. With $\phi_o = 41$ degrees, $A_o = 0.87$; that is, only 13% of the applied load reaches the cylinder. If $d_o > d_s$, the interface pressure may be less than $0.13\, p_v$, because the arching shear stresses may distribute over a larger area, and, thus, reduce the required confining stress to maintain the integrity of the soil arch.

When backpacking is employed, agreement between the arching theory and cylinder experiments is good.[4.6] Further, experimental results have shown that the intergranular arching stresses are preserved on repeated dynamic loading. There is, however, the possibility that an outrunning wave or a direct-induced wave could loosen the cover and debilitate the arching stresses. The consequences of this possibility should be weighed in any design involving multiple loadings.

Another method for enhancing the strength of some buried structures (for example, fuel tanks) is to use internal pressurization. Internal pressurization increases the buckling load, but it also increases the effective stiffness of a cylinder.[4.3, 4.24] As a consequence, it will usually be desirable to use backpacking over pressurized cylinders.

4.4.1.8 Interface Pressure. It has been demonstrated that within limits the interface pressure on flexible cylinders may be calculated from strain measurements.[4.22] This is accomplished by calculating the deformed radius of curvature at the point of interest from the shell theory relation

$$\rho = \frac{1}{\frac{1}{r} - \frac{\epsilon}{c}\left(1 - \frac{c}{r}\right)} \tag{4.18}$$

where ϵ = unit strain in outer fiber due to bending

r = original radius of curvature

ρ = deformed radius of curvature

c = distance from neutral axis to extreme outer fiber

Then, since the thrust, N, is readily calculated from strain measurements, the interface pressure may be determined from the equation

$$p_i = \frac{N}{\rho} \tag{4.19}$$

Equations 4.18 and 4.19 are useful if it is desired to know the actual loads on buried cylinders.

4.4.1.9 Criteria. A minimal set of criteria and specifications which is considered adequate for fully buried cylinders under the conditions stipulated in the above paragraphs is as follows:

Deflection	$\Delta y/D \leq 0.05$
Cylinder stress	$N < \sigma_{allow} A$
Buckling	$p_{i(cr)} < p_{i(allow)}$
Backpacking	$\sigma_{yL} = p_{i(allow)} < p_v$
Cover	$d_o \geq 3D/4$
Soil control	confined compression tests for M_s
Backfill	granular fill compacted to 90% AASHO T-99 or greater
Bedding.	shaped to cylinder curvature to depth of D/8

Obviously, other criteria and refinements of these will be necessary depending on the nature of the particular installation. In all installations, care should be exercised to avoid deleterious influences of clay layers beneath a buried structure. Likewise, the backpacking should be located so that it does not debilitate the buckling resistance of the structure.

Thus far, only circular cylinders have been considered. Other shapes might prove advantageous in some circumstances—square tubes have been tested,[4.25, 4.26] and there may be some advantage in using a section whose upper portion has a shape close to that of the stable arch form of Figure 4.1.

4.4.2 Design Method

The equations necessary for the design of horizontally buried cylinders are given in previous sections; it remains to delineate a step-by-step design procedure. A general methodology is adaptable to all buried structures irrespective of geometry, provided appropriate modifications for resistance are substituted for those of the cylinder. An example is presented to demonstrate the procedure.

It is required to design a horizontally buried cylinder with a 17-foot internal diameter and a length-to-diameter ratio of 4 to resist a 600-psi side-on overpressure from a 1 Mt surface burst. Bedding and backfill are to consist of a granular soil with a compacted density of 120 pcf, an angle of friction of 42 degrees, zero cohesion, and an at-rest coefficient of lateral earth pressure of 0.45.

1. Determine the loading characteristics, including the vertical stress at midcylinder height, p_e, and the vertical stress at the elevation of the crown, p_v. Assume a configuration as indicated in Figure 4.8, then

Dead load . . . . $p_e = \left(\frac{120}{144}\right)31 = 25.8$ psi

$p_v = \left(\frac{120}{144}\right)22 = 18.3$ psi

Live load . . . . 600 psi

Total load . . . . $p_{et} = 626$ psi

$p_{vt} = 618$ psi

From Figure 3.2, the angle of the wave front with the surface will be approximately

$$\beta = \sin^{-1} \frac{C}{U_{avg}} = \sin \frac{1,300}{15,360} = 4.85 \text{ deg}$$

based on the average shock speed between ground zero and the range corresponding to 600 psi.[4.27] Based on the velocity at the range corresponding to 600 psi

$$\beta = \sin^{-1} \frac{1,300}{6,100} = 12.3 \text{ deg}$$

Thus, for practical purposes, the loading may be considered as a plane-wave loading.

The durations[4.13] and rise-time of the loading (Equation 3.3) will be

$$\tau = 1.01 \text{ sec}$$

$$t_{50} = 0.040 \text{ sec}$$

$$t_r = \frac{z \cos\beta}{2\, C_d} = \frac{18 \cos 5}{2(1,300)} = 6.9 \text{ msec}$$

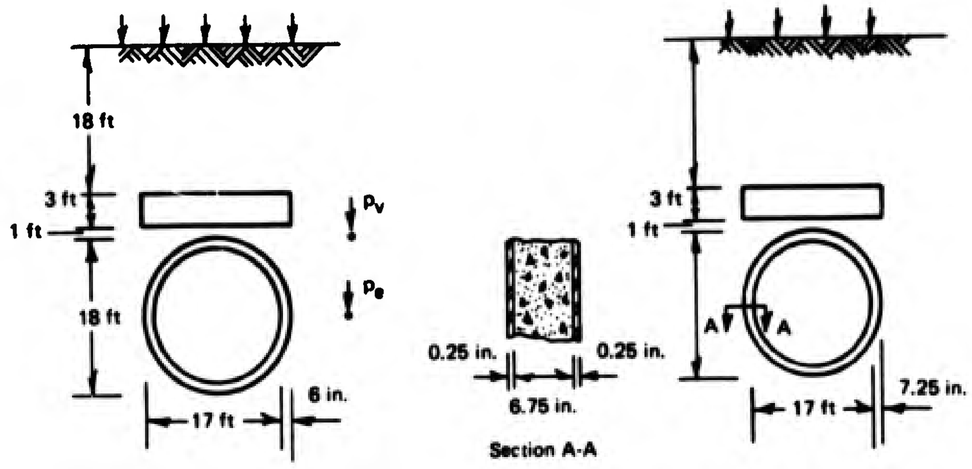

(a) Approximate configuration.

(b) Design dimensions.

Figure 4.8. Example of a buried cylinder design.

2. Determine the soil properties corresponding to midheight of the cylinder. Find M_s from confined compression data using fluid pressure for the loading or, lacking such data, use[4.14]

$$M_s = 1{,}000\,p^{0.8} = 1{,}000(626^{0.8}) = 17{,}300 \text{ psi}$$

and

$$\nu_s = \frac{K_o}{1 + K_o} = \frac{0.45}{1 + 0.45} = 0.31$$

3. Estimate the arching and calculate the thrust. Because backpacking is being used, the net load to the cylinder will be less than 20% of the peak surface pressure; thus,

$$A \simeq 0.8$$

In those cases where no backpacking is employed, arching may be estimated from the relations[4.13]

$$A = 0.2 - 0.2\left(1 - \frac{d_o}{D}\right)^2 \qquad \text{for } \frac{d_o}{D} < 1.0$$

$$A = 0.2 \qquad \text{for } \frac{d_o}{D} > 1.0$$

By Equation 3.2,

$$L_w = 3.7(1^{1/3})(1{,}300)(600^{-1/2}) = 196.2 \text{ ft}$$

$$\alpha_z = \frac{1}{1 + \frac{22}{196.2}} = 0.90$$

and by Equation 4.12 for a **DLF** = 1,

$$N = 0.9[1(1 - 0.80)](600)(9)(12) = 11{,}670 \text{ lb/in.}$$

4. Determine an approximate section stiffness by assuming

$$M = 0.005\, p_i\, D^2 = 0.005(12.0)(216^2) = 27{,}000 \text{ in.-lb/in.}$$

Use a composite section consisting of liner plates and a concrete core. Then using the approximate relation for combined stress,

$$\sigma_{allow} = \frac{N}{A} + \text{DLF}\,\frac{M}{S}$$

With the allowable stress expressed as the yield stress divided by a factor of safety

$$\frac{\sigma_y}{\text{F.S.}} = \frac{N}{\frac{b}{n} + t_p} + \frac{\text{DLF}\, M}{t_p\, b} \qquad (4.20)$$

where b = distance from center cf gravity to center of gravity of the liner plates

t_p = plate thickness

n = ratio of modulus of steel to modulus of the concrete used

For σ_y = 50,000 psi, **F.S.** = 1, **DLF** = 2, **n** = 8, and t_p/b = 0.04 in Equation 4.20,

$$\frac{50{,}000}{1} = \frac{11{,}670}{\frac{b}{8} + 0.04\,b} + \frac{2(27{,}000)}{(0.04\,b)(b)}$$

Therefore, **b** = 6.0 inches and t_p = 0.25-inch plate.

Steps 5 through 7 are not necessary for designs where sufficient backpacking is used to achieve maximum arching. They are included for use where maximum arching is not a goal and the calculated arching needs checking against the initially assumed value.

5. The corresponding section stiffness in terms of the concrete is

$$EI = \frac{30 \times 10^6}{8}\left[(6.0 - 0.25)^3 \frac{1}{12} + 2(0.25)\left(\frac{6.0}{2}\right)^2\right]$$

$$= 76.3 \times 10^6 \text{ lb-in.}$$

6. Determine $M_s/(EI/D^3)$ and find the corresponding value of $(\Delta y/D)/(p_v/M_s)$ from Figure 4.3

$$\frac{M_s}{EI/D^3} = \frac{17{,}300}{76.3 \times 10^6/(17.5 \times 12)^3} = 2{,}100$$

$$\frac{\Delta y/D}{p_v/M_s} = 1.98$$

Also determine the moment from the experiment curve, Figure 4.6, and iterate from step 4 as necessary until the estimated and calculated moments agree.

7. Calculate the depth to the plane of equal settlement from the top of the backpacking.

$$\frac{d_e}{D} = \frac{1}{2K_o} = \frac{1}{2(0.45)} = 1.11$$

$$d_e = 1.11 \times 17.5 = 19.4 \text{ ft}$$

Determine the arching coefficient from Equation 4.4a with $d_o = d_e$

$$\Omega = \frac{2(19.4)}{17.5}(1.98 - 1) = 2.17$$

and the arching from Figure 3.8; the arching without backpacking is found to be 30%. With backpacking, ϵ_c/ϵ_s and A depend on the thickness and yield strength of the backpacking.

8. Calculate the thickness of backpacking for $A = 0.8$ from Equation 3.39 using $\epsilon_s = p_e/M_s$ and a F.S. = 2

$$t_{L(0.87)} = 2\,\frac{25.8/17{,}300}{0.05}\left(\frac{4.0}{3.06} + 1\right)21.57 = 2.96 \text{ ft}$$

$$t_{L(0.8)} \approx 2.96(0.8/0.87) = 2.72 \text{ ft}$$

where $A_{gh} = 2\,\dfrac{d_o}{D^2}\left(1 + \dfrac{D}{L}\right)H = 2\,\dfrac{17.57}{17.57^2}\,(1 + 0.25)\,21.57 = 3.06$

9. The required yield stress of the backpacking is

$$\sigma_{yL} = (1 - \tan 42)\,618.3 = 58 \text{ psi}$$

10. Determine the conformance with design criteria and the factor of safety for the various possible modes of collapse:

a. Deflection—Where no backpacking is used, the peak vertical diametral contraction is readily calculated from step 8. In those circumstances, the effective vertical and horizontal peak stresses on the cylinder are 438 psi and 278 psi, respectively. With backpacking the corresponding peak stresses are 125 psi and 278 psi; thus, there will be a vertical diametral elongation of approximately

$$\frac{\Delta y/D}{p_v/M_s} \approx -1.98\left(\frac{278 - 125}{438 - 278}\right) = -1.90$$

or

$$\Delta y/D \approx -1.90\,\frac{618}{17{,}300} = -0.0679$$

$$\Delta y = -0.0679(17.5)(12) = -14.25 \text{ in.}$$

This deflection is a little larger than the 5% permitted by the criterion, but it would be permissible for transient loading. The factor of safety against caving would be

$$\text{F.S.}\Big|_{\text{caving}} = \frac{0.20}{\Delta y/D} = 2.95$$

b. Wall crushing—Refer to the sketch and employ Coulomb's equation:

$$F \approx (c + p_u K_o \tan\phi_o) d_e$$

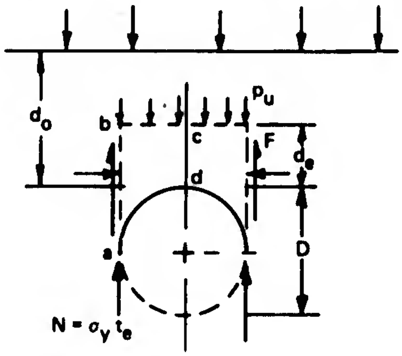

From vertical equilibrium of block abcd, neglecting the weight of the block,

$$\frac{p_u D}{2} = (c + p_u K_o \tan\phi_o) d_e + \sigma_y t_e$$

or

$$p_u = \frac{c d_e + \sigma_y t_e}{\frac{D}{2} - d_e K_o \tan\phi_o}$$

The allowable load for incipient yielding is

$$p_{y(allow)} = \frac{2 \sigma_y t_e}{(1 - A) D}$$

Thus,

$$F.S.\Big|_{wall} = \frac{(1 - A)(c d_e + \sigma_y t_e)}{\sigma_y t_e \left(1 - \frac{2 d_e}{D} K_o \tan\phi_o\right)} \qquad A < 1.0$$

For the design cylinder in granular soil, $c = 0$, $d_e = D/2$ K_o, $\tan\phi_o \approx A_o$

$$F.S.\Big|_{wall} = \frac{1 - A}{1 - A_o} = \frac{1 - 0.80}{1 - 0.87} = 1.5$$

c. Seam or joint strength—This should not be a problem if the seams are properly welded.

d. Transitional buckling—$\tilde{B} = 0.75$, $\tilde{C} = 0.675$

$$\frac{\tilde{B}\tilde{C}}{96}\left(\frac{E_s}{E\,I/D^3}\right) = \frac{(0.75)(0.675)}{96}\,1{,}575 = 8.3$$

$$\frac{R}{t_e} = \frac{D/2}{\sqrt[3]{12\,I}} = \frac{(17.5)(12)/2}{\sqrt[3]{12(2.54)}} = 34.9$$

$$\frac{L}{R} = 8$$

Then, from Figure 4.7

$$\frac{1}{12}\left(\frac{p_{cr}\,R^3}{E\,I}\right) = 1.9$$

and

$$p_{cr} = 1.9(12)\,\frac{76.3 \times 10^6}{8.75^3} = 1{,}503 \text{ psi}$$

Without backpacking,

$$\text{F.S.}\Big|_{\text{buckle}} = \frac{p_{cr}}{p_o(1 - A)} = \frac{1{,}503}{626(1 - 0.2)} = 3.0$$

On comparing the factors of safety, it is clear that a better design would result if a steel with an 80,000-psi or higher yield strength were used and if the backpacking thickness were reduced about 20%. This would result in a decrease in the vertical deflection and in a higher factor of safety against wall crushing.

The suggested modification to the above design would provide a factor of safety of slightly over 1 against failure and a factor of safety of about 3 against collapse. Completing the design involves consideration of the end caps, of penetrations, of longitudinal bending, and of durability.[4.1] Note that if the usual ellipsoidal or spherical end caps are employed, the effective cylinder stiffness will be greater near the ends than at midspan. Thus, there will be a tendency to attract load near the ends unless backpacking is used. With proper consideration of the potential load concentration and load distribution, proportioning of end caps and penetrations proceeds as in normal pressure vessel design.[4.28]

4.4.3 Finite Element Analysis

The following paragraphs discuss and exemplify the use of the finite element method in the analysis of soil–structure systems. Only the pertinent characteristics, advantages, and limitations of the stiffness method for this application are discussed as the method has become well known and there are a number of books on the subject.[4.29, 4.30, 4.31]

For those who are not familiar with the stiffness method, it involves subdivision of the free field and the inclusion into elements whose stiffness matrices are known. The element stiffness matrices are then combined into a so-called global or system matrix which is used in the determination of displacements and stresses corresponding to given material properties, boundary conditions, and loading. Virtually all of the process involved, except for the preparation of a portion of the input, can be carried out with any one of a number of computer programs and installations depending upon the characteristics of the problem.

Presently (1971) the following classes of codes exist:

1. Two-dimensional
   a. Linear—static and dynamic
   b. Linear with slip and crack subroutines—static and dynamic
   c. Nonlinear—static and dynamic
2. Three-dimensional (linear)—static and dynamic

The fact that such codes exist does not mean that they are adequate in all respects. Work is still in progress, for example, to provide better constitutive relations for the nonlinear codes. Three-dimensional nonlinear programs are under development.

In general, good solutions can be achieved economically for systems that can be represented as plain strain, or axisymmetric (two-dimensional) models.[4.32] In a limited spatial region, solutions can be obtained for three-dimensional models;[4.33] however, three-dimensional solutions require too much computer time to be economically feasible except for special problems.

Finite element programs developed by Wilson and Farhoomand[4.32-4.34] have been modified[4.35] and employed by Takahashi of NCEL to study the behavior of buried cylinders and the effectiveness of backpacking. Static and dynamic runs were obtained for the five configurations shown in Figure 4.9. Typical mesh (including element and nodal point numbers), boundary conditions, loading, and material properties for cylinders with one diameter of cover over the crown are given in Figures 4.10 and 4.11.

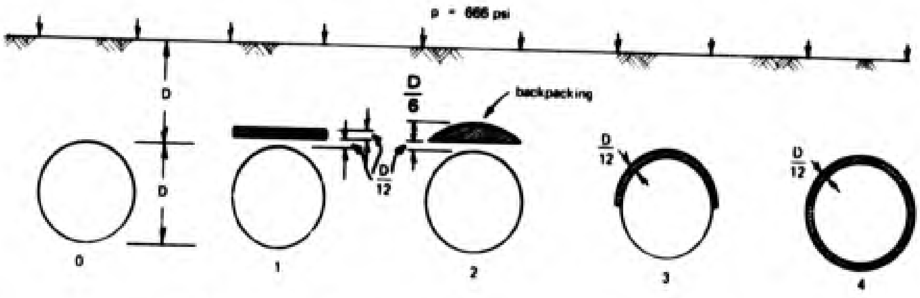

Figure 4.9. Backpacking configurations for buried cylinders.

As is inferred by the list of material properties on Figure 4.11, variations in material properties throughout the system are easily handled. Representative displacement and stress contours from the output data are shown in Figures 4.12 through 4.16 for the selected cases. These plots are for uniformly distributed static loading over the surface. They show the remarkable difference in stress distribution attributable to inclusion stiffness.

Radial and shear stress distribution on the extrados of the cylinder without backpacking are shown in Figure 4.17. Solutions with and without interface slippage are plotted for comparison. Comparative output data for the cylinder without backpacking and for the case of uniform all-around backpacking are listed in Table 4.2. In this case the stresses in the cylinder are reduced by a factor of 3 by the use of backpacking. Much greater reductions are possible. (All-around backpacking for blast load conditions may not be satisfactory for one of several reasons, including the tendency of the cylinder to vibrate within the backpacking.)

As previously indicated, constitutive properties are not too important in static solutions, providing the effect of stiffness on loading is correctly modeled. By contrast, constitutive properties, particularly the unloading shear modulus, are exceedingly important in blast loading as most of the response time at a given point occurs during unloading.

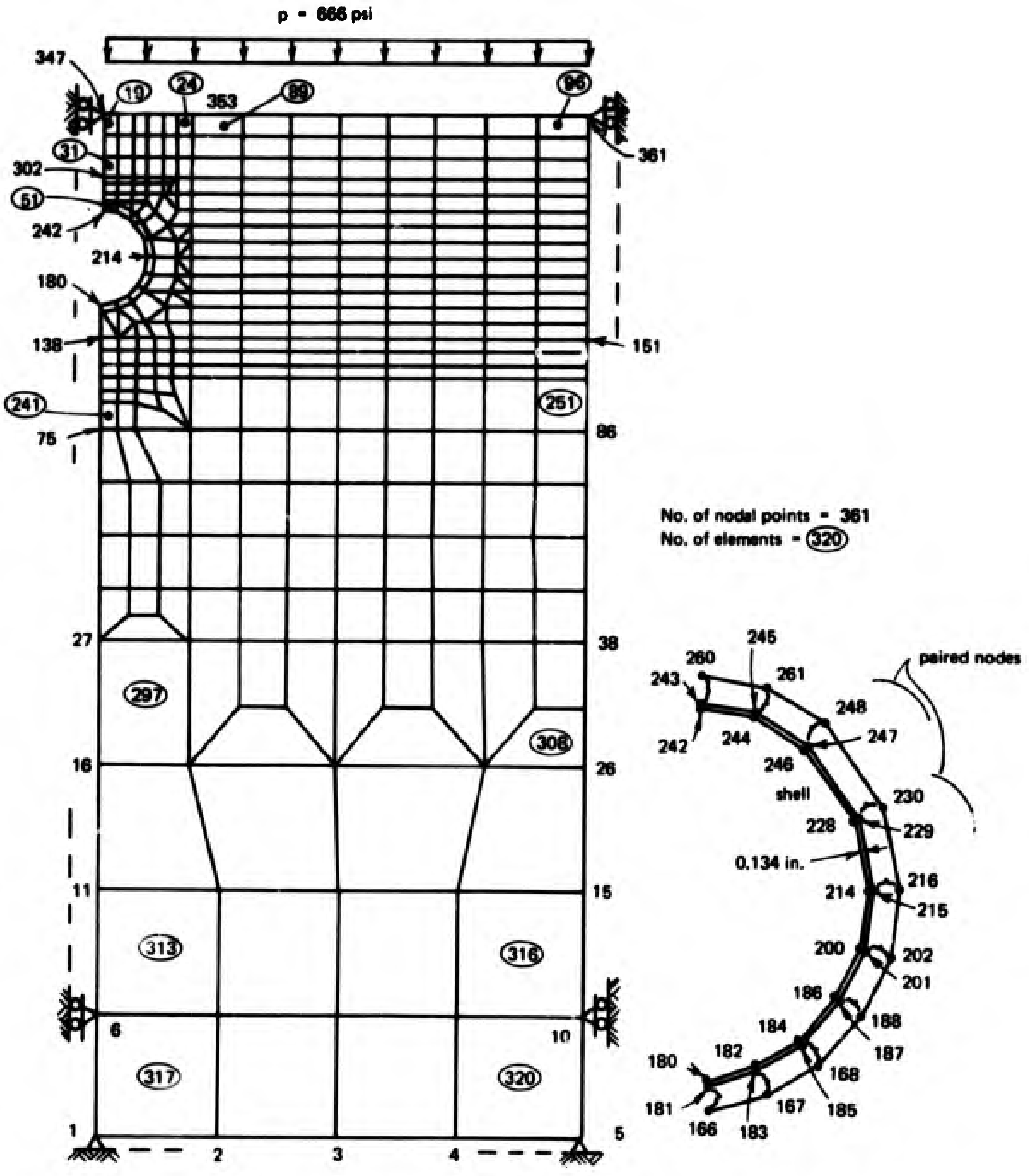

(a) Complete mesh.

(b) Paired nodal points at outer surface of cylinder for all schemes.

Figure 4.10. Finite element mesh for buried cylinder.

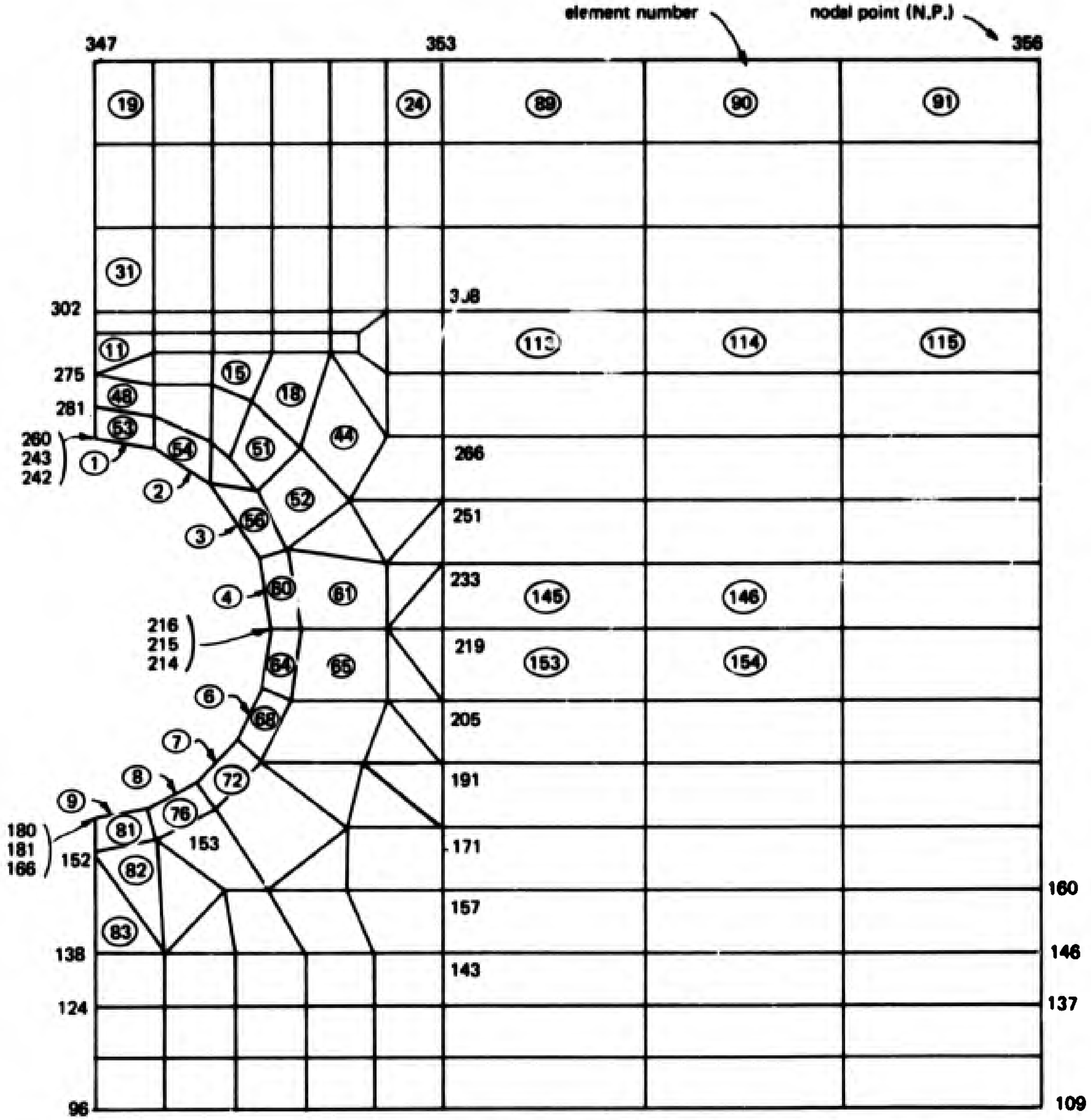

Material Properties

No.	Modulus of Elasticity (psi)	Poisson's Ratio	Material
1	35,160,000	0.3	cylinder
2	690	0.0	backpacking
3 & 4[a]	30,800	0.355	backfill
5[b]	2,700	0.333	topsoil
6[c]	12,140	0.27	middle soil layer
7[d]	12,800	0.333	bottom soil layer

[a] Bounded by N.P. 138, 143, 353, 347.
[b] Bounded by N.P. 143, 151, 361, 353.
[c] Bounded by N.P. 11, 15, 151, 138.
[d] Bounded by N.P. 1, 5, 15, 11.

Figure 4.11. Enlarged finite element mesh (configurations 0, 3, and 4).

Table 4.2. Deformations and Stresses for Buried Cylinders

Parameter	Configuration 1 No Interface Slip or Backpacking			Configuration 1 Interface Slip and No Backpacking			Configuration 4 Interface Slip and Circular Backpacking		
	α^a	β^b	γ^c	α	β	γ	α	β	γ
Diametral Deformation, in.									
Vertical	-0.4138	+0.0165	-0.4303	-0.5057	+0.0164	-0.4893	-0.0361	+0.0177	-0.0184
Horizontal	+0.1336	+0.0092	+0.1428	+0.1624	+0.0093	+0.1717	+0.0159	+0.0095	+0.0254
Maximum Relative Slippage									
Nodal point (229-230)	NA[d]	NA	NA	0.1027	NA	NA	0.3496	NA	NA
Stress in Shell, psi									
At crown, f_{min}	-59,378	+18,817	-40,561	-78,383	+18,794	-59,589	-1,717	+19,755	+18,038
At springline, f_{min}	-99,431	+18,738	-80,693	-82,351	+18,768	-63,583	-2,042	+19,739	-17,697
At springline, f_{min}	-10',060	+18,788	-82,272	-82,357	+18,818	-63,539	-1,983	+19,781	-17,798
At invert, f_{min}	-58,372	+18,868	-39,504	-78,999	+18,817	-60,182	-1,743	+19,779	-18,036
Stress in Backpacking, psi									
Above crown, f_z	NA	NA	NA	NA	NA	NA	-22[e]	-1.55	-24
At springline, f_r	NA	NA	NA	NA	NA	NA	-4	-1.69	-6
At springline, f_z	NA	NA	NA	NA	NA	NA	-3	+0.14	-3
At invert, f_z	NA	NA	NA	NA	NA	NA	-22	+0.14	-22
Stress in Soil, psi									
Above crown, f_z	-657	-5.91	-663	-681	-5.93	-687	-91[e]	-1.13	-92
Above springline, f_r	-507	-6.78	-514	-534	-6.77	-541	-278[e]	-0.74	-279
Above springline, f_z	-520	+9.70	-510	-783	+9.17	-773	-1,427	+1.79	-1,425
Below springline, f_r	-569	-5.61	-575	-544	-5.83	-550	-251[e]	-0.78	-252
Below springline, f_z	-524	+10.69	-513	-825	+10.03	-815	-1,446	+1.83	-1,444
Below invert, f_z	-623	-6.79	-630	-683	-6.91	-690	-288	-0.23	-288

[a] α —Surface pressure only, 666 psi.
[b] β —Internal pressure only, 150 psi.
[c] γ —Surface and internal pressure combined.
[d] NA—not applicable.
[e] Large reduction due to presence of backpacking.

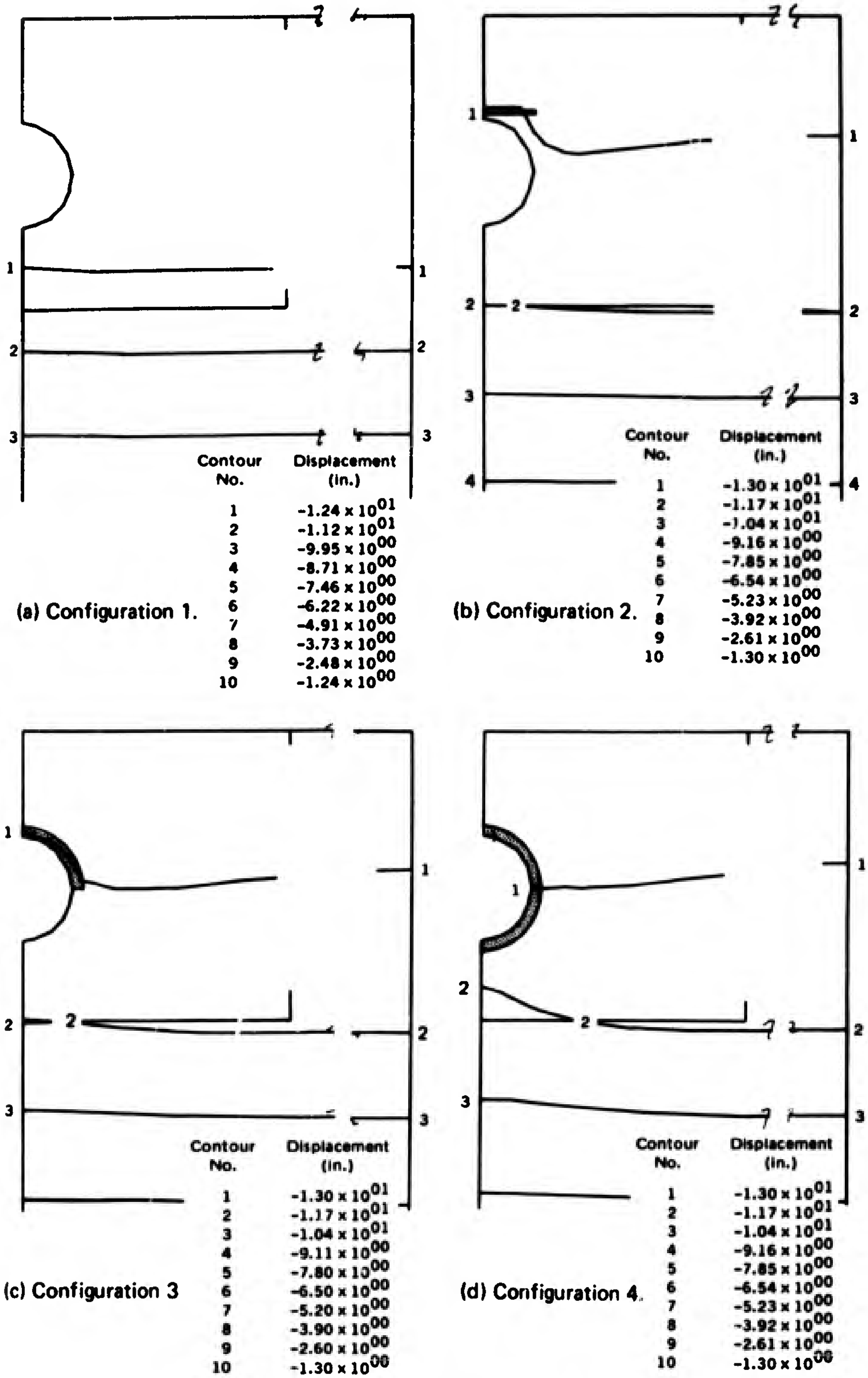

(a) Configuration 1.

Contour No.	Displacement (in.)
1	-1.24×10^{01}
2	-1.12×10^{01}
3	-9.95×10^{00}
4	-8.71×10^{00}
5	-7.46×10^{00}
6	-6.22×10^{00}
7	-4.91×10^{00}
8	-3.73×10^{00}
9	-2.48×10^{00}
10	-1.24×10^{00}

(b) Configuration 2.

Contour No.	Displacement (in.)
1	-1.30×10^{01}
2	-1.17×10^{01}
3	-1.04×10^{01}
4	-9.16×10^{00}
5	-7.85×10^{00}
6	-6.54×10^{00}
7	-5.23×10^{00}
8	-3.92×10^{00}
9	-2.61×10^{00}
10	-1.30×10^{00}

(c) Configuration 3

Contour No.	Displacement (in.)
1	-1.30×10^{01}
2	-1.17×10^{01}
3	-1.04×10^{01}
4	-9.11×10^{00}
5	-7.80×10^{00}
6	-6.50×10^{00}
7	-5.20×10^{00}
8	-3.90×10^{00}
9	-2.60×10^{00}
10	-1.30×10^{00}

(d) Configuration 4.

Contour No.	Displacement (in.)
1	-1.30×10^{01}
2	-1.17×10^{01}
3	-1.04×10^{01}
4	-9.16×10^{00}
5	-7.85×10^{00}
6	-6.54×10^{00}
7	-5.23×10^{00}
8	-3.92×10^{00}
9	-2.61×10^{00}
10	-1.30×10^{00}

Figure 4.12. Static vertical displacement contours.

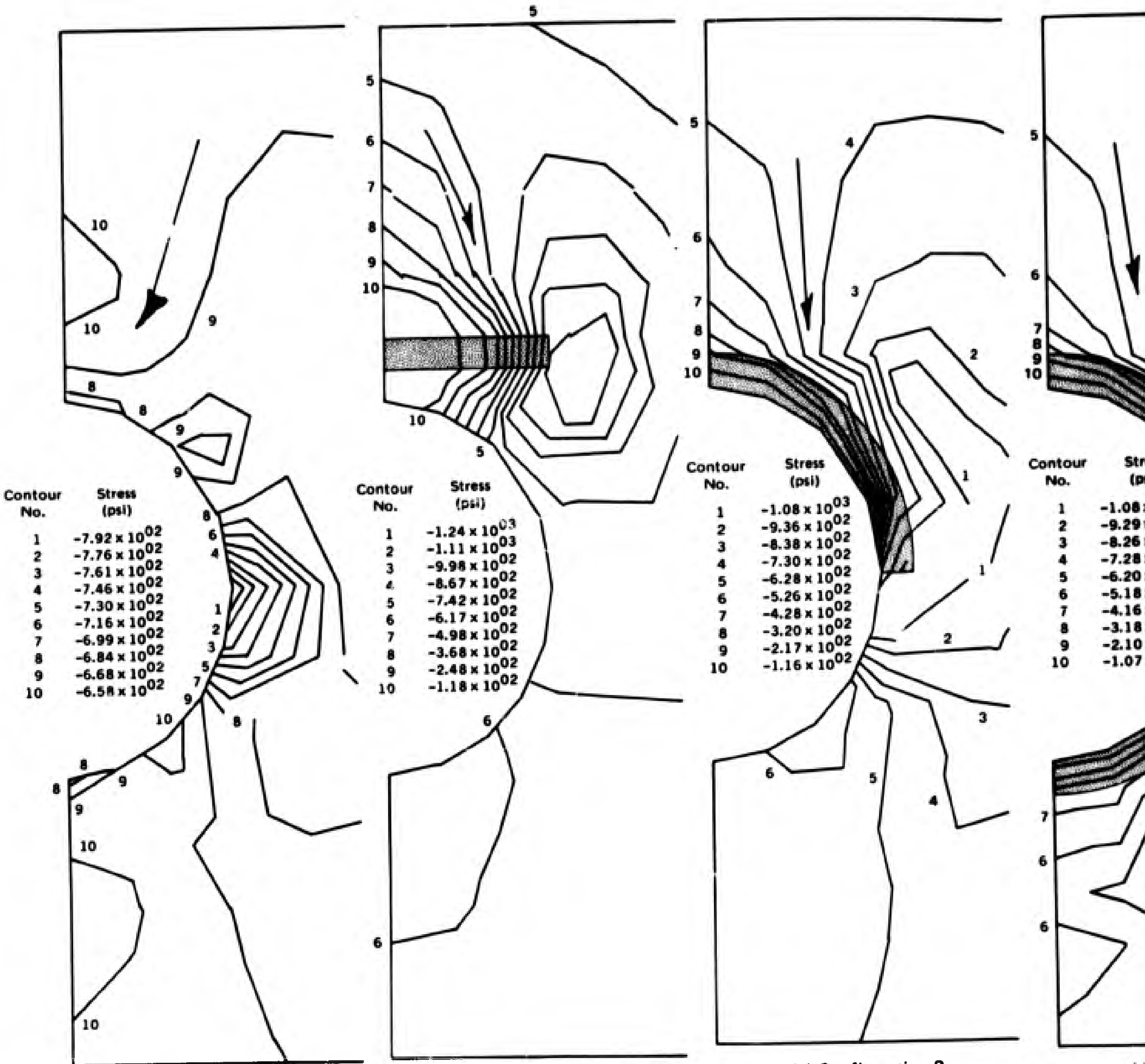

(a) Configuration 1.

(b) Configuration 2.

(c) Configuration 3.

Figure 4.13. Comparison of static minimum stress patterns.

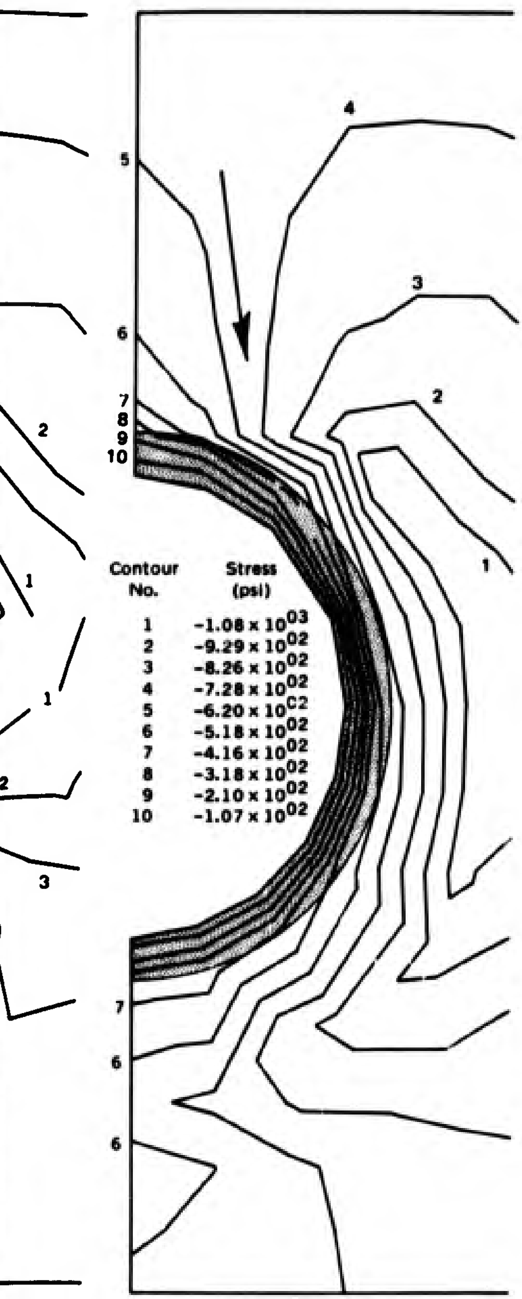

(d) Configuration 4.

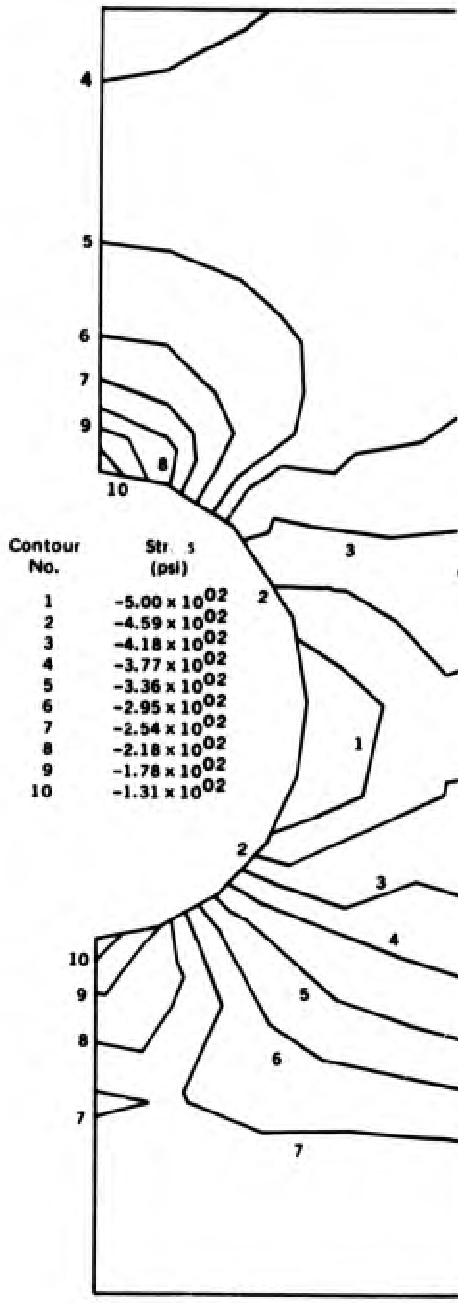

(a) Configuration 1.

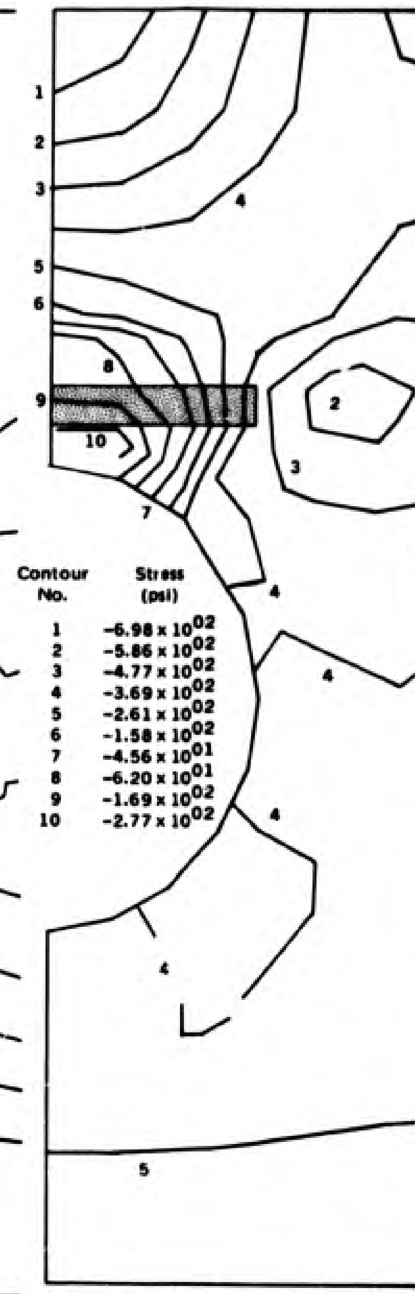

(b) Configuration 2.

Figure 4.14. Comparison of

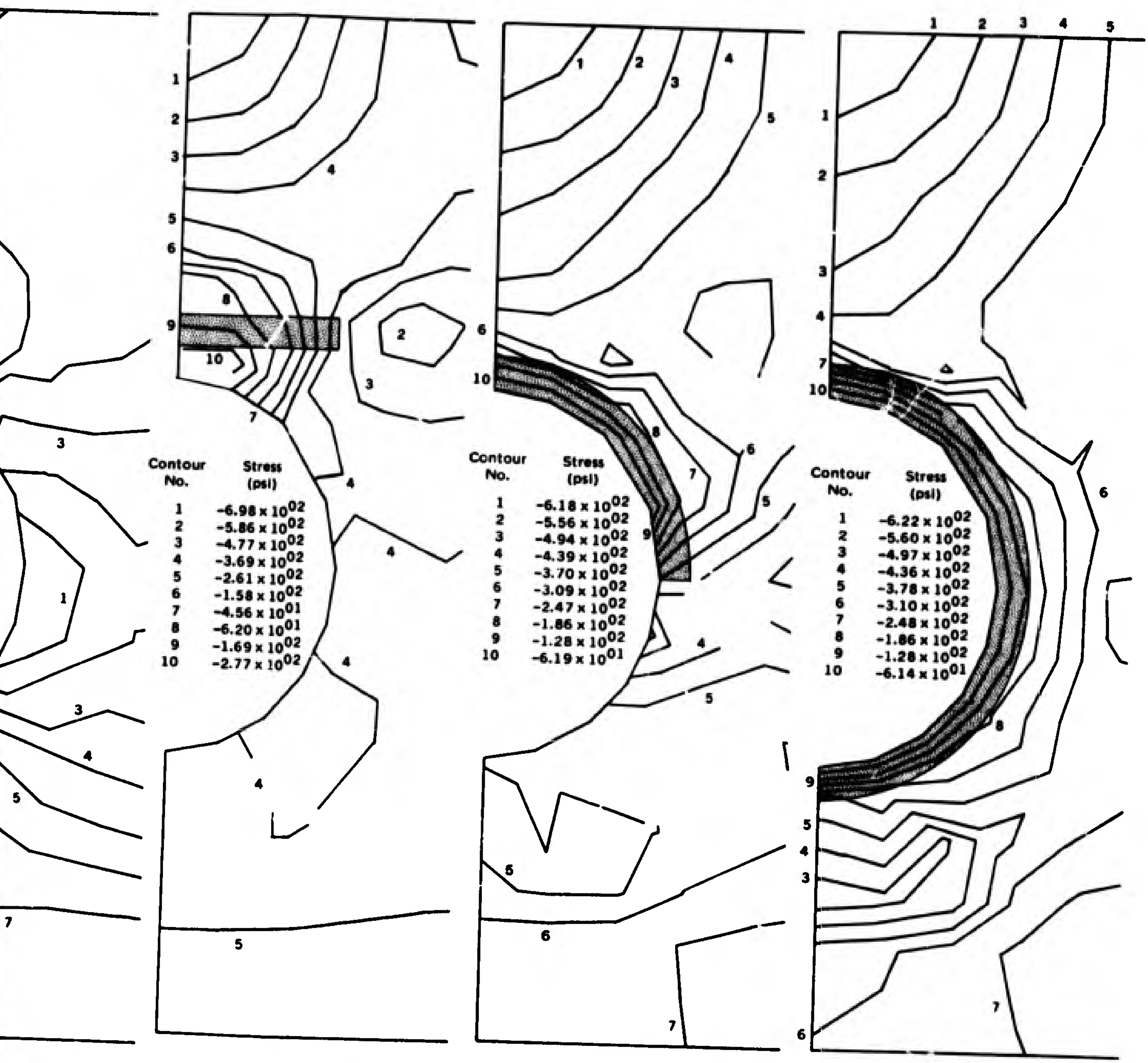

ation 1.

(b) Configuration 2.

(c) Configuration 3.

(d) Configuration 4.

Figure 4.14. Comparison of static horizontal stress patterns.

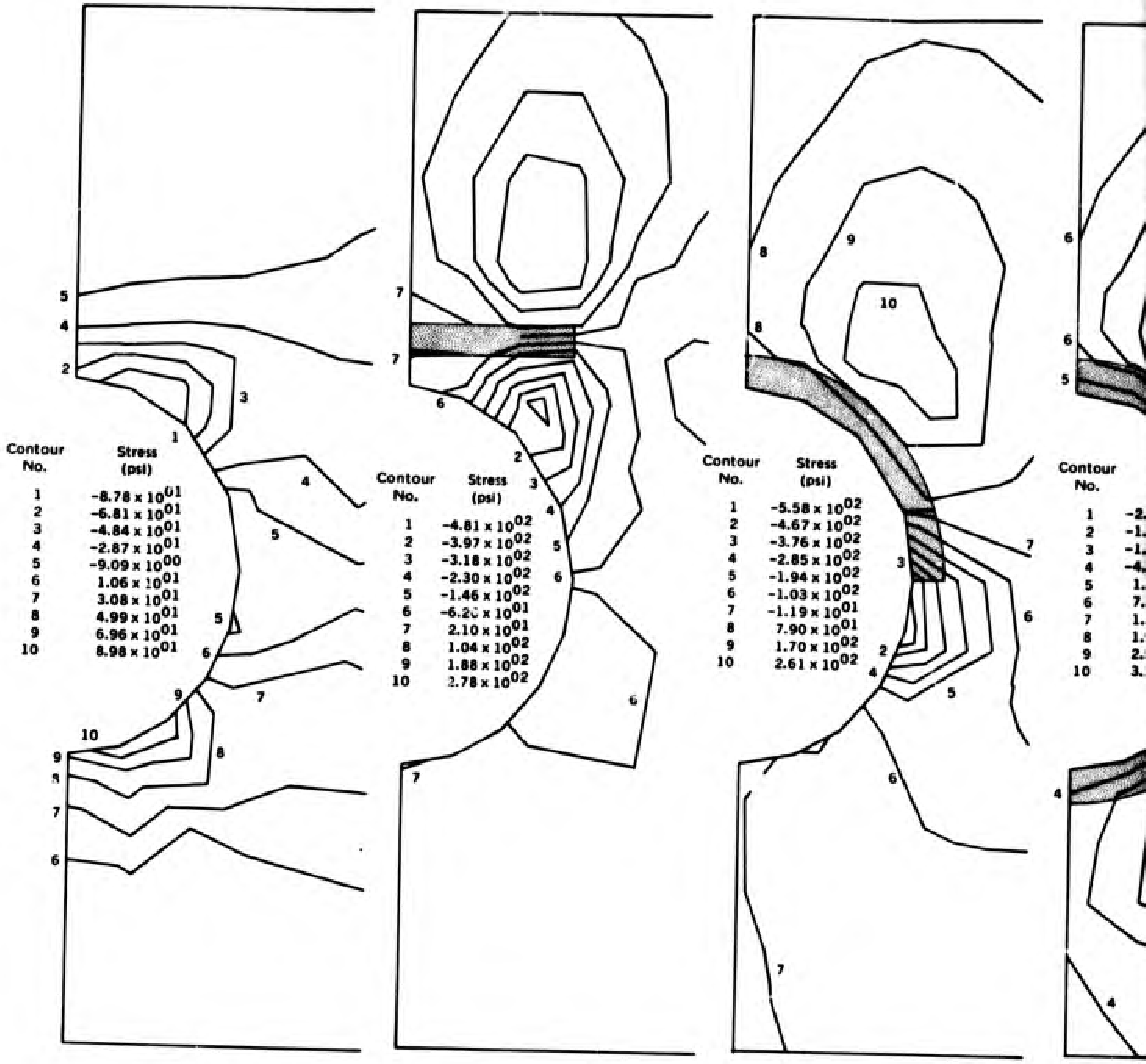

(a) Configuration 1.

(b) Configuration 2.

(c) Configuration 3.

Figure 4.15. Comparison of static shear stress patterns.

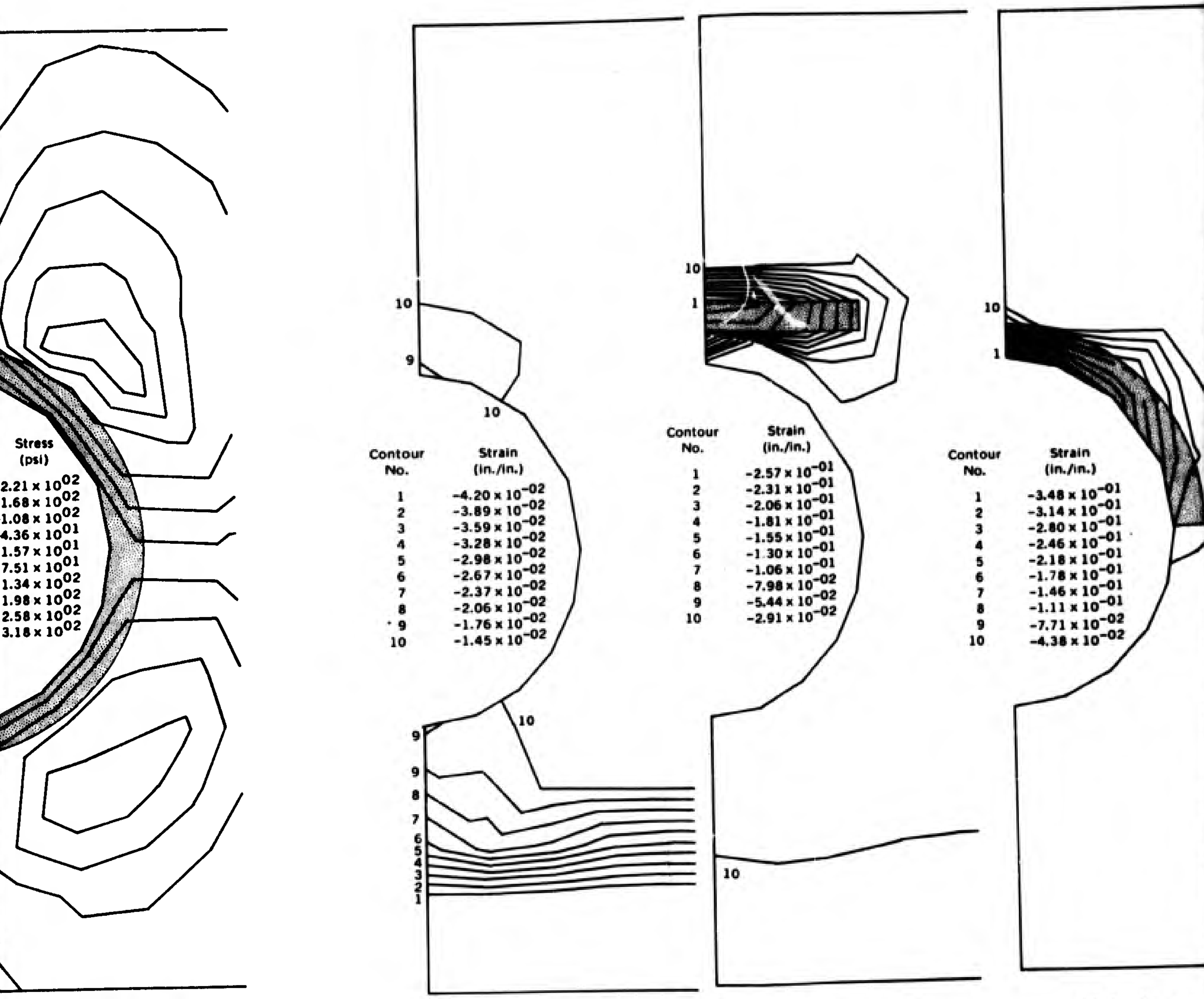

(d) Configuration 4.

(a) Configuration 1

(b) Condiguration 2.

(c) Configuratio

Figure 4.16. Comparison of static minimum strain pat

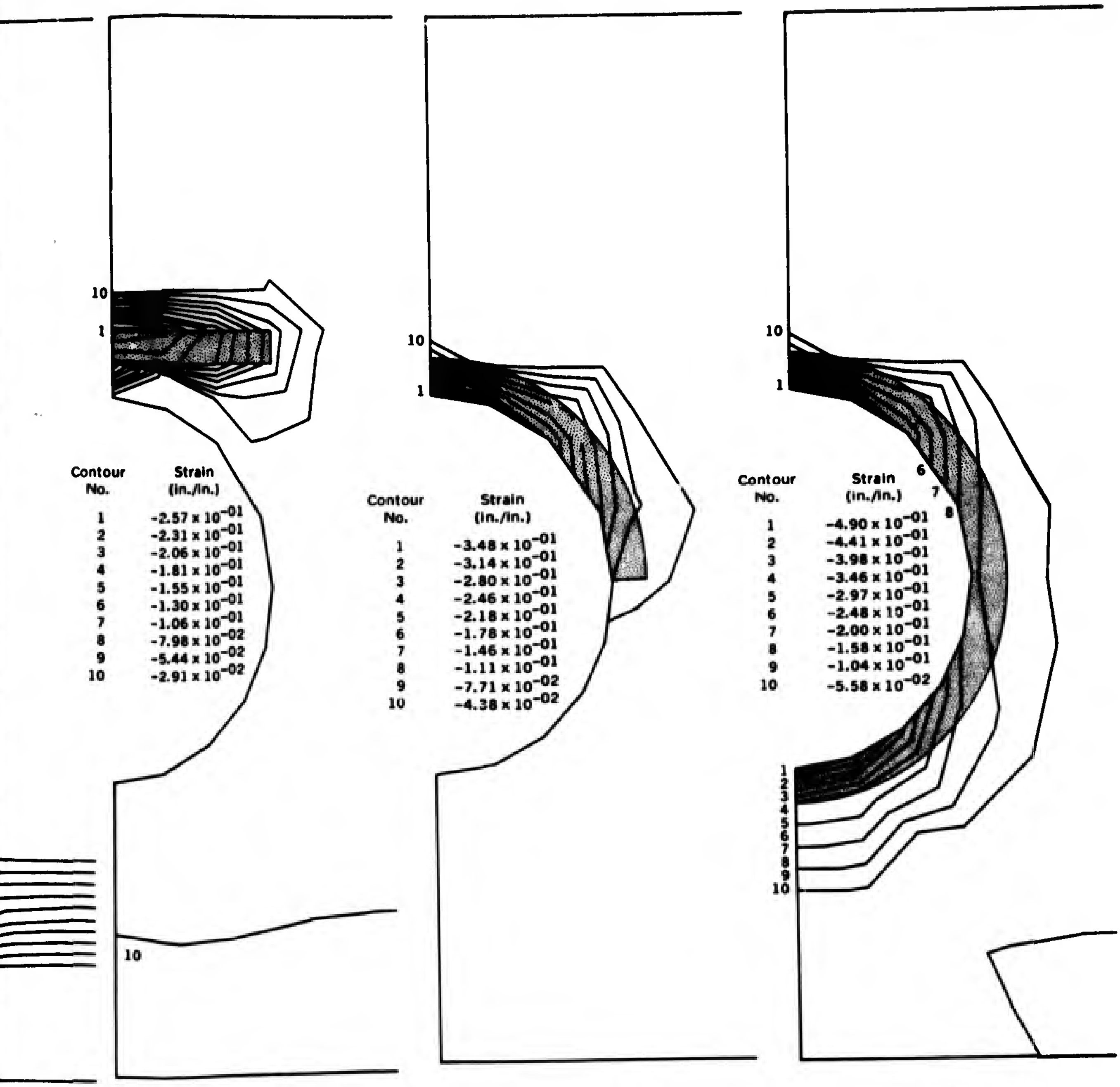

n 1. (b) Condiguration 2. (c) Configuration 3. (d) Configuration 4.

Figure 4.16. Comparison of static minimum strain patterns.

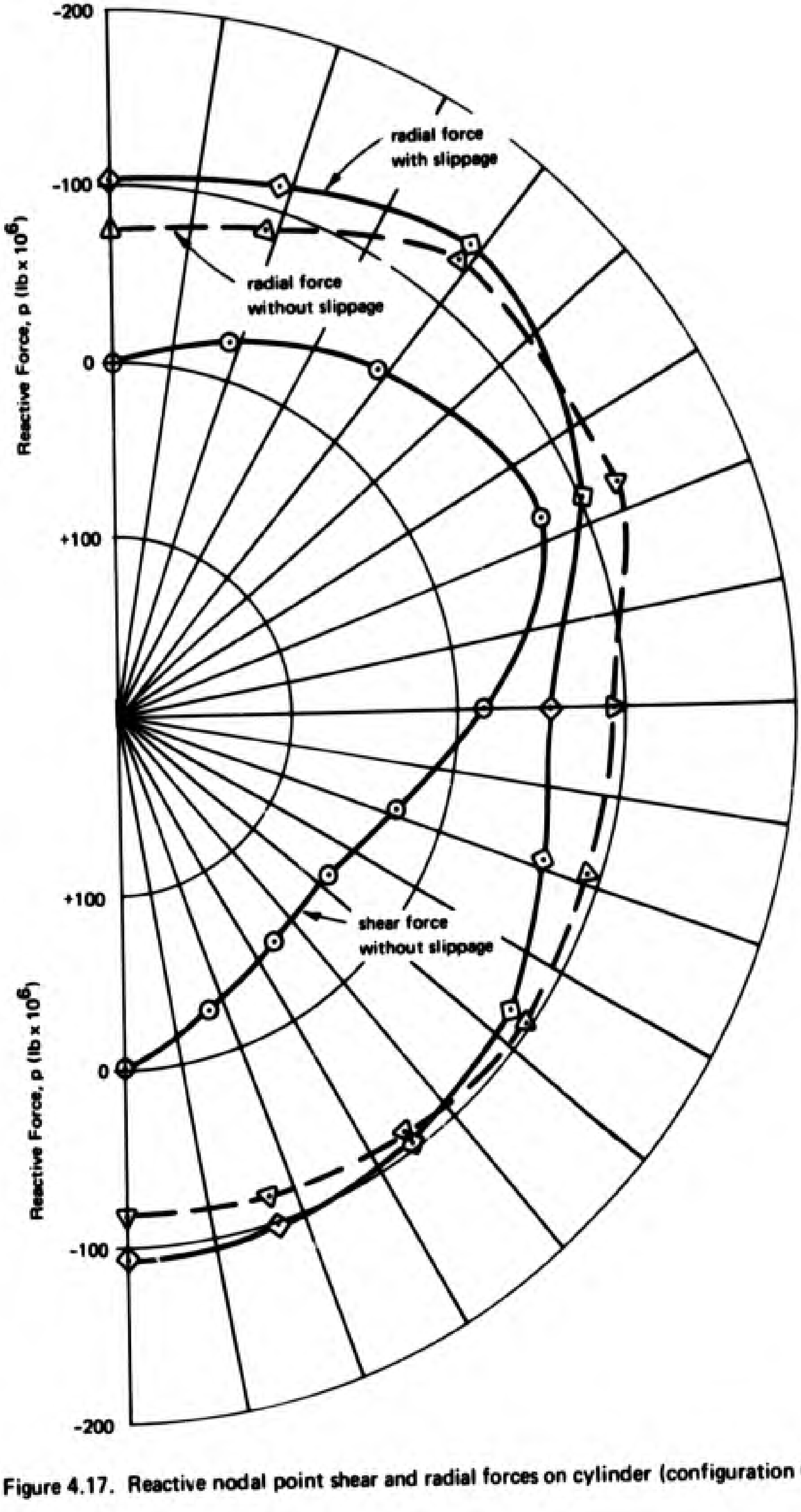

Figure 4.17. Reactive nodal point shear and radial forces on cylinder (configuration 0).

Computer runs have been made for identical geometries to investigate the influence of soil nonlinearity and backpacking on dynamic response. Comparative results of the stresses at the springline are indicated in Figure 4.18. With nonlinear material properties, the peak stress is about one-half of that for the system with linearly elastic material properties. For a backpacking thickness of one-twelfth of the diameter, placed as in configuration 1 of Figure 4.9, the peak stress was reduced by another factor of 2 or more. Curiously, the wave shapes and times to peak deflection are about the same for the three cases of Figure 4.17. A similar result was evident at the crown.

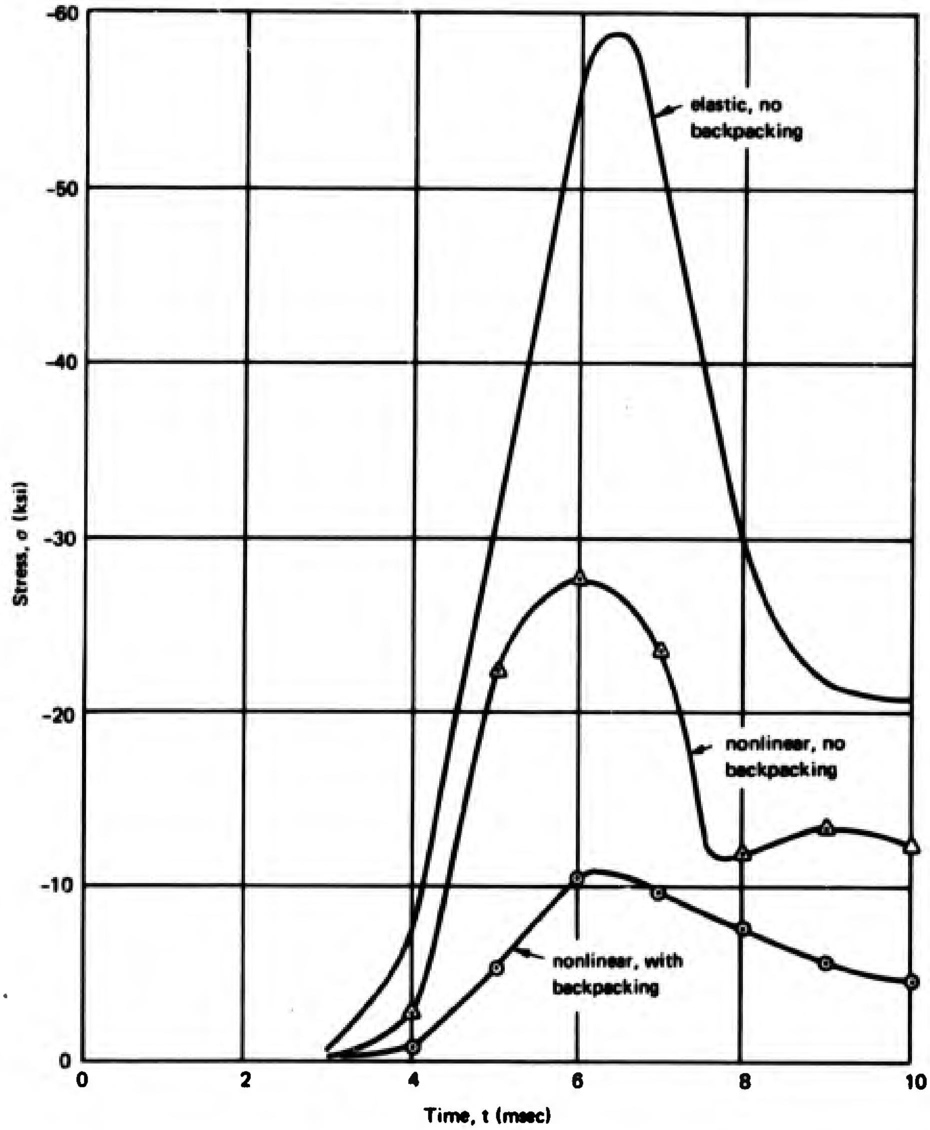

Figure 4.18. Minimum stress at springline of buried cylinder (configuration 4).

The manner in which displacement contours concentrate in the backpacking is indicated in Figure 4.19. The figure shows a contour plot of vertical displacements at a time of 6 msec after application of the plane-wave loading at the surface. Series of such plots have been made into movies showing the amplitude–time behavior of the system.

As stated previously, static and dynamic linear three-dimensional solutions are also achievable with the finite element method. Figures 4.20 through 4.25 show a system model and output data for a culvert loaded by the overburden. The culvert is a 60-inch-diameter, 2-2/3-in. x 1-in. corrugation of 10-gage plate. In an emergency, culverts may be employed as shelters, because they usually have a factor of 6 or more load capacity in excess of their design load, and because the required radiation protection can be provided with minimal modification. The culvert configuration was chosen as the first three-dimensional soil–structure system to be calculated at NCEL because of its relative simplicity. Further, the configuration may be considered as an entrance tunnel to a mounded protective facility.

As indicated in Figure 4.20, only one-quarter of the system was analyzed because of symmetry. Different moduli were used for soil layers further from the top because the soil modulus increases with applied stress (overburden).

Fifteen hundred and sixty-eight 8-nodal hexahedron solid elements were used to represent the soil, and 84 shell elements were employed to model the culvert. The culvert was represented by a plate of equivalent thickness (0.387 inch) to properly model the stiffness of its transverse section. No correction was made for the corrugations; thus, the longitudinal stresses in the cylinder would be expected to be greater than those where circumferential corrugated plate is used. Stresses in all elements and deflections at all nodal points were obtained as output data; however, space limitations permit visual display of only a small portion of this data.

Vertical soil stress contours in the Y-Z plane and in the X-Y plane are shown in Figures 4.21 and 4.22, respectively. As may be observed, the interface stress at the crown is about 15 psi as compared to 10 psi predicted with the arching relation in the example design. At the invert, the normal stress is about 16 psi. The horizontal stress at the springline is about 15 psi. It is interesting to note from Figure 4.22 that the vertical soil stress is greater about 1 to 2 feet above the culvert than it is at the crown.

Horizontal stress contours in the Y-Z plane are shown in Figure 4.23. Perhaps the most significant aspect of the horizontal stress is the rapid dispersal of the stress concentration adjacent to the springline.

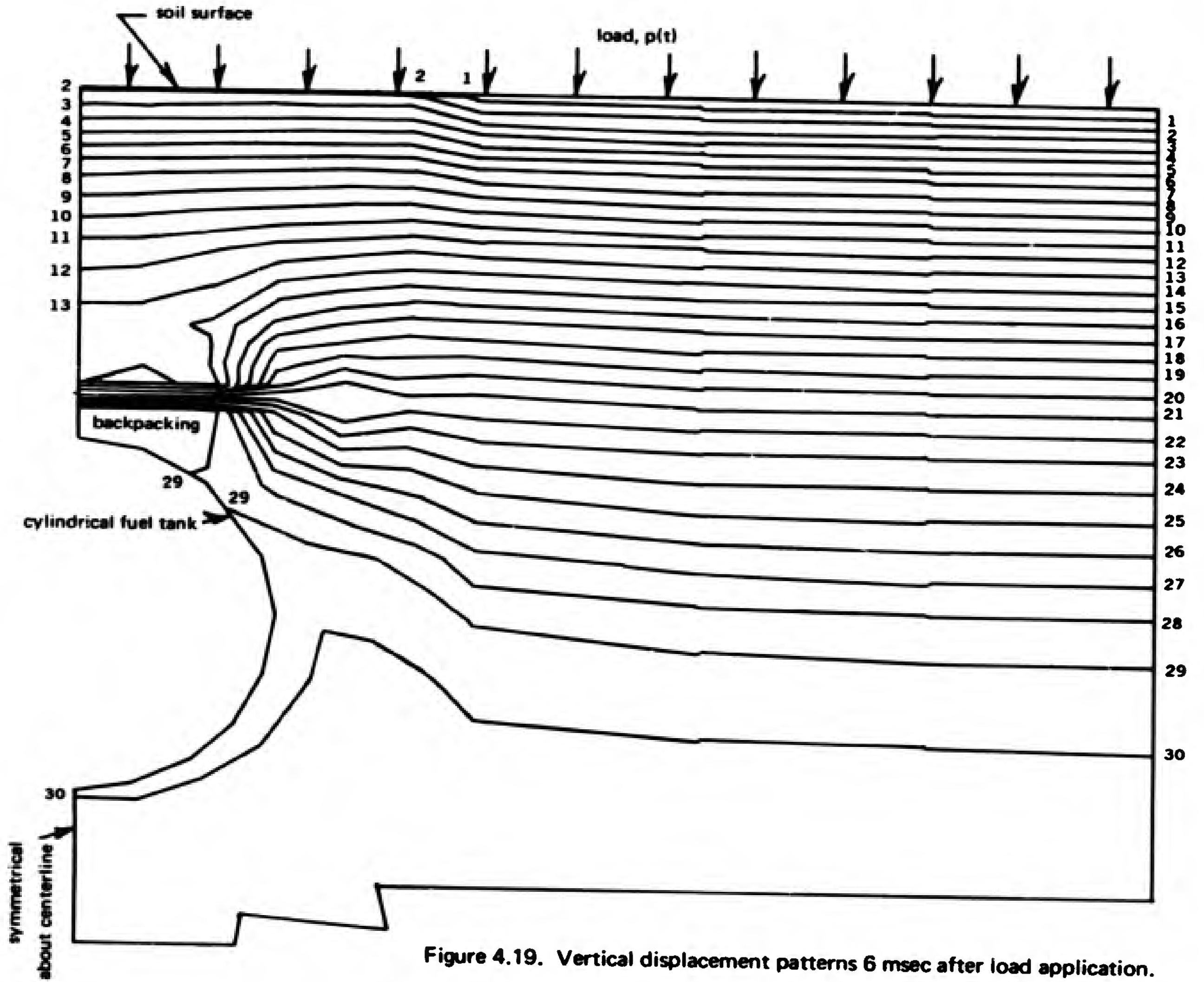

Contour No.	Displacement (in.)
1	-1.50×10^{00}
2	-1.45×10^{00}
3	-1.40×10^{00}
4	-1.35×10^{00}
5	-1.30×10^{00}
6	-1.25×10^{00}
7	-1.20×10^{00}
8	-1.15×10^{00}
9	-1.10×10^{00}
10	-1.05×10^{00}
11	-1.00×10^{00}
12	-9.50×10^{-01}
13	-9.00×10^{-01}
14	-8.50×10^{-01}
15	-8.00×10^{-01}
16	-7.50×10^{-01}
17	-7.00×10^{-01}
18	-6.50×10^{-01}
19	-6.00×10^{-01}
20	-5.50×10^{-01}
21	-5.00×10^{-01}
22	-4.50×10^{-01}
23	-4.00×10^{-01}
24	-3.50×10^{-01}
25	-3.00×10^{-01}
26	-2.50×10^{-01}
27	-2.00×10^{-01}
28	-1.50×10^{-01}
29	-1.00×10^{-01}
30	-5.00×10^{-02}

Figure 4.19. Vertical displacement patterns 6 msec after load application.

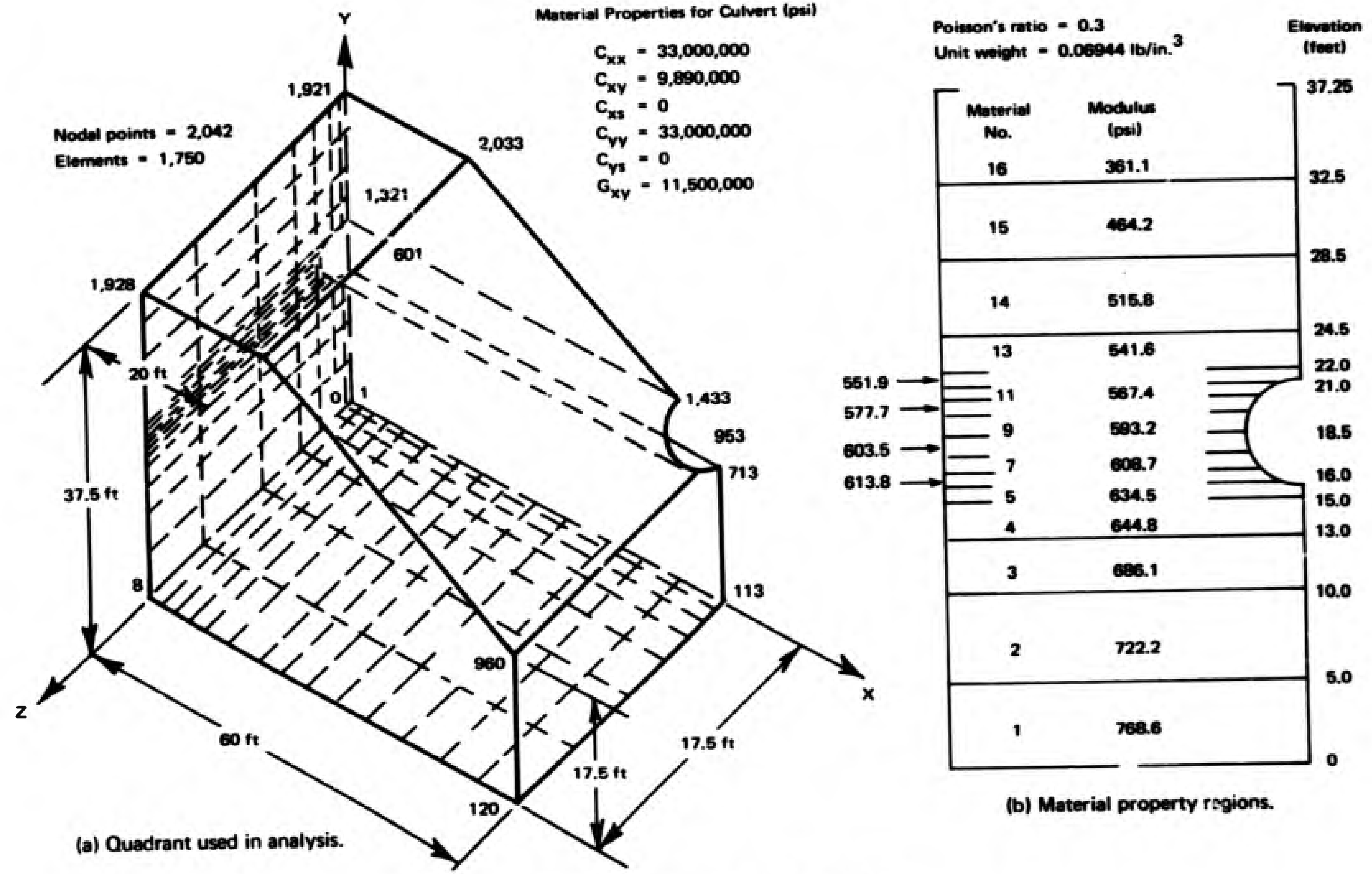

(a) Quadrant used in analysis.

(b) Material property regions.

Figure 4.20. Soil–culvert system model.

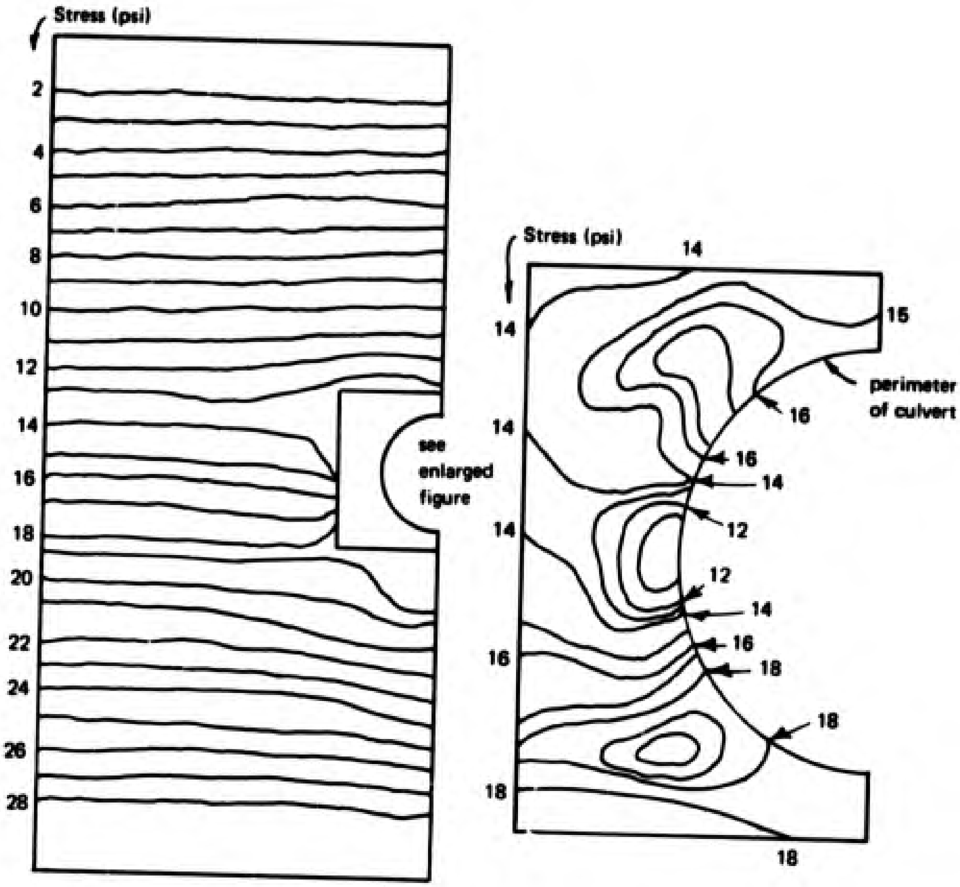

Figure 4.21. Vertical soil stress contours (Y-Z plane).

Stresses and forces in the culvert are shown in Figures 4.24 and 4.25. The contour plots in Figure 4.24 show the longitudinal and circumferential stresses in the extrados of one-half of the developed longitudinal section. At the center springline the circumferential stress in the extrados is about 11,100 psi.

The peak longitudinal stress is about 18,000 psi for the modeled plate, although, it would be less for a longitudinally corrugated culvert.

Forces and deflections on the transverse sections at midlength and one-quarter of the total culvert length from one end are shown in Figure 4.25. It is interesting to note that the thrust at the springline is about double the thrust at the crown and invert. Moments at the crown and springline are about equal in amplitude but of opposite sign.

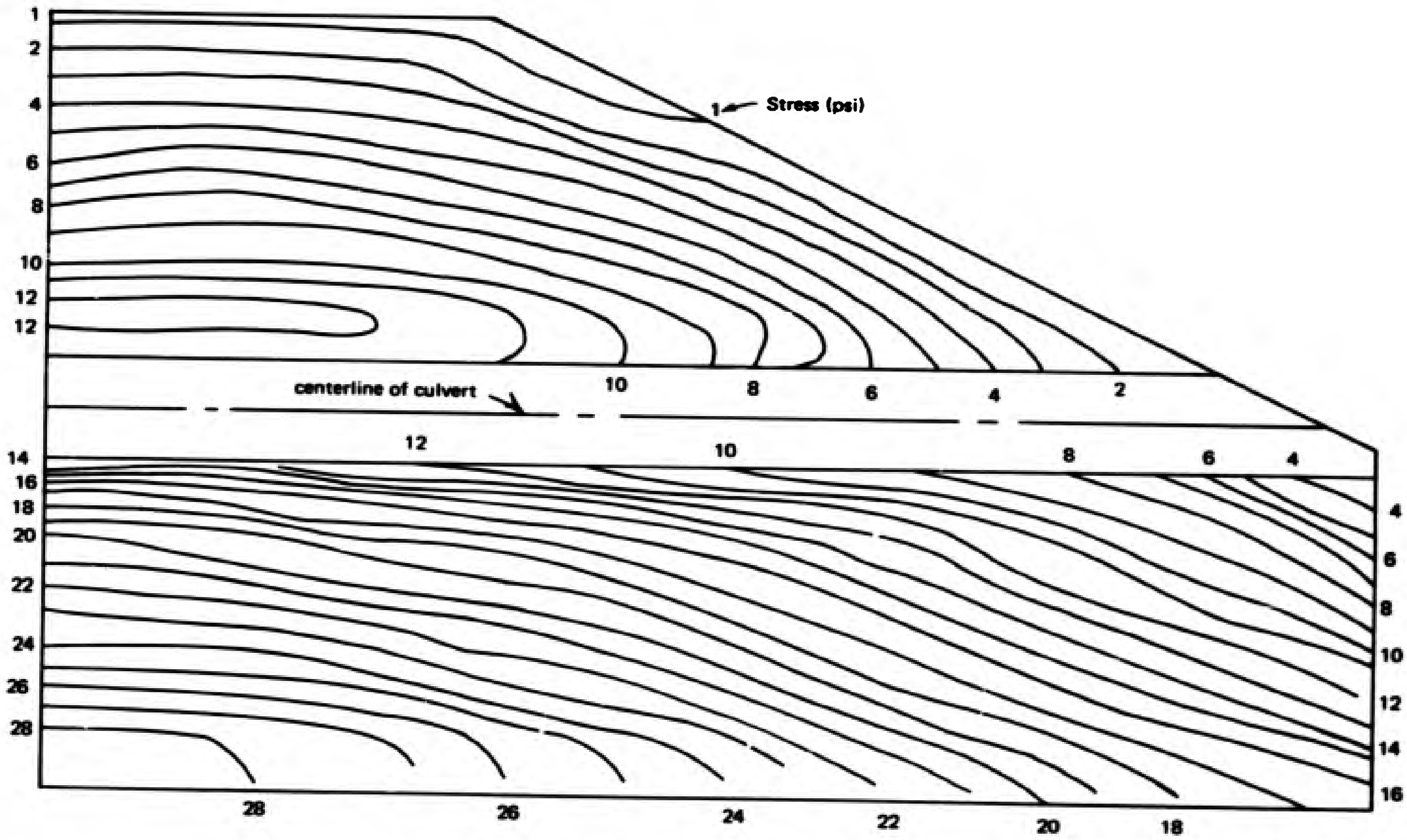

Figure 4.22. Vertical soil stress contours (X-Y plane).

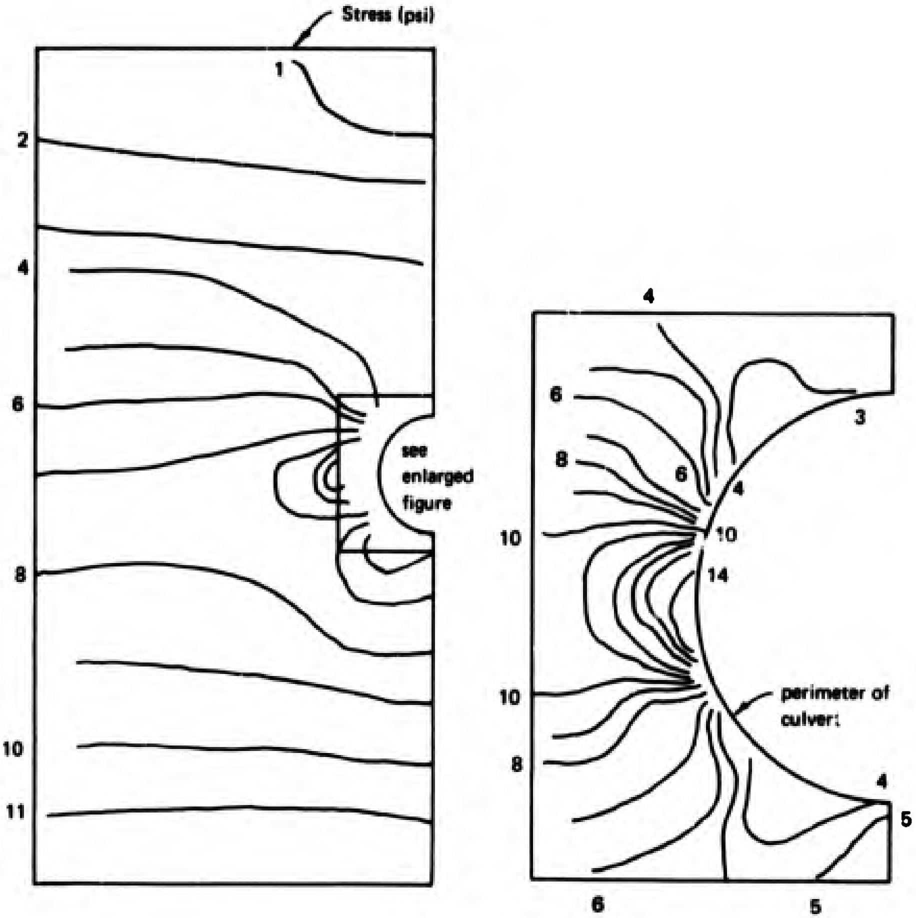

Figure 4.23. Horizontal soil stress contours (Y-Z plane).

Horizontal diametral expansion at the center section was 1.27 inches, and the vertical diametral shortening was 1.35 inches. The corresponding vertical deflection determined in the design was 1.77 inches; the deflection by the Iowa formula neglecting deflection lag was 2.14 inches. Absolute displacement of the invert at the center section was 4.77 inches. This is the amount of camber that should be provided initially to assure that the longitudinal axis of the culvert is straight when the embankment is completed.

The linear three-dimensional finite element solution gives deflections that are in approximate agreement with values from the approximate theory. Thrusts and moments are, however, about a factor of 2 larger than the approximate theory. It may also be noted from Figure 4.25a that the thrust at the crown and invert is only about one-half that at the springline. Test results indicate that the thrust difference is much more uniform around the extrados. Magnitudes from the approximate theory are regarded as more nearly correct than the elastic three-dimensional solution; nonetheless, the stress and deflection distribution from the three-dimensional solution is informative. Incorporating interface slip capability and nonlinear material properties would undoubtedly improve the results but at a greatly increased cost.

Analysis of soil—structure systems by the finite element method may be readily applied to a variety of configurations. It must be remembered, however, that numerous difficulties may arise, including errors from large abrupt changes in soil properties, errors from improper mesh gradation at boundaries, unloading instability, etc.

This chapter has dealt exclusively with horizontally buried, circular cylinders. Some tests have been performed on noncircular sections,[4.16] and the methods described are generally adaptable to other section geometries.

As a second problem, static runs were made on a fuel capsule which had been tested in the laboratory and in a field test.[4.3, 4.24] Dynamic runs for this problem are currently (April 1972) being attempted.

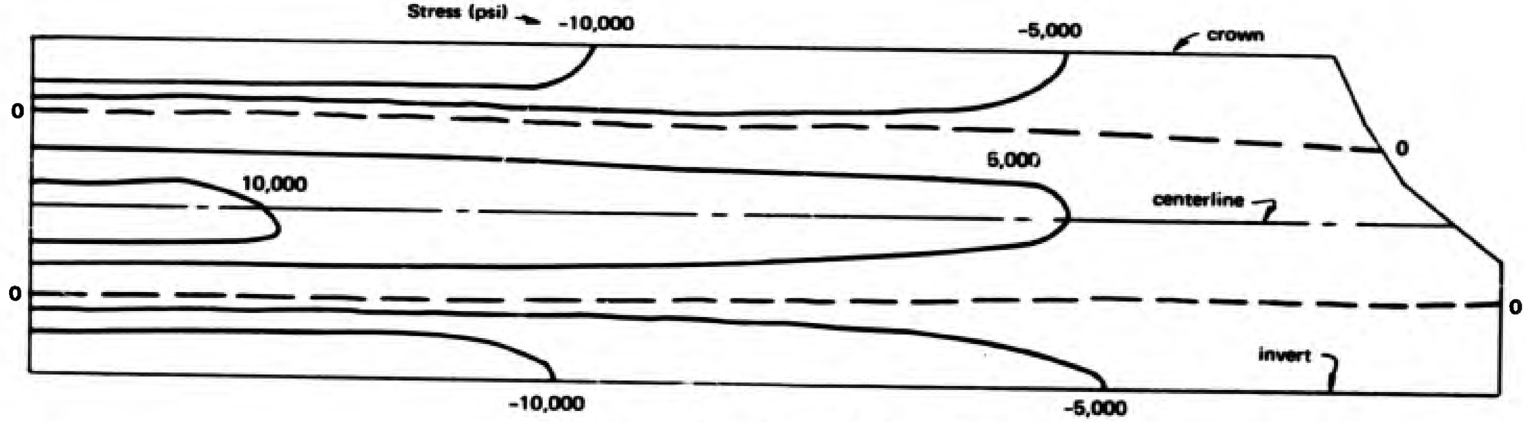

(a) Circumferential stress at extradcs.

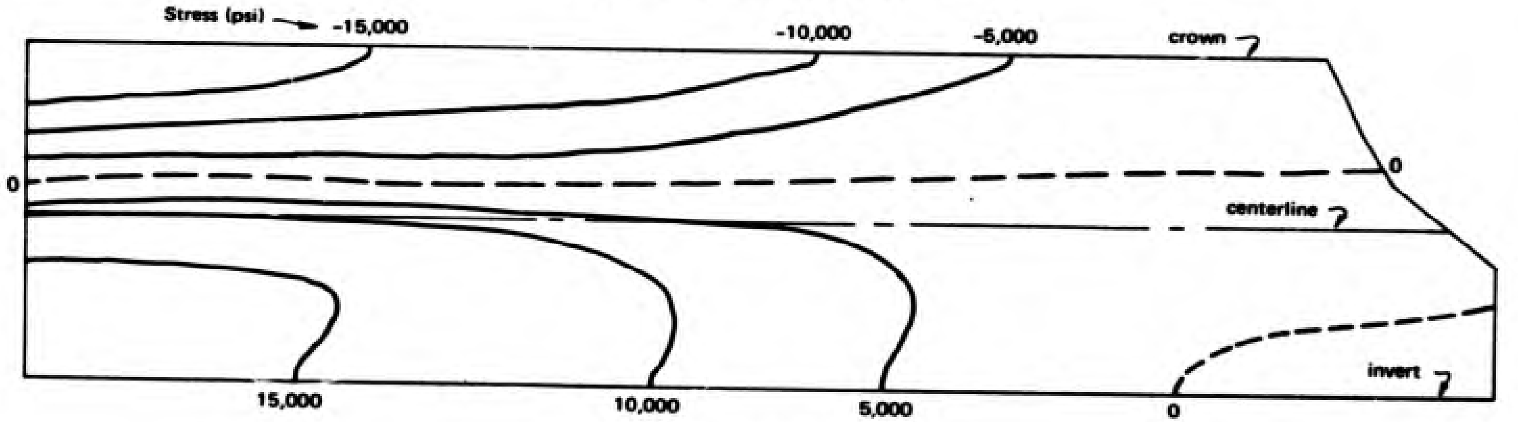

(b) Longitudinal stress at extrados.

Figure 4.24. Stress contours on developed longitudinal half-section.

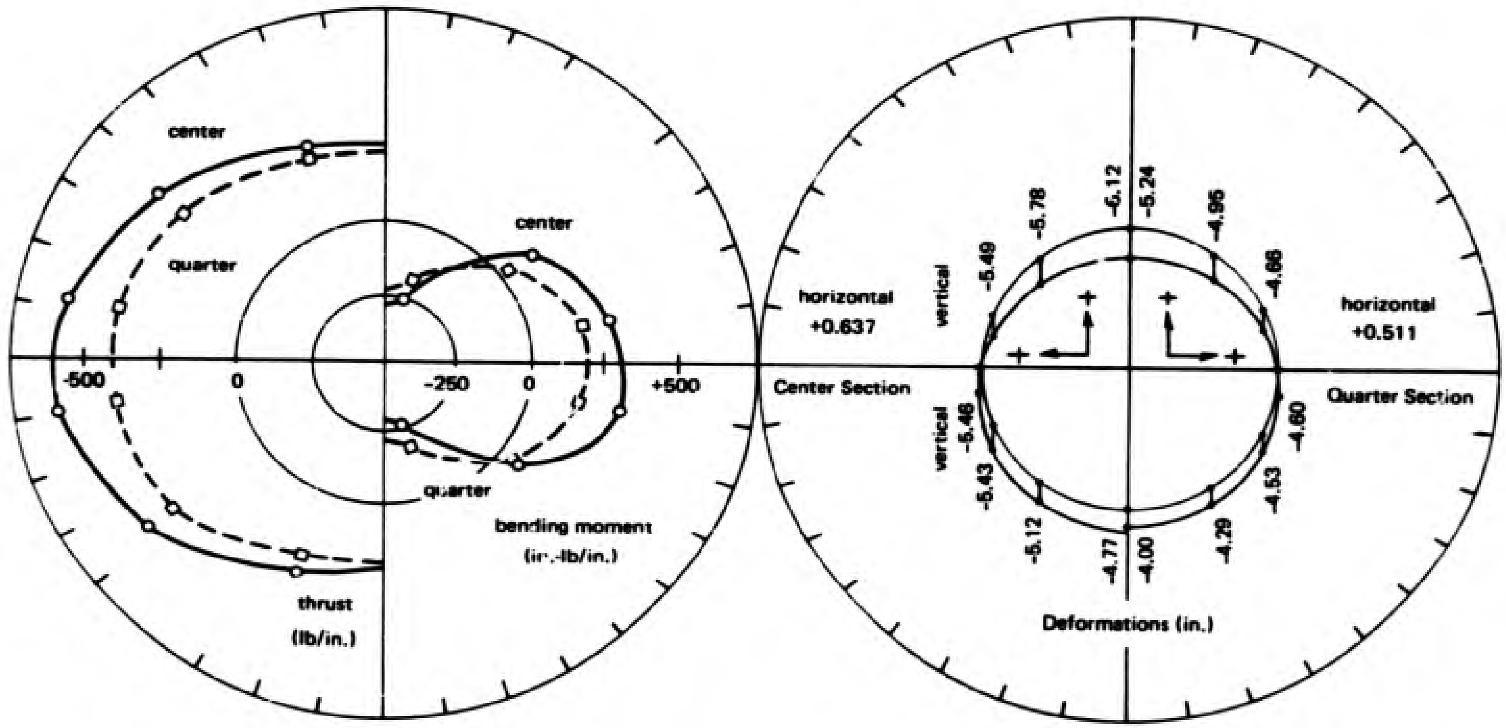

(a) Thrust and bending moment.

(b) Horizontal and vertical deformations.

Figure 4.25. Forces (thrust and moment) and deflections on transverse section.

4.5 REFERENCES

4.1. Highway Research Board. National Cooperative Highway Research Report 116: Structural analysis and design of pipe culverts, by R. J. Krizek, et al. Washington, D. C., 1971.

4.2. Ministry of Aviation. Translation TIL/T.4480: The form of stable semi-arches and arches (O Formakh Ustoichivykh Polusvodov i Svodov), by V. V. Sokolovkii. London, England, Jan. 1960. (Translation of: Prikladnaya Matematika i Mekhanika, vol. 20, no. 1, 1956, pp. 73-86) (AD 245810; TT61-27046)

4.3. Naval Civil Engineering Laboratory. Technical Report R-728: Static and dynamic tests of model pressurized underground fuel storage containers, by W. E. Gates and S. K. Takahashi. Port Hueneme, Calif., May 1971. (AD 726160)

4.4. Iowa State College. Engineering Experiment Station. Bulletin No. 153: The structural design of flexible-pipe culverts, by M. G. Spangler. Ames, Iowa, Dec. 1941.

4.5. Naval Civil Engineering Laboratory. Contract Report CR 69.019: Dynamic response analysis of two-dimensional structures with initial stresses and nonhomogeneous damping, by I. Farhoomand, E. Rukos, and E. L. Wilson. Berkeley, Calif., University of California, Jan. 1970. (Contract N62399-69-C-0016) (AD 874628L)

4.6. J. R. Allgood. "Structures in soil under high loads," American Society of Civil Engineers, Proceedings, Journal of the Soil Mechanics and Foundations Division, vol. 97, no. SM3, Mar. 1971, pp. 565-579.

4.7. J. Q. Burns. An analysis of circular cylindrical shells embedded in elastic media, Ph.D. thesis, University of Arizona. Tucson, Ariz., 1965.

4.8. J. R. Allgood. "Balanced design and finite element analysis of culverts," paper presented at 51st Annual Meeting, Highway Research Board, Washington, D. C., Jan. 17-21, 1972.

4.9. R. K. Watkins and A. P. Moser. "Response of corrugated steel pipe to external soil pressures," paper presented at the 50th Annual Meeting, Highway Research Board, Washington, D. C., Jan. 18-22, 1971.

4.10. Air Force Weapons Laboratory. Technical Report No. AFWL-TR-65-98: Pressure distribution on underground structural cylinders, by K. Höeg. Kirtland Air Force Base, N. M., Apr. 1966. (Contract AF 29(601)-6368)

4.11. J. N. Kay and R. J. Krizek. "Adaptation of elastic theory to the design of circular conduits," Institution of Engineers, Australia, Civil Engineering Transactions, Apr. 1970, pp. 85-90.

4.12. Naval Civil Engineering Laboratory. Technical Report R-678: Response of buried cylinders in the near-crater region, by J. R. Allgood, T. K. Lew, and R. D. Rail. Port Hueneme, Calif., May 1970. (AD 708010)

4.13.———. Contract Report CR 68.010: Design of cylindrical reinforced concrete tunnel liners to resist air overpressures, by A. J. Hendron, et al. Urbana, Ill., N. M. Newmark Consulting Engineering Services, Jan. 1968. (Contract NBy-62218) (AD 837422L)

4.14. U. Luscher. "Buckling of soil-surrounded tubes," American Society of Civil Engineers, Proceedings, Journal of the Soil Mechanics and Foundations Division, vol. 92, no. SM6, Nov. 1966, pp. 211-228.

4.15. Classified reference.*

4.16. Naval Civil Engineering Laboratory. Technical Note N-773: Critical pressures for radially supported cylinders, by C. V. Chelapati. Port Hueneme, Calif., Jan. 1966. (AD 627082)

4.17. E. J. Yoder. Principles of pavement design. New York, Wiley, 1959.

4.18. Army Engineer Waterways Experiment Station. Technical Report No. 1-682: Response of horizontally oriented buried cylinders to static and dynamic loading, by A. F. Dorris. Vicksburg, Miss., July 1965.

4.19.———. Technical Report No. 1-750: Response of a buried prototype communication conduit to static and dynamic loading, by A. F. Dorris and G. E. Albritton. Vicksburg, Miss., Dec. 1966.

4.20.———. Technical Report No. 1-821: Behavior of flexible cylinders buried in sand under static and dynamic loading, by G. E. Albritton. Vicksburg, Miss., Apr. 1968.

4.21. Air Force Weapons Laboratory. Technical Report No. AFWL-TR-64-122: A study of static and dynamic resistance and behavior of structural elements, by R. L. Marino. Kirtland Air Force Base, N. M., July 1965. (Contract AF 29(601)-5372) (AD 468736)

4.22. Naval Civil Engineering Laboratory. Technical Report R-582: Influence of soil modulus on the behavior of cylinders buried in sand, by J. R. Allgood, J. B. Ciani, and T. K. Lew. Port Hueneme, Calif., June 1968. (AD 670477)

4.23. University of Detroit. Department of Engineering Mechanics. Report on Contract NBy-32254: Inelastic buckling of an elastically supported buried cylinder, by D. A. DaDeppo. Detroit, Mich., Apr. 1965.

* Classified reference list available to qualified requestors.

4.24. Naval Civil Engineering Laboratory. Technical Note N-1199: Reduction of stresses in buried structures, by S. K. Takahashi and R. N. Murtha. Port Hueneme, Calif., Dec. 1971. (AD 736601)

4.25. Military Engineering Experimental Establishment. Report RES. 48.3/5: Blast loading of square tubes, by P. S. Bulson. Christchurch, Hampshire, England, Feb. 1965.

4.26.———. Report RES. 47.5/13: Static and dynamic loading of brittle square tubes, by C. J. Allison. Christchurch, Hampshire, England, Feb. 1969.

4.27. RAND Corporation. Report R-425-PR: A review of nuclear explosion phenomena pertinent to protective construction, by H. L. Brode. Santa Monica, Calif., May 1964.

4.28. J. F. Harvey. Pressure vessel design: nuclear and chemical applications. Princeton, N. J., Van Nostrand, 1963.

4.29. J. S. Przemieniecki. Theory of matrix structural analysis. New York, McGraw-Hill, 1968.

4.30. O. C. Zienkeiwicz. The finite element method in structural and continuum mechanics. New York, McGraw-Hill, 1967.

4.31. M. F. Rubinstein. Structural systems: statics, dynamics, and stability. Englewood Cliffs, N. J., Prentice-Hall, 1970.

4.32. University of California. Structural Engineering Laboratory. Report No. 68-1: A computer program for the dynamic stress analysis of underground structures, by E. L. Wilson. Berkeley, Calif., Jan. 1968. (Contract DACA-39-67-C-0020) (AD 832681)

4.33.———. Structural Engineering Laboratory. Report No. SESM 70-20: SAP; a general structural analysis program, by E. L. Wilson. Berkeley, Calif., Sept. 1970. (Contract DACW 68-67-C-004)

4.34. I. Farhoomand. Nonlinear dynamic stress analysis of two-dimensional solids, Ph.D. thesis, Department of Civil Engineering, University of California, Berkeley, Calif., Sept. 1970.

4.35. Naval Civil Engineering Laboratory. Technical Report R-743: Stress analysis of multicomponent structures, by A. B. Nosseir, S. K. Takahashi, and J. E. Crawford. Port Hueneme, Calif., Oct. 1971. (AD 733659)

5.0 OTHER CONFIGURATIONS

5.1 CABLES AND PIPES

The principles of buried cylinders apply to similarly oriented buried cables and pipe. There are also problems with: (1) potential damage from nearby boulders, (2) longitudinal bending, (3) passage through interfaces of high impedance mismatch, and (4) connections to structures. There are also the possibilities of (1) late-time cable failure due to slumping of the sides of a crater, and (2) a very shallow buried pipe or cable being bounced out of its trench.*

A summary of cable tests performed in HEST and other tests is given in Reference 5.2. Basically, it has been learned that some crushing will occur in bundles of cables at pressures of about 3,000 psi, and that design of cable systems to survive in high overpressure regions requires care and good judgement.

Potential damage from boulders is of little consequence in trenched installations where the character of the backfill can be controlled. It is, however, a dominating factor in plowed installations. In either case the maximum size of the boulders will govern the thickness of sand or other cushion required or, alternately, whether a shield must be used over or around the cable.

The relative motion of a cable or a boulder in a soil field may be calculated from Equation 3.10. This equation gives the relative displacement due to the impedance mismatch with the enveloping soil. It does not include inertial effects which may be important at high overpressures. Approximate analysis indicates that relative displacement due to inertial effects are important at high overpressures ($p_o > 600$ psi depending on the soil); however, test results are not available for checking this. In the usual circumstance where the relative displacement of a boulder with respect to the soil is greater than the relative displacement of the cable with respect to the soil, there is a possibility of the boulder damaging the cable—especially in a multiple burst attack.

* This actually happened in a field test.[5.1]

A number of the cable failures that have occurred in field tests[5.3] have been attributed to slumping of the sides of the crater downward and toward the center. In large (100-to-500-ton) high-explosive shots, cable breakage occurred about 2 seconds after detonation zero. For a surface nuclear detonation, corresponding motions would be expected to occur at a later time and be of a larger magnitude. For the 500-ton TNT shot of Operation PRAIRIE FLAT, breakage occurred at surface overpressures of 1,500 psi and greater. The critical overpressure would be expected to be much higher for surface nuclear detonations.

A vulnerability assessment of a large diameter cable is given in Table 5.1.[5.4] These results indicate the need for a sand cushion or for a mechanical shield in rocky soils or at soil–rock (or other soft–hard) surfaces.

Table 5.1. Vulnerability Assessment Summary for a 3-Inch Cable With a 2-Inch Copper Cone[5.4]

Media	Critical Overpressure[a] (psi) for—			
	Air or Contact Burst		Penetration Burst	
	1 Mt	10 Mt	1 Mt	10 Mt
Soft–hard	2,500	1,000	–	–
Soft	6,000	3,000	10,000	6,500
Medium	10,000	7,000	7,000	3,000
Hard	10,000	10,000	10,000	8,000
Rock inclusion	1,300	1,300	–	–

[a] Onset of damage was assumed to occur when cable strain exceeded 4%.

A reasonable maximum allowable strain for cable is 4%; however, most electrical cable can withstand at least 12% strain prior to rupturing.

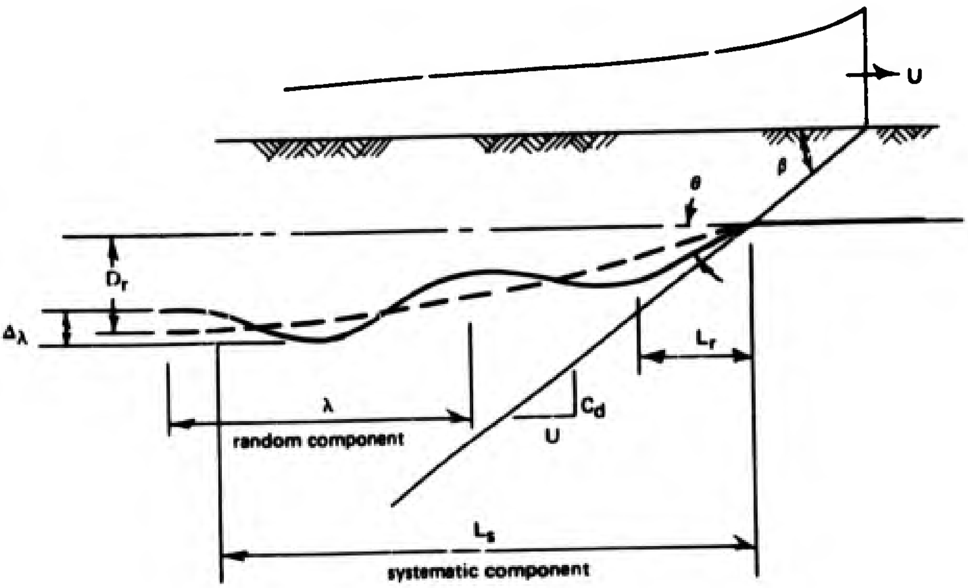

Figure 5.1. Deflection of a buried cable subjected to a blast wave.

For steel pipe, rock penetration would not be a serious problem; however, longitudinal bending might be. As is indicated schematically in Figure 5.1, as a blast wave moves in the general direction of a buried pipe or other long structure there occurs systematic and random components of displacement and concomitant stresses. The systematic component is attributable to compaction of the pressurized soil relative to the unloaded field. The random component is caused by natural inhomogeneities in the soil field. Information on random displacement is available from experience with various installations. For example, it has been found that footings only 20 feet apart may experience differential settlements of 50% of their total settlements.[5.4]

Using this as a criterion, Karagozian[5.4] proposes the following equation for predicting the random displacement

$$\Delta_\lambda = \frac{D_r}{(1 + 50/\lambda)} \qquad (5.1)$$

where Δ_λ = amplitude of random displacement

D_r = amplitude of systematic component of the displacement = $D_1 + D_2$

λ = wavelength of random component, $\approx$ 25 feet

D_1 = systematic component of displacement from air blast

D_2 = systematic component of displacement from direct-induced wave

The peak amplitude of the systematic component attributable to air blast may be approximated by

$$D_{r1} = K_1 \frac{I_t}{\rho C_d} \tag{5.2}$$

where I_t = impulse to the time that the wave reflected from the basement rock reaches the cable

K_1 = constant to account for compaction of the media (K_1 = 1.2, 1.4, and 1.7 for hard, medium, and soft soils, respectively)

The amplitude of the systematic component attributable to direct-induced motion is highly dependent upon the ground profile near the crater; consequently, it is best estimated from runs of ground motion codes of similar profiles. Lacking such information, D_{r2} may be estimated from the relation

$$D_{r2} = \frac{5\,W^{5/6}}{C_d\,R^{1.5}} \tag{5.3}$$

where D_{r2} = peak downward amplitude of the direct-induced motion for a surface burst (inches)

W = weapon yield (Mt)

R = range (kft)

C_d = seismic velocity of the soil (kft)

An outward and upward component of direct-induced motion of larger amplitude may occur close to the crater at relatively late times. Fortunately, the velocity associated with these late-time motions is only about 2 fps. The amplitude of late-time motions is best determined from computer ground motion runs.

In the neighborhood of the juncture of a shock front with a buried pipe, Figure 5.1, bending stresses develop from the attendant rotation; this rotation may be conservatively estimated as[5.5]

$$\theta = \theta_1 + \theta_2 = \tan^{-1}\frac{D_r}{L_s} + \tan^{-1}\frac{\Delta_\lambda}{L_r} \tag{5.4}$$

where L_s = length of systematic component

L_r = length of random component = $\lambda/4$

The minimum possible length of the systematic component is

$$L_{s_{min}} = \frac{D_r}{\epsilon_s (C_d/U)} \tag{5.5}$$

where ϵ_s = vertical soil strain

C_d = seismic velocity of stress wave

U = shock front velocity

Undoubtedly, L_s will be greater than the length given by Equation 5.5 due to soil sliding past the cable as it is deformed. With θ known from Equation 5.4, it is a simple matter to determine the induced moment from

$$M = M_1 + M_2 = EI\left(\frac{\theta_s}{L_s} + \frac{\theta_r}{L_r}\right) \tag{5.6}$$

Corresponding stresses and strains are readily determined.

Nuclear or high-explosive detonations off to the side of a pipe will develop stresses that may cause failures unless expansion–contraction joints or loops are provided. With the high normal stresses from large yield detonations, interface shear stresses sufficient to produce yielding and rupture could be developed within a few tens of feet; however, this is not likely to occur unless the pipe is restrained as by a T-joint or other means. Care should be taken to design the system so that undesired restraint is avoided at joints, pumping stations, and valves. Also, materials which are subject to brittle failure should not be used.

One must consider the possibility of pipes and cables being bounced out of shallow trenches by shock waves. This has happened in a high-explosive test where cables were placed in sand in a shallow trench through a rock field. It would not be expected to occur in a soil field unless there were a high impedance mismatch between the soil field and a trench fill material.

Where pipe or cable passes through a soil–rock interface, there is particular danger of shear failure from differences in displacement of the two media. The displacement of initially juxtaposed points may be estimated for the different media using Equations 5.2 and 5.3. The relative deflection found from subtracting the two defines the amount of overexcavation that must be made in the harder material near the interface and the amount of deformable material that must be placed around the cable at that juncture to avoid failure.

A similar problem is involved where pipes or cables join structures. In this instance, the induced stresses will be attributable both to difference in stress wave transmission time and to random component displacement.

Failure is avoided by placing a soft material around the pipe or cable in the vicinity of the structure to accommodate the relative motion as indicated in Figure 5.2. This technique has been successfully used with several systems that were in the plastic zone adjacent to 100- and 500-ton high-explosive craters.

In summary, the critical conditions for buried cables are: (1) the possibility of damage from rock inclusions projected into a cable by the stress wave, and (2) shear, tension, compression, or flexural failure at soft–hard interfaces. Damage from rock inclusions may be averted by using a sand cushion around the cable or by placing a mechanical shield around the cable. Failure at interfaces may be prevented by placing a soft material of appropriate thickness around the cable at the interface and by allowing adequate axial movement.

Critical conditions for buried pipe include: (1) passages through soft–hard interfaces, and (2) restraint points. Damage at soft–hard interfaces is avoided by essentially the same means used for cables. Failure from restraint may be avoided by using soft materials around the restraint or by other means that provide for the expected motions.

The required motions are estimated by calculating the relative movement of the structure with respect to the soil and the relative motion of the cable with respect to the soil. Then, the peak relative motion of the cable with respect to the structure can be determined.

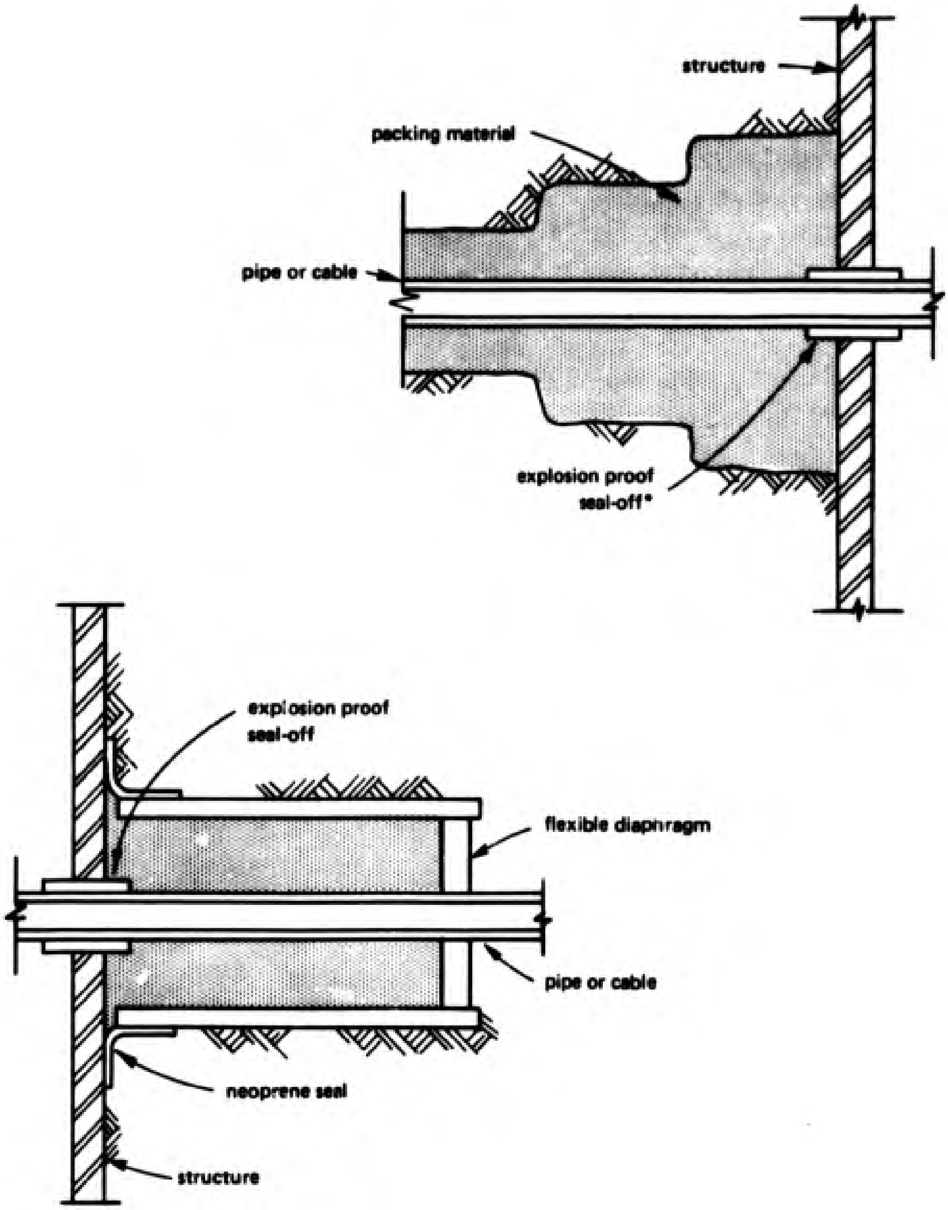

Figure 5.2. Connections to buried structures.

5.2 FOOTINGS AND FOUNDATIONS

The dynamic behavior of footings and foundations is dependent on the soil constitutuve properties, its stress history, and upon the extant environmental conditions. Fortunately, the problem is not recondite for most practical design situations. The reason is that for the common case of long-duration blast loading, the dynamic effects result in temporary increases in load capacity, but the longer term effects are essentially static.[5.6, 5.7]

In some circumstances, punching failure will occur in a dynamically loaded footing, while a corresponding statically loaded footing fails in the classical "logarithmic spiral" mode.[5.8] The reason for this is thought to be attributable to inertial forces in the outer passive Rankine zones that provide resistance for a sufficient amount of time to force failure along the planes of radial shear.

If this explanation is correct, then it would appear that where there is an overburden load, the probability of punching failure is enhanced. The reason is that the mass (and inertial resistance) would increase faster than the increase in shear resistance.

In many situations, such as in a buried arch, the blast load constitutes a large surcharge that provides confinement on one side of a foundation. The capacity of the foundation is not enhanced greatly, however, as restraint is not increased on the interior side of the foundation.

In summary, for most configurations, the design of footings and foundations for long-duration (megaton) blast loads can be accomplished by static methods. Dynamic effects cause a temporary increase in excess of the static bearing capacity, but their effects are minor. The immediately following paragraphs summarize static relations and influences common to the design of protective structures and give an indication of the character of the dynamic response of footings.

The bearing capacity equation is[5.9, 5.10]

$$q_{ult} = k_c c N_c + \frac{1}{2} k_\gamma \gamma B N_\gamma + \gamma D_f N_q \qquad (5.7)$$

where q_{ult} = unit bearing capacity at failure (FL^{-2})

k_c = shape factor for component of resistance manifested by soil cohesion

c = soil cohesion (FL^{-2})

k_γ = shape factor for component of resistance attributable to soil weight

γ = apparent density of soil (FL^{-3})

B = width of footing (L)

D_f = depth of overburden, both sides of footing (L)

N_c, N_γ, N_q = bearing capacity factors, functions of ϕ, from References 5.9 and 5.10.

The shape factors are

Footing Shape	Shape Factor	
	k_c	k_γ
Strip	1.0	1.0
Square	0.8	1.3
Circular	0.6	1.3

N_γ and N_q are plotted in Figure 5.3. N_c is not plotted because the first term in Equation 5.7 is time dependent if c is not zero. Equation 5.7 is valid for dynamic loading only if c is sufficiently small that the first term is negligible; otherwise, time effects alter the results.

A general equation for the bearing capacity of footings on granular soil with or without overburden on one side is[5.10]

$$q_{ult} = \frac{k_\gamma \gamma B N_\gamma}{2} \hat{G} \tag{5.8}$$

where $\hat{G} = 1 + \dfrac{\hat{p} \ln[1 + (1 - \hat{p})^2 D_e']}{(1 - \hat{p})^2}$

$\hat{p} = \dfrac{L + (\pi B/2)}{2L + 2B + \pi B}$; $\hat{p} = 1$ for $B = L = 0$

L = length of footing

B = width of footing

$D'_e = 2 D_e N_q / k_\gamma B N_\gamma$

D_e = difference in height of overburden on opposite sides of the footing

and the other parameters are as previously defined. The corresponding ultimate deflection is given by

$$\delta_{ult} = \hat{G} B / k'_n \tag{5.9}$$

where $k'_n = 1 + \ln(1 + 0.25 \hat{\rho}^2 k_\gamma D'_e)$

A typical response for a footing on dry sand is indicated in Figure 5.4. The initial portion of the load–displacement curve may be characterized by the relation

$$\frac{q}{q_{ult}} = \frac{\delta}{\delta_{ult}} e^{1-\delta/\delta_{ult}} \tag{5.10}$$

where q and δ are, respectively, the corresponding load and displacement, and where q_{ult} and δ_{ult} are calculated from appropriate preceding equations.

Groundwater reduces the displacements of foundations[5.7, 5.11] under dynamic loading partly by the development of negative pore pressures. Thus, for saturated soil conditions, Equations 5.7 and 5.8 will give adequate, but conservative results.

Plotting peak load and peak deflection from tests of footings with different overburden on one side gives curves of the type shown in Figure 5.5. It is interesting to note from Figure 5.5 that as the overburden pressure increases, the peak load–peak deflection curves tend to approach a limit where no further resistance is achieved from increasing the overburden.

Load–deflection curves for cohesive soils may also be characterized by relations of the form of Equation 5.7 provided q_{ult} and δ_{ult} are calculated from relations for cohesive soils and provided one includes a factor to account for the increase in strength with strain rate. Relations for determining the static resistance and data on the strain rate sensitivity of soil are given in Reference 5.12.

Due to the variable and nonhomogeneous properties of soil, the error band for displacement predictions of footings on dense granular soils must be expected to be ± 50%. The variability would be even greater for less densely compacted materials.

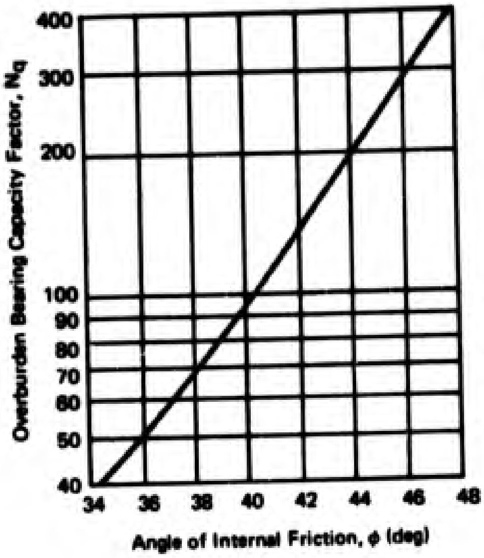

(a) Overburden bearing capacity factor.

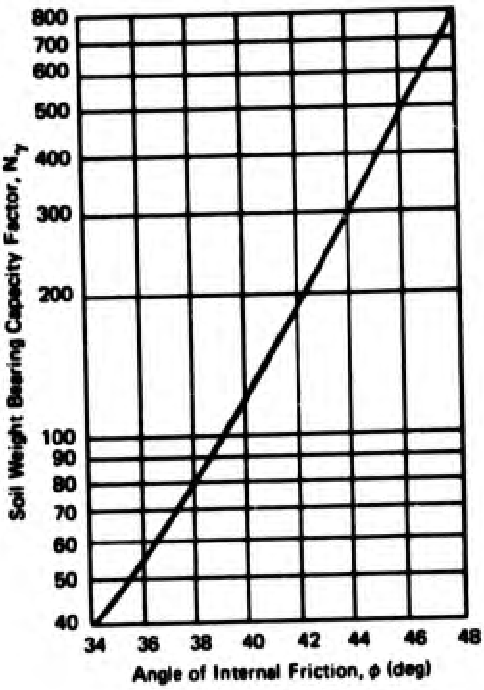

(b) Soil weight bearing capacity factor.

Figure 5.3. Footing bearing capacity factors. (From Reference 5.10)

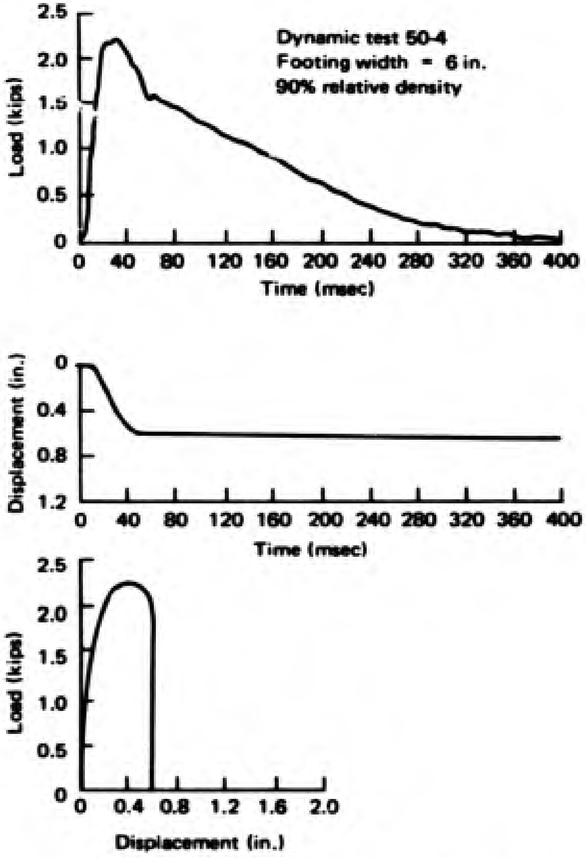

Figure 5.4. Dynamic response of square footings on dry sand. (From Reference 5.10)

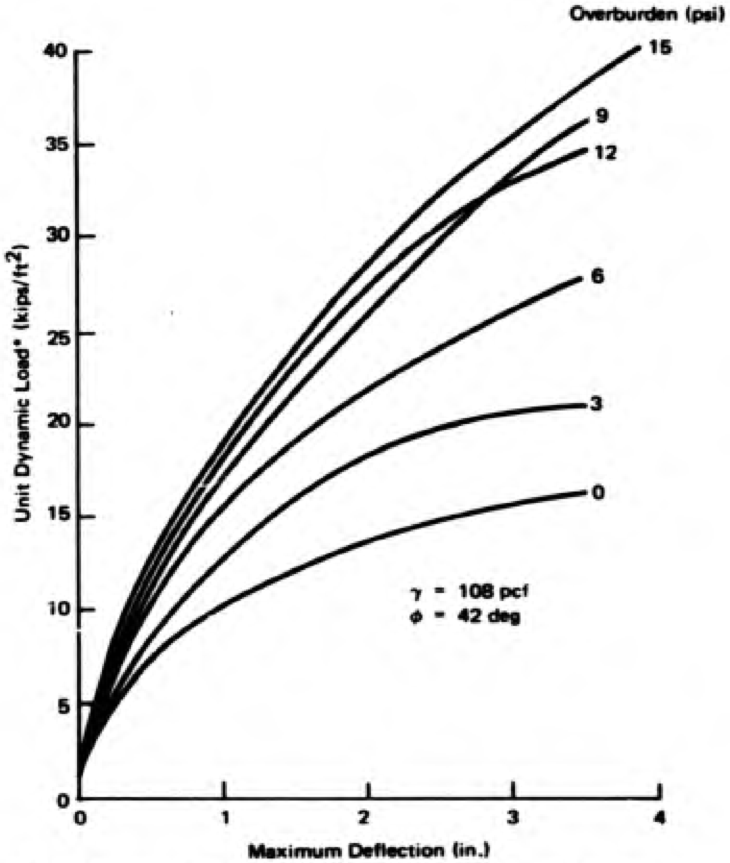

* Long-duration blast load on strip footing on dry sand with overburden on one side.

Figure 5.5. Dependence of footing resistance on overburden pressure. (From Reference 4.22)

In saturated foundations, stresses are transmitted through the pore fluid and through the mineral skeleton of the soil. If the pore pressure is sufficiently large, liquefaction may occur. Loose sands are particularly susceptible to liquefaction because they contract on shearing, thereby reducing the effective stress. Dense sands dilate under shear deformation; nonetheless, liquefaction is still possible if the pore pressure is sufficiently large. The designer should keep this possibility in mind in designing footing and foundation systems for protective facilities.

5.3 VERTICAL CYLINDERS

5.3.1 Vertical Capsule and One-Dimensional Stress Cells

As used here, the term vertical capsule refers to vertically oriented cylinders with flat or domed ends whose crowns are below the surface. Such inclusions are well suited for operations centers and other similar shelters because their geometry permits great strength with a near minimum of materials, and ease of shock-isolating interior platforms. They are also used for one-dimensional stress cells and for other purposes.

Under plane-wave loading from an air blast, the stress on the cylindrical section is only about one-half or less than that on a similarly located horizontal cylinder. However, vertical capsules are usually stiff in the axial direction, and they tend to collect load. It is virtually mandatory, therefore, that backpacking be used to reduce the effective axial stiffness—especially if their height is large compared to their diameter. Information on the response of vertical capsules and relations for designing backpacking for them are given in the following paragraphs.

When a stiff vertical capsule in a soil field is loaded by an essentially plane stress wave, the soil tends to compact at the sides, producing a downward directed shear on the structure as shown in Figure 5.6. This shear and the load on the top are resisted by the foundation reaction at the bottom, by inertia, and by an upward directed shear near the bottom of the cylinder. Studies indicate that there is a neutral, shear plane about one-third of the distance up the cylinder from the bottom.

Abbott[5.13] has shown that the load concentration on vertical cylinders in sand depends on the height-to-diameter ratio as follows:

$$\frac{p_i}{p_y} \propto 1 + \frac{H'}{2\alpha D} \tag{5.11}$$

where H' = height of cylinder
α = experimental constant

Equation 5.11 may be combined with Equation 3.33 to account for the principal parameters by modifying the geometry factor in the arching equation so that

$$A_{gv} = \frac{A_g}{1 + \dfrac{H'}{2\alpha D}} = \frac{4d_o/D^2}{1 + \dfrac{H'}{2\alpha D}} \qquad (5.12)$$

Arching is now determinable, since the vertical strain in most vertical cylinders is negligible compared to the soil strain. Thus, with $\epsilon_c/\epsilon_s = 0$ and $H = H'$ in Equation 3.33,

$$\Omega = -A_{gv} H \qquad (5.13)$$

and the arching may be readily determined from Equation 3.30 for any specific case. The negative value of Ω in Equation 5.13 assures that the interface pressure on top of a vertical cylinder will be greater than the applied load. It is, in fact, possible to experience interface loads on vertical cylinders of 2.5 or more times the load at the same elevation in the free field. This undesirable condition may be avoided by placing backpacking over the structure to reduce the effective stiffness of the inclusion consisting of the structure and the backpacking.

Ironically, the load attracted to a buried cylinder through negative arching increases with depth of cover. Thus, if a stiff vertical cylinder is used without backpacking, it should be placed close to the surface. Backpacking should be required unless there is some reason that it cannot be used. The thickness of backpacking required for maximum arching is obtained by substituting Ω from Equation 5.13 into Equation 3.39.

A plot of the required thickness of liner to achieve maximum arching as a function of depth-of-cover-to-diameter ratio for various diameter-to-height ratios and a given soil-strain-to-backpacking-hardening-strain ratio is shown in Figure 5.7. Thickness for other soil-strain-to hardening-strain ratios are obtainable by direct proportion. As expected, the required thickness increases rapidly for shallow depths of burial and approaches an asymptote rapidly for depths of burial above about two diameters. The plot of Figure 5.7 is only applicable to capsules in well-compacted granular soil fields.

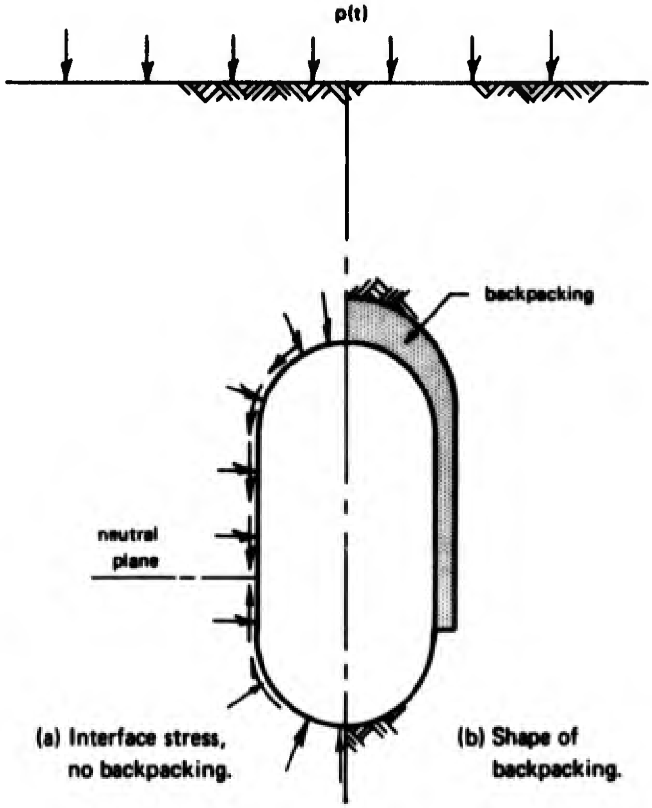

Figure 5.6. Vertical capsule sections.

Development of maximum arching may not be desirable, because transferring the load to the soil on the sides will result in an increase in the lateral stress on the cylinder. Backpacking changes the compaction pattern completely and, likewise, alters the shear distribution on the sides of the cylinder. For long cylinders, it may be desirable to minimize the coefficient of friction at the interface to reduce the net axial load.

Once the load transmitted to the structure has been determined, checking for buckling and other modes of failure is a fairly routine matter. As with horizontal cylinders, finite element analysis of the design provides useful information on the behavior and resistance of the system.

Detailed information on tests of buried, vertical capsules and on a finite element analysis of such structures may be found in Reference 5.14.

Vertical cylinders with flat ends and small diameter-to-height ratios (wafers) are sometimes used as one-dimensional soil stress cells. Such cells are made very stiff with respect to the soil so that in Equation 3.33, $\epsilon_c/\epsilon_s \ll 1$ and $\Omega \approx -4H/D$. By making $H/D \ll 1$, arching over the gage will be negligible, and registered stress will be within a few percent of the mean stress in the direction of the axis at the gage location.

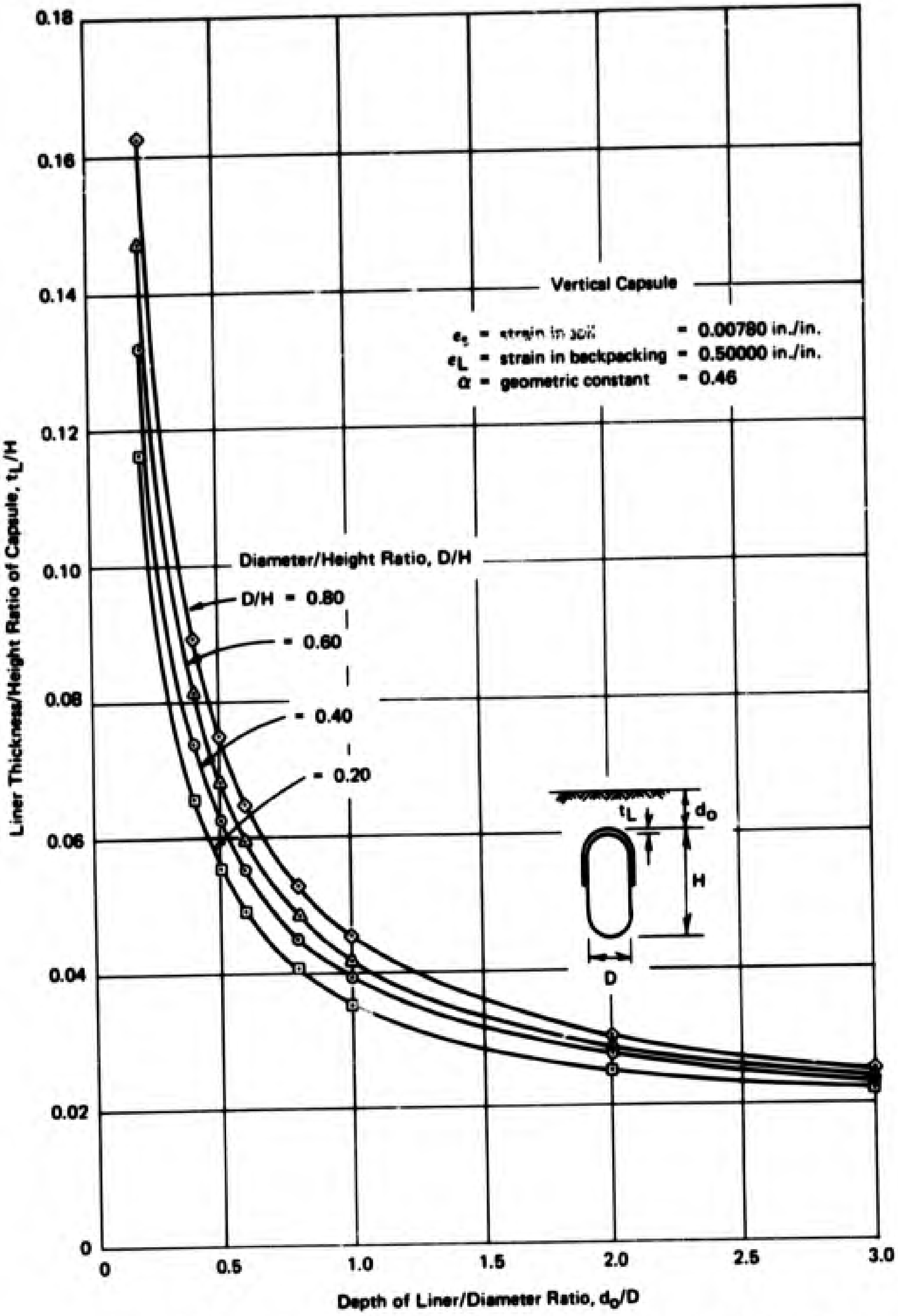

Figure 5.7. Thickness of liner and depth of cover for maximum arching over capsule. (Prepared by S. K. Takahashi of the NCEL staff.)

Wafer gages will respond correctly to dynamic stress waves only if the rise time of the wave is greater than about five transit times. This condition will virtually always be met for stress waves in soil fields unless the soil is saturated. Where the rise time is less than the transit time, arching is likely to occur around the gage.

5.3.2 Silos

Two basic types of silos, referred to respectively as one-piece and two-piece silos, are illustrated in Figure 5.8. Two-piece silos have the advantage that much of the shock from the air blast on the top surface is dissipated into the soil through the upper footing, thus, effectively reducing the shock which is transmitted to the missile suspended in the lower cylinder.[5.14] A disadvantage of two-part silos is their susceptibility to misalignment from large ground motions.

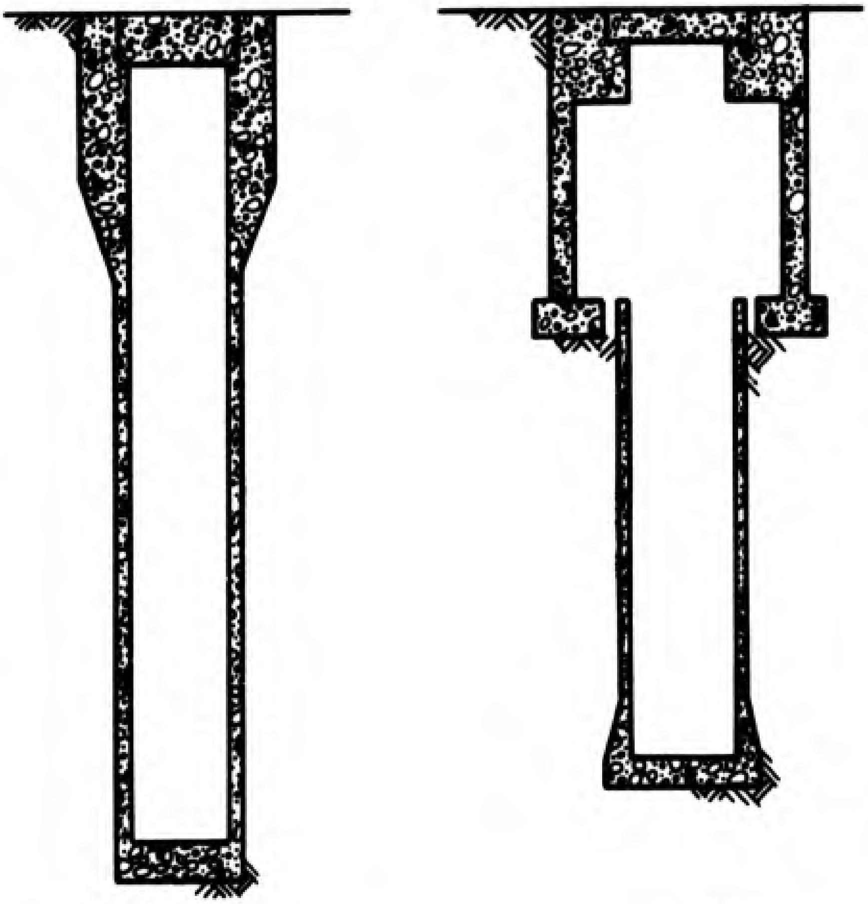

(a) One-piece silo.

(b) Two-piece silo.

Figure 5.8. Typical silo configurations.

One-piece silos have opposite advantages and disadvantages.[5.16] They can be designed to greater hardnesses than two-piece silos; further, their response is easier to model. Dominant characteristics of the early-time vertical motion may be depicted in terms of the damped one-degree-of-freedom system where the spring stiffness is that attributable to the foundation reaction on the bottom and the shear on the sides. The downward shear load on the sides must be included in the forcing function. At relatively late times, the silo motion is essentially the same as the soil field.

Naturally, the response of a silo is highly dependent upon the characteristics of the enveloping field; however, for basically granular soil fields the behavior is approximately as follows:

a. The blast load on the top of the silo causes a stress front to propagate down the silo to the bottom. The reflected wave subsequently bounces up and down through the cylinder walls causing the silo to vibrate for a relatively long time. The transmitted wave stresses the bottom foundation causing the cylinder to move initially downward relative to the surrounding soil and to produce upward shears on the extrados.

b. Then, the slower wave moving down through the soil compacts the soil producing downward motion of the soil with respect to the silo and predominantly downward interface shears.

c. There follows a rebound period where the relative motions may be positive or negative and, subsequently, a movement of the silo with the soil field.

Radical departure from the described behavior can occur for silos in low bearing strength, low hysteresis soils. Under these conditions the initial and final displacement of the silo will be downward with respect to the soil and there may be a strong elastic rebound.

In addition to the air-blast pressure on the top, a silo is loaded by interface shear on the extrados of magnitude $\tau_e = \mu K_o p_v$, where μ equals the coefficient of friction between the soil and the silo, K_o equals the at-rest coefficient of lateral earth pressure, and p_v equals the vertical soil stress in the free field adjacent to the silo. As a first approximation, the dynamic coefficient of lateral earth pressure may be taken as the static value, and the interface shear may be considered as acting only on the upper two-thirds of the cylinder. The reaction on the bottom of the silo, $r_f = \sigma_r A$, may be determined with Equation 3.19 of Section 3.2.

With expressions for the interface shear and the foundation reaction available as indicated, the relative deflection in the vertical direction may be found from the second order differential equation

$$m \frac{d^2 y_r}{dt^2} + \frac{\pi D^2}{4} r_f = \pi D\left(\frac{D}{4} - \frac{\mu K_o H}{3}\right)p \qquad (5.14)$$

where y_r = relative displacement of the silo with respect to the soil

r_f = foundation reaction

D = outside diameter of silo

m = mass of silo

p = surface pressure

and the other terms are as previously defined. Equation 5.14 is readily solved by numerical or graphical techniques.

Relative deflection in the horizontal direction may be estimated by applying the horizontal component of the soil stress over the blastward side and using r_f from Equation 5.14 as the reaction on the opposite side. A parallel equation to that of Equation 5.14 permits determination of the horizontal relative displacement.

Field tests have shown that as the system rebounds, a gap may be left between the soil and the silo on the blastward side.[5.15] Field tests also show that slip of the soil relative to the silo tends to be an intermittent phenomena.[5.16] Where the silo extends below the water table, the lower part of the silo may be loaded in advance of the upper part by the high velocity ground stress waves in the saturated soil. This may enhance the rotation of the silo.

Detailed tests and analysis of silos have been performed, although most of this information is in the classified literature.[5.17, 5.18] Three-dimensional dynamic finite element codes are becoming available which permit reasonably refined analysis of soil–silo systems.

5.4 ARCHES

Buried arches are of limited usefulness as protective shelters for several reasons. One is that arches tend to develop larger moments than a counterpart cylinder. This is especially true where the foundation is an integral part of the arch as shown in Figure 5.9a. As such an arch is loaded, the floor is deflected upward relative to the springline, thereby developing large moments in the arch between the haunch and the springline.[5.19]

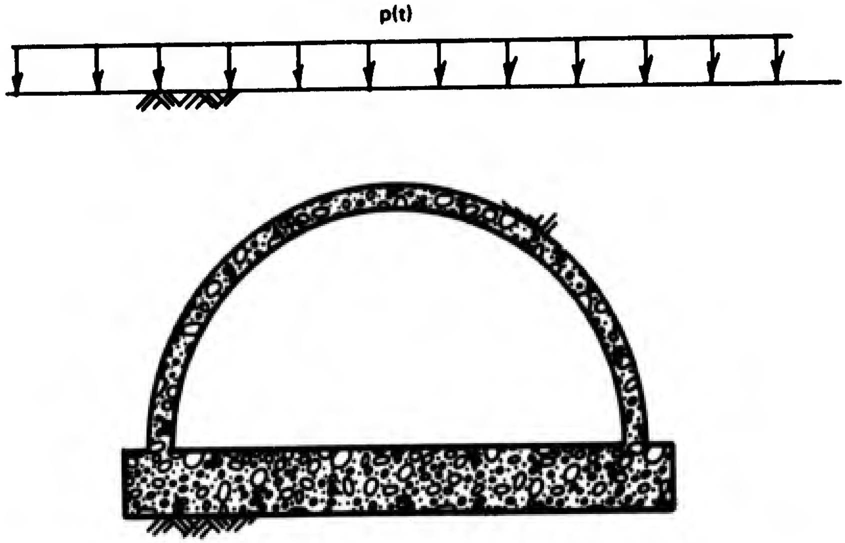

(a) Integral floor and shell.

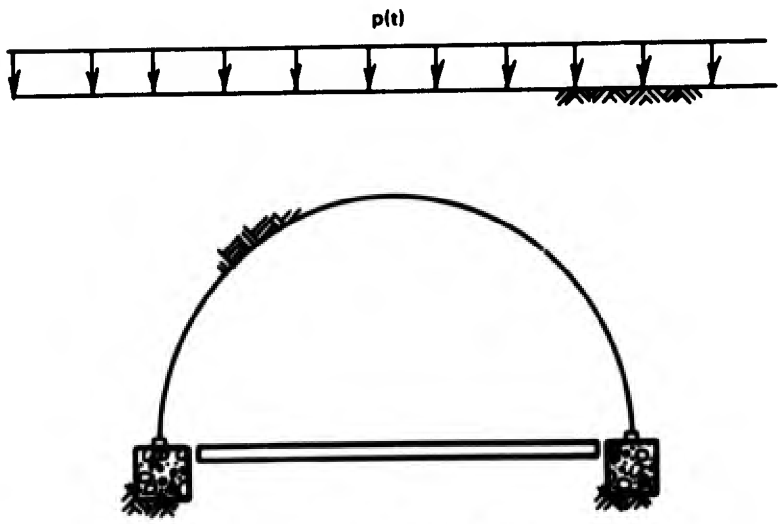

(b) Separate floor and footing.

Figure 5.9. Alternative buried arch geometries.

Large moments in the arch are avoided by use of footings separated from the floor slab as indicated in Figure 5.9b. The additional advantage is that the accelerations of the floor slab are significantly reduced. Unfortunately, with the configuration of Figure 5.9b, the arch and footings may experience large downward deflections with respect to the floor slab. As a consequence, the use of arches as shelter is usually limited to nuclear blasts of less than about 150 psi overpressure unless excellent foundation conditions prevail. This is especially true where there is a likelihood of multiple loading.

One advantage of the punching action depicted is that it transfers load away from the structure to the surrounding soil. Thus, punching produces an effect equivalent to that of backpacking with horizontal cylinders. A combination of backpacking and punching may enhance the load capacity of fully buried arches at the discretion of the designer.

For practical purposes, an arch with footings behaves as a hinged arch, the deflection modes of which are shown in Figure 5.10. When an arch is covered, most of these modes are difficult to excite and, even if they can be excited, they damp out quickly. As would be expected, the added mass of an earth cover tends to increase the periods of the various modes. Contrariwise, the stiffening effect of the soil tends to decrease these sames periods.

Experiments show that buried metal arches vibrate in the first inextensional symmetrical mode under compressive excitation in the direction of the axis of symmetry.[5.19] The stiffening effect of the soil is more influential on the period than the added mass. Another effect of the confining soil is to quickly damp out most structural vibrations.

As would be expected, arch response is highly dependent on the soil stiffness (modulus). Small reductions in density result in large increases in deflection. The influence of soil modulus, E_s, and other principal variables may be seen on studying the charts of Figure 5.11.[5.20] These charts are for a standard 24-foot by 48-foot circular arch buried in a nonsaturated, uniform, granular soil field. The charts are based upon an approximate theory and are intended only to show the influence of the dominant parameters and to effect preliminary designs.

A study of the referenced charts and of available experimental data[5.19, 5.21-5.25] leads to the realization that:

1. The maximum relative deflection occurs in a few transit times.

2. A large increase in footing width is necessary to permit a relatively small increase in load capacity for a given limit deflection.

3. Assuming ordinary granular soil conditions, surface loads above about 150 psi cannot be resisted if the allowable relative deflection between the footing and the floor slab is limited to 2 inches.

4. A small increase in pressure will occur within the shelter equivalent to the adiabatic compression due to the reduction in volume caused by the footings punching into the supporting soil.

Next to punching of the footings, failure of the end walls ranks as the most troublesome problem in the design of arch shelters. Domed ends or thick end walls may be used with reinforced concrete arches.[5.26] With corrugated metal arches, a stiffener at midheight tied to dead-men in the backfill has been found to be an effective method of strengthening end walls.[5.27]

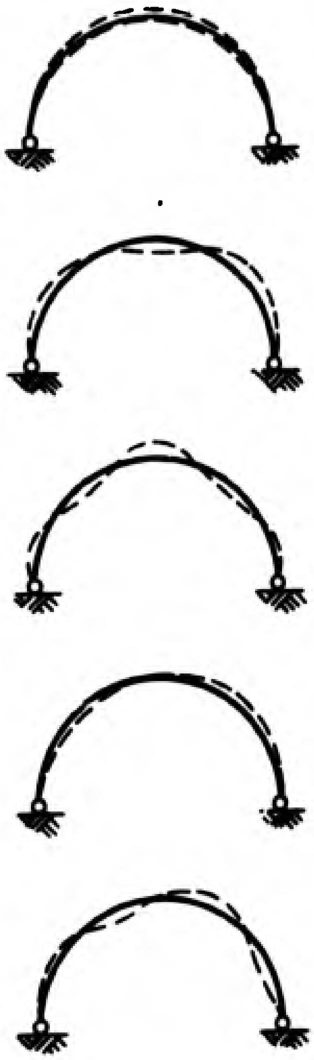

I. Extensional Mode

Sometimes called compression mode

II. Inextensional Modes

A. Symmetrical

1. First symmetrical (bending-compression)

2. Second symmetrical (bending-compression)

B. Asymmetrical

1. First asymmetrical (lateral bending mode, flexural mode, deflection mode)

2. Second asymmetrical

Figure 5.10. Deflection modes of a hinged arch.

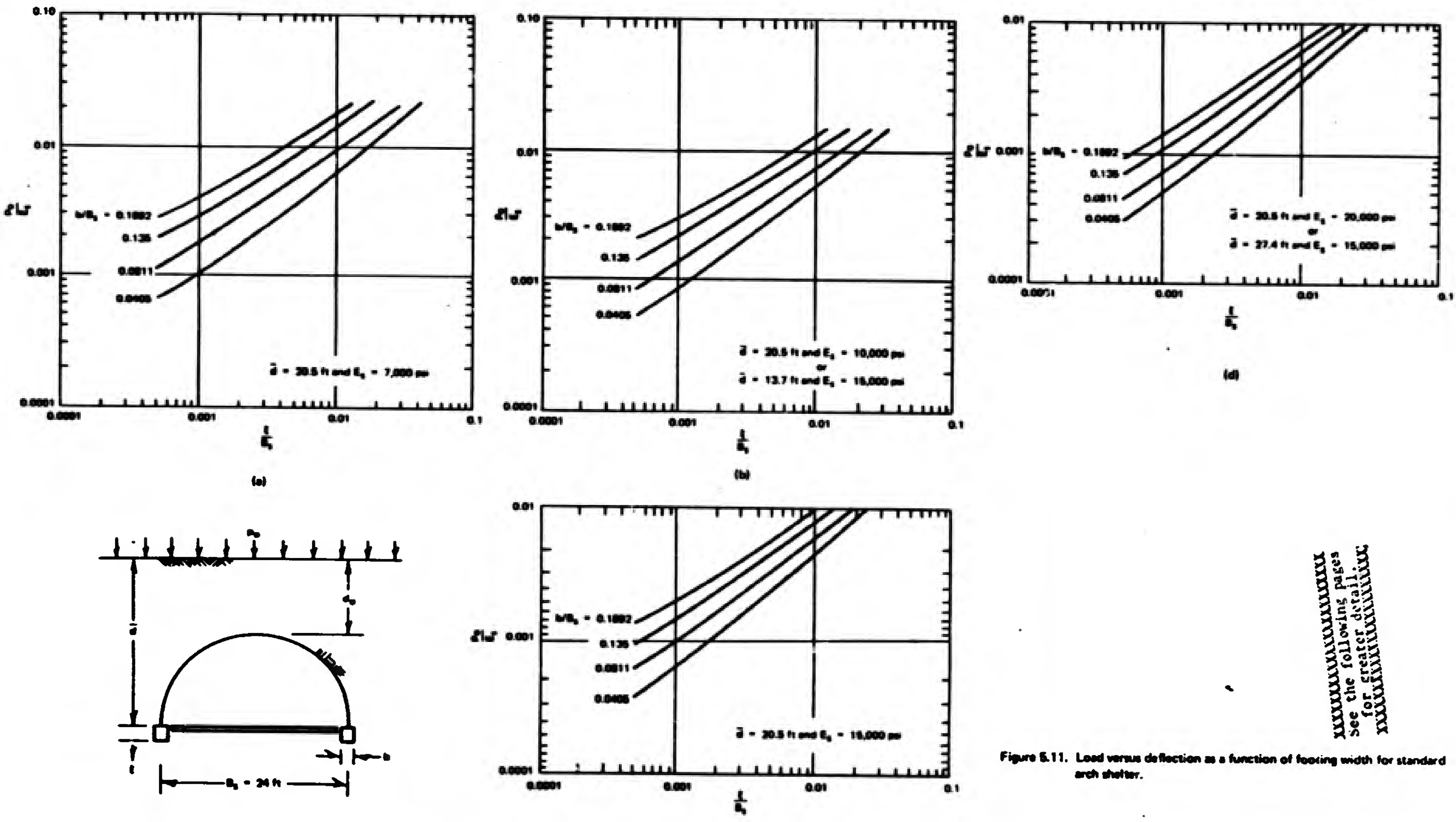

125.1

125.2

XXXXXXXXXXXXXXXXXXXXXX
See the following pages
for greater detail.
XXXXXXXXXXXXXXXXXXXXXX

Figure 5.11. Load versus deflection as a function of footing width for standard arch shelter.

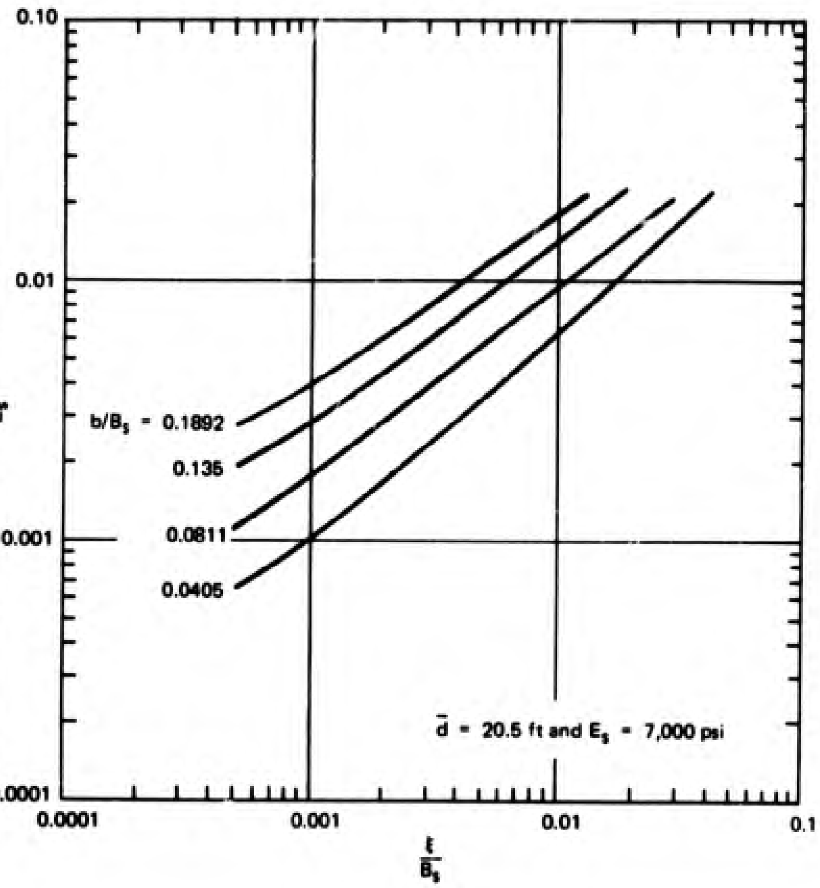

(a)

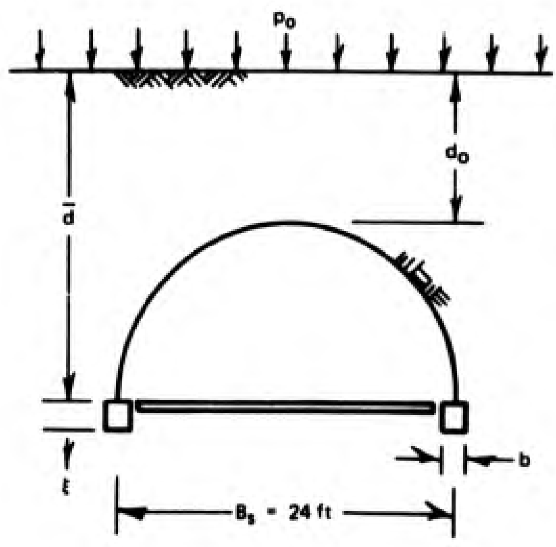

125.1

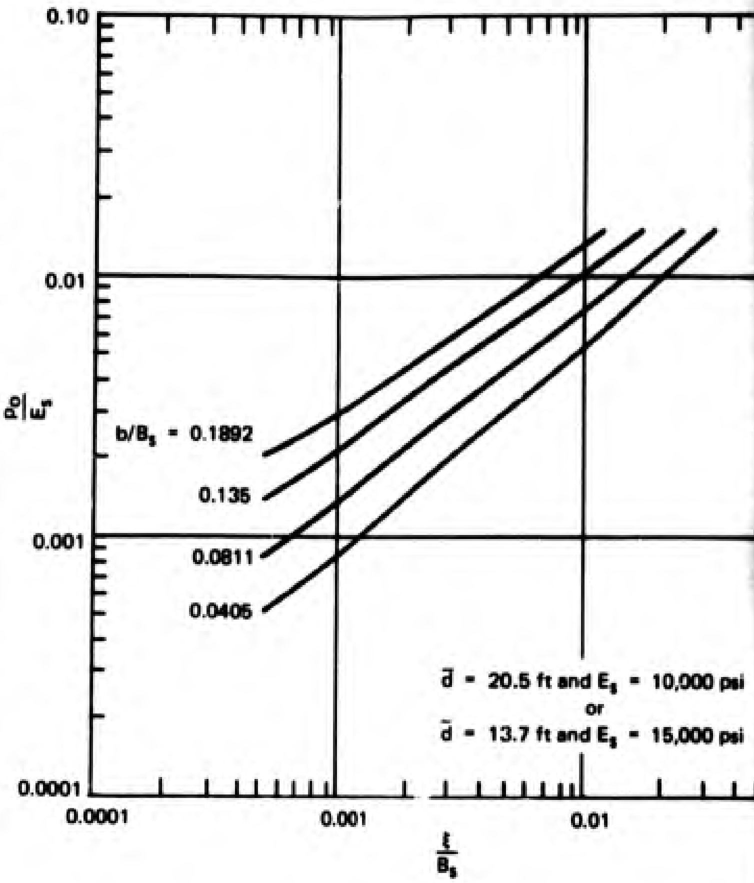

(b)

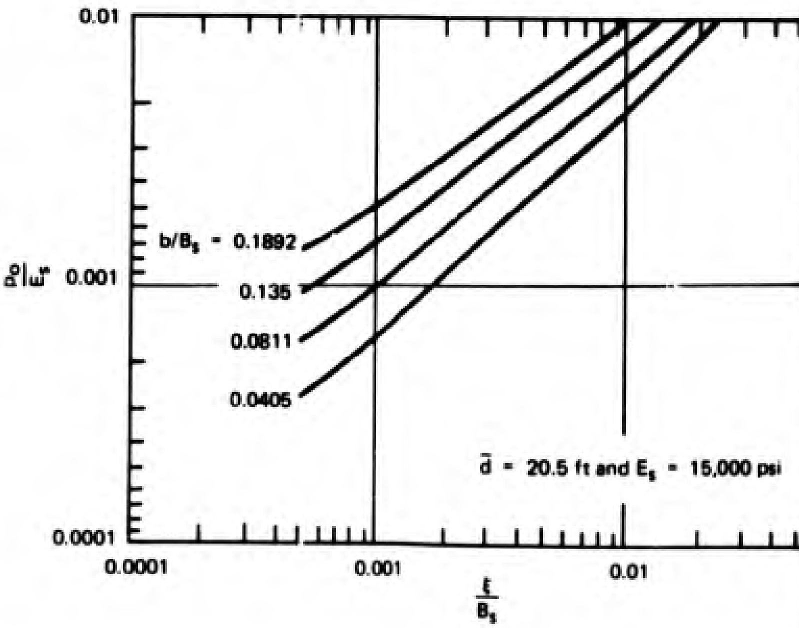

(c)

125.2

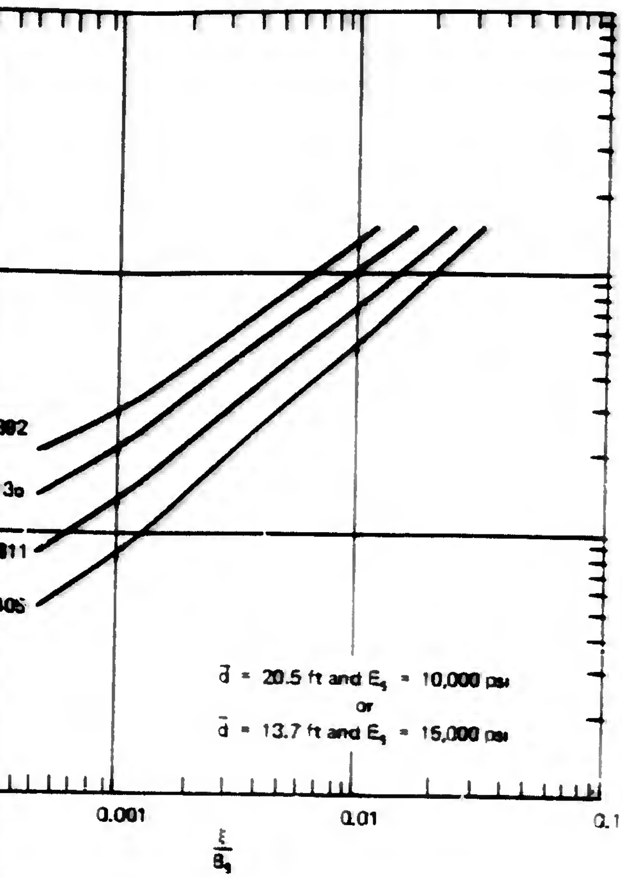

(b)

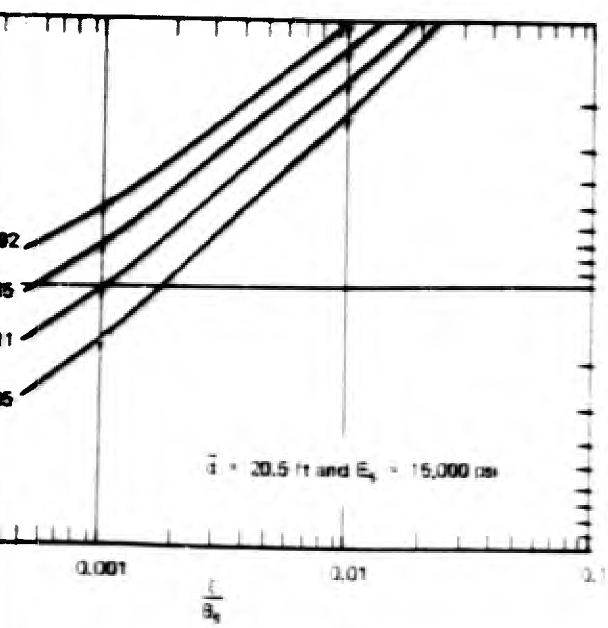

(c)

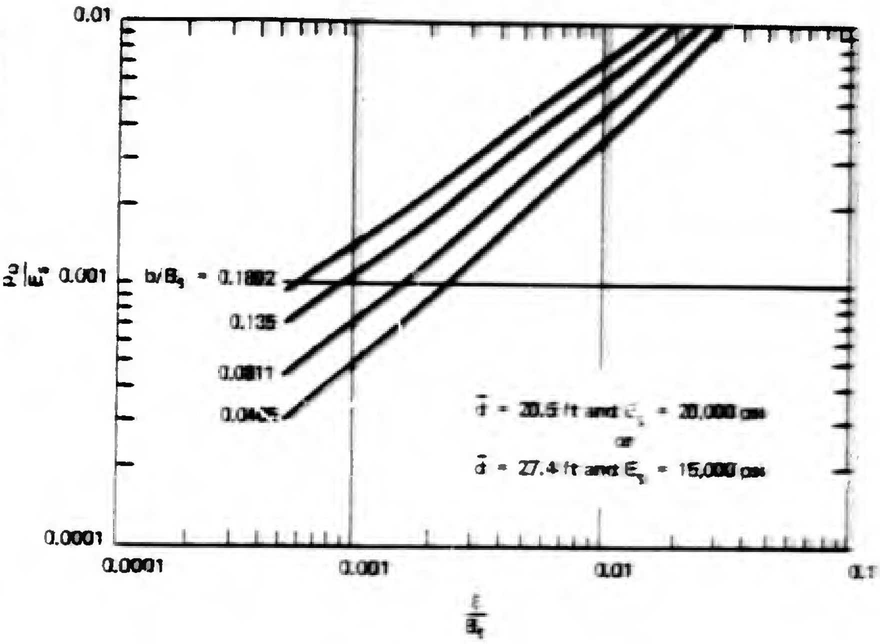

(d)

Figure 5.11. Load versus deflection as a function of footing width for standard arch shelter.

Maintaining the integrity of seals on multiple loading or on overload is also a difficult problem with arch shelters. Considering the problems of maintaining the integrity of the seals between the footings and the floor slab and other limitations, it would seem preferable to avoid the use of arches as shelters for resisting the effects of nuclear weapons. Cylinders or other "closed" geometries are preferable for most such applications.

5.5 DOMES, SPHERES AND THREE-DIMENSIONAL STRESS CELLS

Above-ground spherical structures are known to have greater inherent strength than cylindrical ones. Shell theory shows that the strength of a sphere in compression is twice that of a cylinder.[5.28] The buckling strength is usually two or more orders of magnitude higher, depending on the thickness-to-radius ratio.[5.29] Thus, one might expect the sphere to be stronger than the cylinder in the buried state. This is not necessarily the case because, for a given radius and thickness, spheres deflect less than cylinders and may not develop active and passive arching stresses in the soil to the same degree that cylinders do.

Tests on models of buried domes[5.30] have shown that soil is effective in preventing buckling in the lower modes. The soil support seems to negate the effects of geometric irregularities in the shell. Available data indicate that there are three general ranges of behavior:

1. Buckling near the energy load (lower buckling load) for thin cover ($d_o \lesssim 0.25R$).
2. Buckling near the theoretical elastic buckling load for medium cover ($0.25R \lesssim d_o \lesssim 0.65R$).
3. Yielding for thick covers ($d_o \gtrsim 0.65R$).

Of course, the occurrence and limits of these stages will be influenced by the stiffness of the shell, the compaction of the soil, and other system parameters. The transitional buckling of uniformly loaded spherical caps with clamped edges has been discussed by Gjelsvik and Bodner.[5.31] Inelastic buckling of shallow spherical shells has been treated by Lee, Ariman, and Hoffman.[5.32]

For fully buried domes, the radius-to-thickness ratio required for resisting the compression loads at overpressures greater than about 100 psi will be sufficient to result in yielding failure. The buckling load can be determined by the computer program described in Reference 5.33.

As with cylinders, care should be exercised in using backpacking over domes to assure that the buckling load remains considerably above the yield load.

Tests on rigid model domes in a granular soil field indicated that the peak radial on-structure stress, passive arching, and free-field stress are about equal for static or blast loading.[5.34] In the referenced tests

1. The peak total vertical load on the dome was 1.02 times the peak load produced by the soil stress over the projection of the dome cross section. (This agrees with results from the arching theory of Section 3.3.6 as applied to the conditions of the experiment.)

2. On unloading, this value was 1.38 due to locking-in of horizontal soil stress.

3. Approximately 20% of the total vertical load to the dome was derived from the tangential component of the on-structure stress on the dome. A friction reducing membrane at the interface reduces the load to the dome.

A fourth order polynomial was used to approximate the load on a rigid dome.

Approximate relations for the natural period, deflection, and ultimate strength of a buried dome are given in Reference 5.35. The loading on a buried dome would be expected to be of the same form and magnitude as the load on the upper portion of a buried sphere.

At shallow depths of cover, the interface pressure depends on the rise-to-span ratio of the dome as indicated in Figure 5.12.[5.36] For depths of cover above about 1.5 diameters, arching reaches a maximum of about 87%. The results shown hold for a dome in a granular soil which can move or punch relative to the soil, thereby developing maximum arching.

To the knowledge of the author, the only tests performed on buried spheres are those on a spherical soil stress cell.[5.37] There have been several theoretical investigations of confined spheres.[5.27, 5.38] These studies show that the stresses in the liner and in the medium are highly dependent on the properties of the liner and the medium. Mow has found that:[5.39]

1. Whereas the stresses in a stiff sphere may be reduced by increasing the thickness, the stresses in a soft liner may actually increase with increase in thickness.

2. The dynamic stress concentration factor around a spherical cavity in an elastic medium is approximately two.

3. Dynamic stress concentration factors are about 20 to 30% higher than their corresponding static values.

By virtue of their double curvature, steel and reinforced concrete spheres are rigid relative to the stiffness of the usual granular soil field.

The compressive stress in the wall of a spherical shell of thickness, t, under external pressure, p, is

$$\sigma = \frac{pr}{2t}$$

No relation is known for the buckling strength of confined spheres; however, the buckling load of unconfined spheres under hydrostatic pressure is[5.29]

$$p_{cr} = \frac{2}{\sqrt{3(1-\nu^2)}} E\left(\frac{t}{R}\right)^2$$

This may be used as a conservative design value since spheres are inherently stiff structures; their efficient use as protective shelters requires the use of backpacking. No test data are available for spheres with backpacking; however, from theoretical considerations it is clear that truly phenomenal load capacities are possible with properly backpacked spheres in granular fields. This is possible because of the development of arching in two directions and because of the relatively high buckling and hydrostatic strength of spheres.

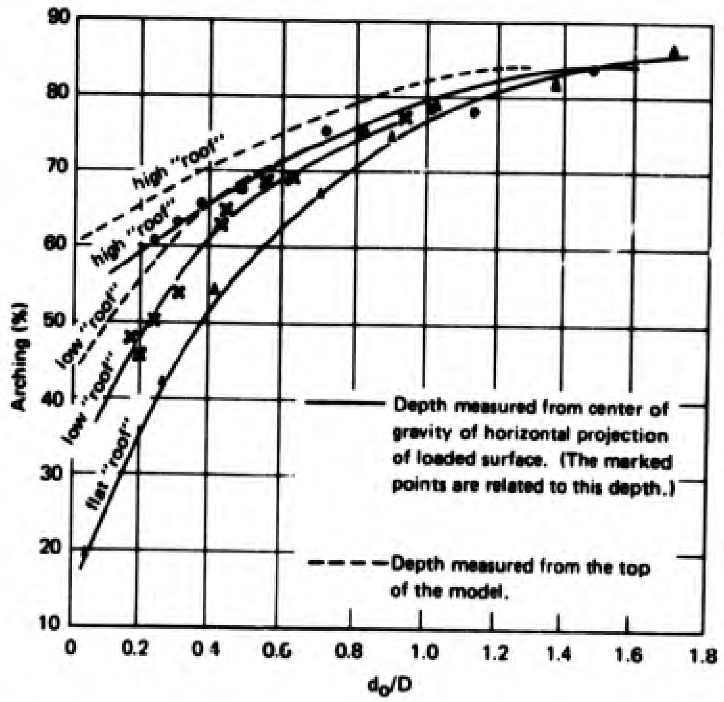

Figure 5.12. Arching versus depth and shape. (From Reference 5.36)

The design methodology for spheres parallels that for horizontal cylinders as given in Section 4.4. The theory of solid, rigid inclusions is given in Reference 5.37.

The direct stress concentration factor from the theory is shown in Figure 5.13. This and similar curves for lateral stress and shear stress[5.37] show that the induced stress is insensitive to changes in the stiffness of the confining media provided the ratio of the modulus of the confining media is greater than about 10. It is this characteristic and the fact that the stress is constant in any given direction through a uniform rigid sphere that lends them to use as soil stress cells.

A recently developed stress cell made from plastic cue-balls with embedded strain gages has proven effective for measuring the complete state of stress at a point in a granular field under static loading.[5.37] The data also indicate that under some circumstances the cell is effective in measuring the state of stress with time under dynamic load conditions. To achieve good dynamic measurements, the rise time and the mass must be such that relative displacement due to stiffness and inertial mismatch is negligible.

5.6 BOX, FRAME, AND OTHER SHELTERS

One may have occasion to use box, frame, diaphragm, or other configurations as buried protective shelters. The purpose of this section is to provide general information and references on these shelter types.

Box structures have been used extensively in field tests as instrumentation shelters to provide protection from weapons effects corresponding to overpressures of the order of 15 psi.[5.40-5.44] Most of these shelters were relatively small and had their roof tops flush with the surface of the ground. Where additional radiation protection is required, earth cover can be provided. Earth cover has the added advantage that even small depths decrease the high frequency content and the peak magnitude of induced accelerations.[5.45]

Studies of the pressure distribution on a simply supported buried flat plate subjected to static or dynamic loads have shown that:[5.46]

1. The ratio of static soil stress to overpressure is higher during unloading than during loading.
2. Above a certain load, the distribution and variation of interface pressure with time remains essentially the same.
3. Interface soil stresses are greater near the edges than at midspan.

The tendency for the stress to be relieved at midspan will, of course, improve as the depth-of-burial-to-span ratio increases.

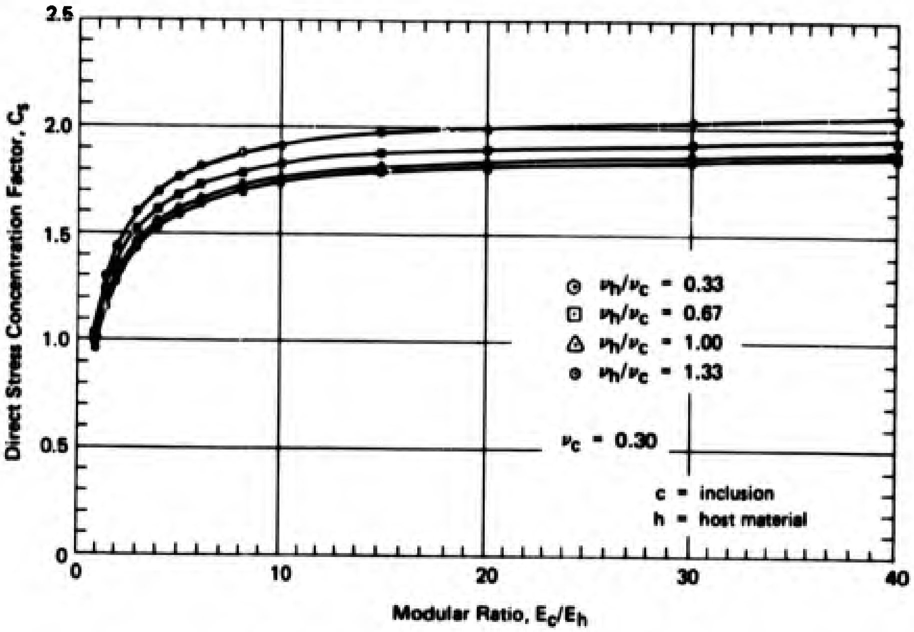

Figure 5.13. Direct stress concentration factor, C_s.

If the depth of cover is sufficient, arching (calculated by the relations of Section 3.3.6) can be developed, thus, enhancing survivability. Estimating the arching over a box structure is complicated by the fact that the side walls are usually stiff with respect to the soil. As a consequence, load is relieved near the center of the roof and is attracted to the perimeter.[5.47] Loading on the side walls will be K_0 times the free-field pressure at the mean depth.[5.48] The upward loading on the floor has about the same magnitude as the load on the roof, although the rise time would be expected to be longer. As with other configurations, load redistribution can be accomplished by the proper backpacking.

Once the loads have been determined, the structural elements may be designed by the methods of Reference 5.49. If greater strength is needed than can be economically achieved with slabs, shallow shells may be employed.[5.50, 5.51] Shallow shells are also useful in multistory, multibay underground structures as indicated in Figure 5.14.

What has been said regarding box structures is also true in essence for buried frame and other parallelepiped structures. It is also true of enclosures with diaphragm roofs, although, such roofs use the strength of the material better than flexural elements.[5.52] Toroids, cyclides, and certain other shells of revolution would constitute good buried shelters; however, the horizontal and vertical cylinder are preferable for most applications.

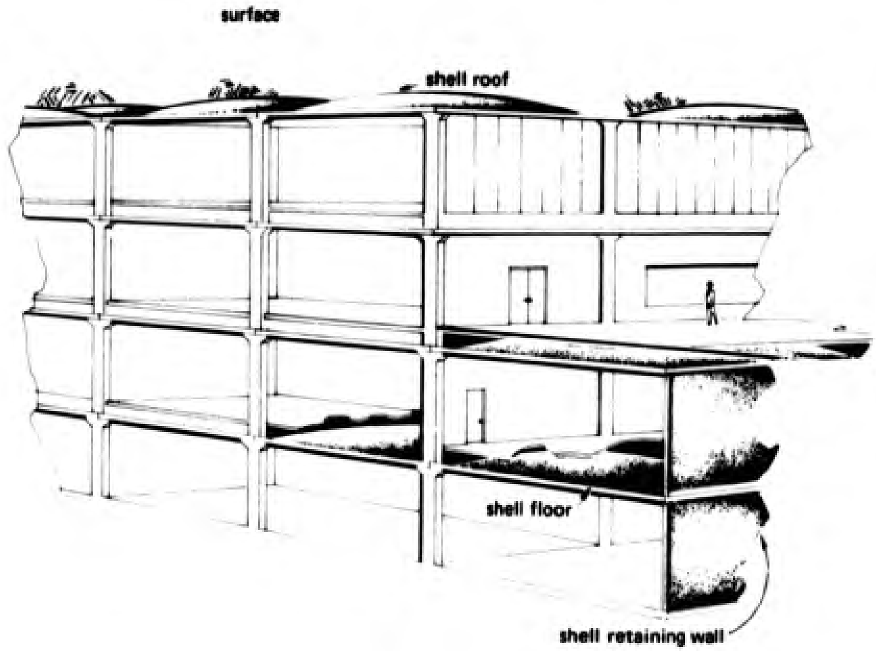

Figure 5.14. Funicular shells in a multistory, multibay building.

5.7 REFERENCES

5.1. Classified reference.*

5.2. Classified reference.

5.3. Defense Atomic Support Agency. Project Officers Report POR-2108 (WT-2108): Operation PRAIRIE FLAT: Strong ground shock measurements, by H. V. Hoffman, F. M. Sauer, and B. Barclay. Washington, D. C., Apr. 1971. (Contract DASA 01-68-C-0082)

5.4. Naval Civil Engineering Laboratory. Contract Report CR 69.015: Vulnerability of buried cables to nuclear detonations, by J. Karagozian. Los Angeles, Calif., John Karagozian, Consulting Engineer, Mar. 1969. (Contract N62399-69-C-0021)

5.5. University of Illinois. Department of Civil Engineering. Final Report on Contract NBy-32279: Attachments and connections to buried structures, by J. D. Haltiwanger, et al. Urbana, Ill., Oct. 1965. (AD 475427)

5.6. Army Engineer Waterways Experiment Station. Technical Report No. S-69-3: A model study of dynamically loaded square footings on dry sand, by J. K. Poplin. Vicksburg, Miss., Mar. 1969.

5.7.———. Technical Report No. S-70-3: Effect of saturation on dynamic response of footings in sand, by J. K. Poplin. Vicksburg, Miss., May 1970.

5.8.———. Technical Report No. S-69-6: Effects of relative density and pulse duration on dynamic response of footings buried in sand, by J. K. Poplin and P. F. Hadala. Vicksburg, Miss., July 1969.

5.9. K. Terzaghi. Theoretical soil mechanics. New York, Wiley, 1943.

5.10. Naval Civil Engineering Laboratory. Technical Report R-664: Dynamic behavior of strip and spread footings buried in sand, by D. G. True and C. R. White. Port Hueneme, Calif., Feb. 1970. (AD 7[illegible]216)

5.11. . Technical Report R-536: Static and dynamic bearing tests on a strip footing in saturated sand, by C. R. White. Port Hueneme, Calif., June 1967. (AD 654712)

5.12. Army Engineer Waterways Experiment Station. Technical Report No. S-68-8: Effect of shallow burial on load–displacement–time response of square footings in clay under impulsive loading, by E. B. Perry. Vicksburg, Miss., Nov. 1968.

* Classified reference list available to qualified requestors.

5.13. Air Force Weapons Laboratory. Technical Report No. AFWL-TR-65-160: Nonlinear static arching for vertically buried prismatic structures, by P. A. Abbott. Kirtland Air Force Base, N. M., Aug. 1966. (Contract AF 29(601)-6002) (AD 801487)

5.14. Naval Civil Engineering Laboratory. Technical Report R-668: Response of buried capsules in the high-overpressure region, by R. J. Odello and J. R. Allgood. Port Hueneme, Calif., Apr. 1970. (AD 705990)

5.15. Classified reference.

5.16. Classified reference.

5.17. Classified reference.

5.18. Classified reference.

5.19. Naval Civil Engineering Laboratory. Technical Report R-375: Shallow-buried model arches subjected to a traveling-wave load, by J. R. Allgood and R. H. Seabold. Port Hueneme, Calif., Oct. 1965. (AD 622552)

5.20.———. Technical Report R-539: Predicting blast-induced body motions of a buried structure with footings, by J. R. Allgood and W. O. Carter. Port Hueneme, Calif., Aug. 1967. (AD 657839)

5.21. Army Engineer Waterways Experiment Station. Technical Report No. 1-660: Model study of a buried arch subjected to a dynamic loading, by R. K. Tener. Vicksburg, Miss., Nov. 1964.

5.22. D. R. Denton and W. J. Flathau. "Model study of dynamically loaded arch structures," American Society of Civil Engineers, Proceedings, Journal of the Engineering Mechanics Division, vol. 92, no. EM3, June 1966, pp. 17-32.

5.23. Army Engineer Waterways Experiment Station. Technical Report No. 1-807: Similitude study of flexible buried arches subjected to blast loads, by J. R. Balsara. Vicksburg, Miss., Jan. 1968.

5.24.———. Miscellaneous Paper No. N-71-3: Dynamic tests of a model flexible-arch-type protective shelter, by T. E. Kennedy. Vicksburg, Miss., Apr. 1971.

5.25.———. Technical Report No. N-70-6: Dynamic response of a model buried field shelter, Project LN314, Operation PRAIRIE FLAT, by T. E. Kennedy. Vicksburg, Miss., Mar. 1970.

5.26. Naval Civil Engineering Laboratory. Technical Report R-191: Design for a cast-in-place concrete shelter, by J. R. Allgood, R. M. Webb, and R. F. Swalley. Port Hueneme, Calif., Dec. 1962. (AD 292930)

5.27. Classified reference.

5.28. W. Flügge. Stresses in shells. Berlin, West Germany, Springer-Verlag, 1960.

5.29. ———. Handbook of engineering mechanics. New York, McGraw-Hill, 1962.

5.30. Z. Getzler and L. Lupu. "Experimental study of buckling of buried domes," American Society of Civil Engineers, Proceedings, Journal of the Soil Mechanics and Foundations Division, vol. 95, no. SM2, Mar. 1969, pp. 605-624.

5.31. A. Gjelsvick and S. R. Bodner. "Nonsymmetrical snap buckling of spherical caps," American Society of Civil Engineers, Proceedings, Journal of the Engineering Mechanics Division, vol. 88, no. EM5, Oct. 1962, pp. 135-165.

5.32. University of Notre Dame. Technical Report No. THEMIS-UND-69-11: Inelastic buckling of shallow spherical shells, by L. H. N. Lee, T. Ariman, and R. E. Hoffman. Notre Dame, Ind., Jan. 1970. (Contract N00014-68-A-0152)

5.33. Air Force Weapons Laboratory. Technical Report No. AFWL-TR-69-146: A computer program for the elastic-plastic analysis of DOME structures and arbitrary solids of revolution subjected to unsymmetrical loadings, by A. P. Capelli, G. L. Agrawal, and V. E. Romero. Kirtland Air Force Base, N. M., Feb. 1970. (Contract F29601-69-C-0024) (AD 866588)

5.34. ———. Technical Report No. AFWL-TR-70-106: Investigation of buried domes, phase 3. Dynamic pressure distribution of small rigid domes, by R. Cramond. Kirtland Air Force Base, N. M., Dec. 1970. (Contract F29601-68-C-0009)

5.35. Classified reference.

5.36. Z. Getzler. "Arching in soil above buried structures," presented at Mechanics Division Seminar, University of California, Los Angeles, Calif., Nov. 19, 1970.

5.37. Naval Civil Engineering Laboratory. Technical Report R-758: Evaluation of a three-dimensional stress cell for granular soils, by T. K. Lew. Port Hueneme, Calif., Feb. 1972.

5.38. A. Coutinho. "Theory of an experimental method for determining stresses, not requiring an accurate knowledge of the modulus of elasticity," in International Association of Bridge and Structural Engineering, Publications, vol. 9, Zurich, Switzerland, 1949, pp. 83-93.

5.39. RAND Corporation. Memorandum RM-3962-PR: Dynamic response of lined and unlined underground openings, by C. C. Mow. Santa Monica, Calif., Mar. 1964. (AD 602456)

5.40. E. T. Selig, K. E. McKee, and E. Vey. "Underground structures subjected to air overpressure," American Society of Civil Engineers, Proceedings, Journal of the Engineering Mechanics Division, vol. 86, no. EM4, Aug. 1960, pp. 87-103.

5.41. Holmes and Narver, Inc. Design manual, AEC test structures, vol. 1. Nuclear weapons effects and blast loading. Los Angeles, Calif., Dec. 1961. (Contract AT(29-2)-20)

5.42.———. Design manual, AEC test structures, vol. 2. Structural response characteristics under dynamic loads. Los Angeles, Calif., Dec. 1961. (Contract AT(29-2)-20)

5.43.———. Design manual, AEC test structures, vol. 3. Design of blast resistant structures. Los Angeles, Calif., Dec. 1961. (Contract AT(29-2)-20)

5.44. Defense Atomic Support Agency. Report DASA 1285(V): Nuclear geoplosics, a sourcebook of underground phenomena and effects of nuclear explosions. vol. 5. Effects on underground structures and equipment, by J. L. Merritt and N. M. Newmark. Washington, D. C., May 1964. (Contract DA-49-146-XZ-027)

5.45. Army Engineer Waterways Experiment Station. Technical Report No. N-71-1: In-structure motion studies for shallow buried protective facilities, phase IIb, by T. E. Kennedy. Vicksburg, Miss., Feb. 1971.

5.46.———. Miscellaneous Paper No. N-68-4: Pressure distribution on a buried flat plate subjected to static and airblast overpressures, by J. P. Balsara and R. S. Cummins. Vicksburg, Miss., Oct. 1968.

5.47. W. B. Truesdale and E. Vey. "An investigation of panel-arching effects in noncohesive soil," in Proceedings of the Symposium on Soil-Structure Interaction, Tucson, Arizona, June 8-11, 1964. Tucson, Ariz., University of Arizona, Sept. 1964, pp. 349-355.

5.48. Air Force Special Weapons Center. Technical Documentary Report No. AFSWC-TDR-62-138: Air Force design manual: Principles and practices for design of hardened structures, by N. M. Newmark and J. D. Haltiwanger. Kirtland Air Force Base, N. M., Dec. 1962. (Contract AF 29(601)-2390) (AD 295408)

5.49. J. R. Allgood and G. R. Swihart. Design of flexural members for static and blast loading. Published jointly by American Concrete Institute, Detroit, Michigan and the Iowa State University Press, Ames, Iowa, 1970. (ACI monograph no. 5)

5.50. Naval Civil Engineering Laboratory. Technical Report R-693: Concrete funicular shells for floors and roofs, by R. J. Odello and J. R. Allgood. Port Hueneme, Calif., Sept. 1970. (AD 712754)

5.51.———. Technical Report R-714: Economics of shallow concrete shells, by R. J. Odello and J. R. Allgood. Port Hueneme, Calif., Mar. 1971. (AD 721689)

5.52. H. P. Harrenstein and R. H. Gunderson. "Yielding membrane concepts," in Proceedings of the Symposium on Soil-Structure Interaction, Tucson, Arizona, June 8-11, 1964. Tucson, Ariz., University of Arizona, Sept. 1964, pp. 430-448.

6.0 OPTIMIZATION

6.1 GENERALITIES OF PROBLEM

Optimization of a soil–structure system should be treated as an integral part of the optimization of a total facility. A reasonable procedure to follow is

1. Set down the objectives
2. Select the input parameters
3. Write the objective function
4. Define the system constraints
5. Set down the system requirements
6. Make "external" analyses
7. Construct functional equations of subsystems
8. Combine these into a system model
9. Program the model and exercise the resulting computer program.

Such a development has been accomplished;[6.1] however, much of the analysis is for a particular macrosystem and is not of general interest. The following paragraphs present only those aspects of the overall problem associated with the selection of an optimal soil–structure system.

Optimization of a single geometry is usually a relatively minor matter. For a dry site, the optimum configuration will result when the load transmitted to the structure is minimum. For example, this is achieved for a horizontal cylinder when backpacking is used and when the depth of cover over the inclusion equals the cylinder diameter. One diameter is usually the minimum depth of cover for which maximum arching can be developed.

The specific problem addressed here is that of finding the best geometry (shape), method of construction (section characteristics), depth of burial, and backpacking for a given loading and site based upon specified volume requirements and unit costs. This constitutes a generalization of the problem of optimizing a single configuration.

6.2 OPTIMIZATION PROCEDURE

The objective of this section is to outline the logic employed in an existing computer program for selecting specific media–structure configuration options for generating near optimum designs to resist a specified threat. A suitable objective–function statement is that the cost of the sum of the components of the selected system shall be minimum. To accomplish the indicated objective, eclectic judgments and approximate relationships were utilized to achieve a tractable problem.

The general logic followed is indicated in the flow diagram of Figure 6.1. Combinations of possible media properties, geologic profiles, and structural geometries utilized may be limited by: (a) choosing representative profiles, and (b) limiting the structural geometries considered to simple shapes. These desiderative restrictions permit achieving rational designs of the more practicable configurations as candidate facility systems.

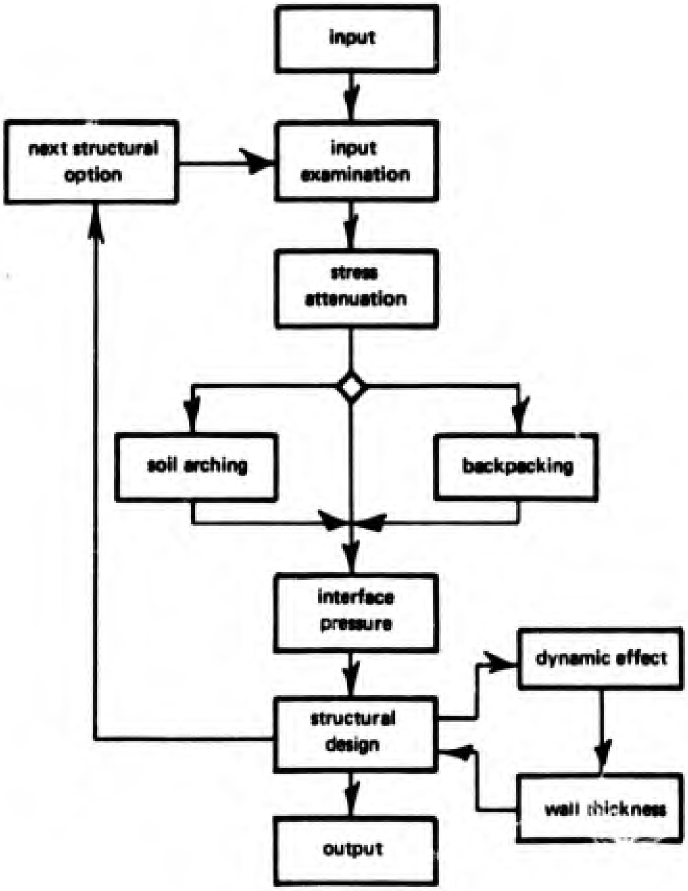

Figure 6.1. General flow diagram.

6.2.1 Structural Analysis Methodology

The soil–structure configurations chosen, Figure 6.2, provide suitable candidates. As may be seen, the options include the box, the arch, horizontal and vertical cylinders, and the sphere; some of these have alternate backpacking and water level conditions. These configurations constitute shapes that are practicable to build and for which at least some experimental information is available.

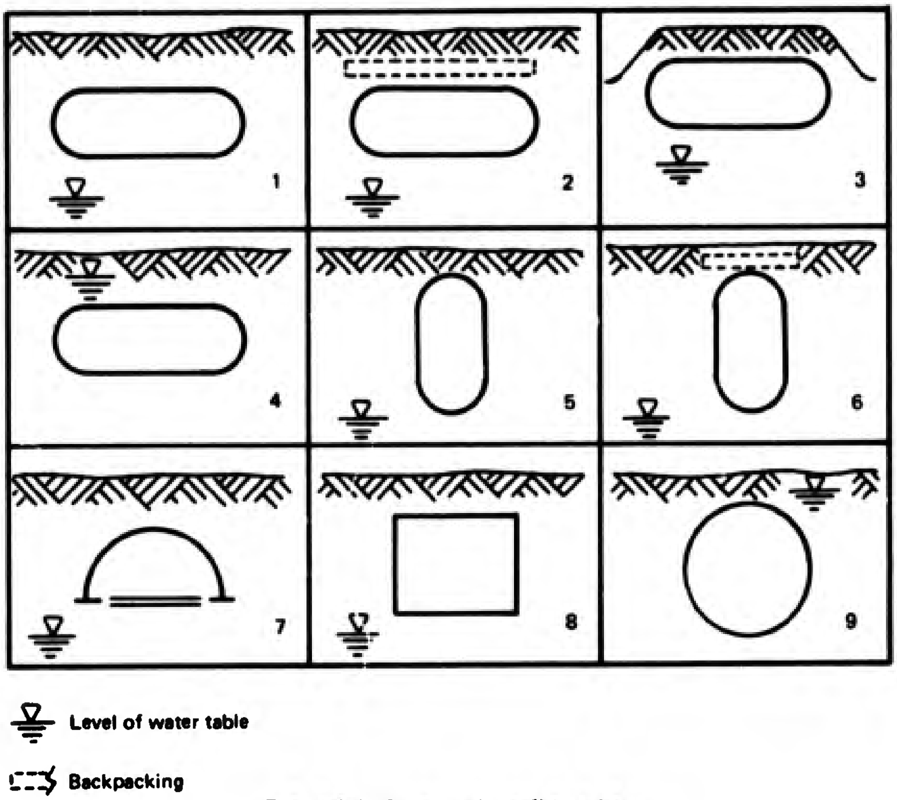

Figure 6.2. Structural configurations.

Configurations 7 and 8 from Figure 6.2, the shallow-buried arch and box, would only be acceptable at overpressures less than approximately 100 psi. Research has shown that at higher pressures the arch may punch downward excessively with respect to the floor slab, thus impairing the integrity of the water seals. Box structures become prohibitively expensive at intermediate or high overpressures, and curved structures are much more efficient at resisting applied loads. Configurations 1 and 5 are particularly suitable geometries for dry sites and intermediate overpressures. For higher overpressures, geometries with backpacking, such as configurations 2 and 6, would be expected to be more economical.

Where the water table is high, backpacking may not be effective; therefore, one must resort to placing the structure in the saturated medium as indicated in configuration 4 or to using earth mounding as indicated in configuration 3. For a high water table, mounding could also be used with the arch and the box; however, the drag forces could get very high, and it would be necessary to control the ambit to assure that the soil–structure system was not penetrated by a log, rock, or other missile. The configurations selected in Figure 6.2 are sufficient for present purposes; however, it may be desirable to modify or extend these depending on the specific application.

What constitutes the best structural option will depend upon the site conditions. Representative site profiles for one optimization program are indicated in Figure 6.3. In this program, approximate ground motions can be developed for each profile with either of two soils with distinctly different stress–strain properties.

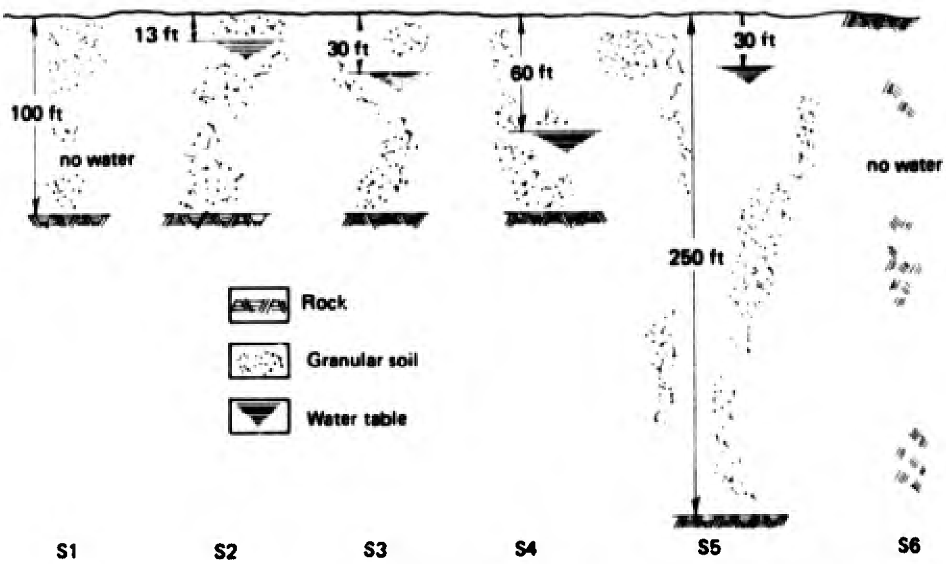

Figure 6.3. Site profiles.

A flow diagram of the steps involved in selecting qualified configurations is shown in Figure 6.4. As may be observed from this figure, various configurations are selected in sequence and examined with respect to the input parameters to eliminate certain configurations. Next, the attenuation factor corresponding to a trial depth of burial is defined, and this is used to determine the pressure at the depth of the structure. Subsequently, designs are generated for configurations not previously eliminated; these designs are "costed out" in later stages of the program to determine their relative cost effectiveness. A flow diagram of the structural design calculations is shown in Figure 6.5. Note that while certain parameters, particularly the depth of burial, are specified as input, they are subsequently changed in the process of achieving an optimum design.

6.2.2 Subroutines

Seven subroutines are used in the design of the various configuration options as follows:

1. ALPHAZ—Determines the attenuation of the stress wave
2. DYNFAC—Computes the dynamic load factor
3. SOARCH—Computes the arching in the soil
4. BKPKG—Designs the backpacking
5. HOST—Design
6. HRCC—Designs the horizontal reinforced concrete cylinder
7. CONCPL—Designs the reinforced concrete section based on equivalent stiffness

Other subroutines employed in the structural design and cost analyses are:

1. PTES—Tests for convergence of a ratio
2. VCAP—Designs domes in vertical cylinders
3. CALCA—Calculates the amount of arching
4. DYNRCC—Calculates the dynamic amplification factor
5. EXCAV—Calculates the cost of excavation
6. GROUT—Computes the cost of grouting
7. STRUCT—Computes the structure cost
8. BACKPK—Calculates the cost of backpacking, backfill, and mounding

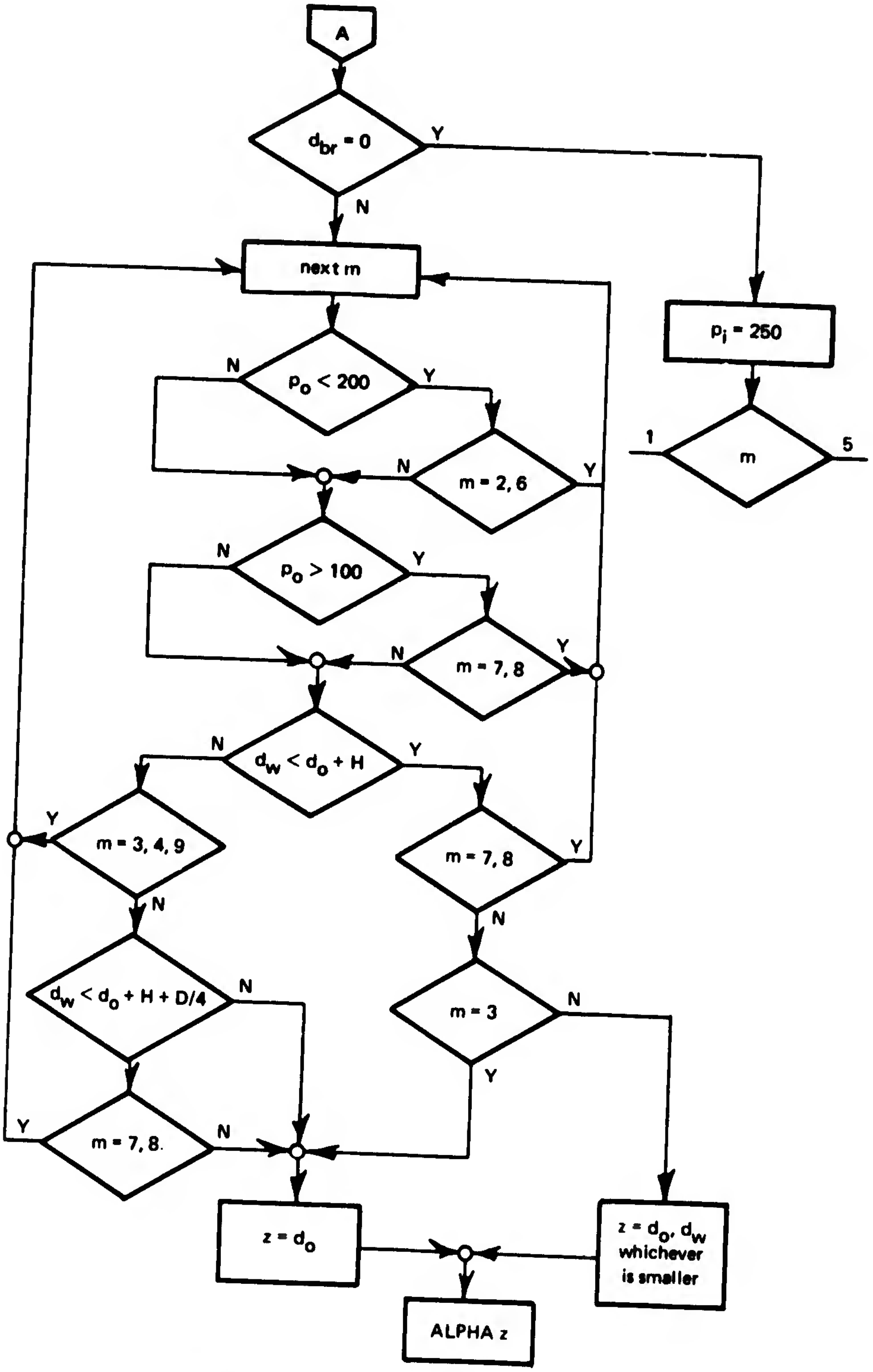

Figure 6.4. Qualification process for structure.

9. CDWATX—Calculates the cost of dewatering

10. CALCST—Calculates the cost of cavity excavation in rocks

11. TCOS—Computes the cost of material in construction

12. IT—Outputs a nominal thickness for steel plate

Detailed relations upon which these subroutines are based are given elsewhere[6.1, 6.2]; the manner in which they are used to effect specific configuration designs is indicated in Figure 6.5.

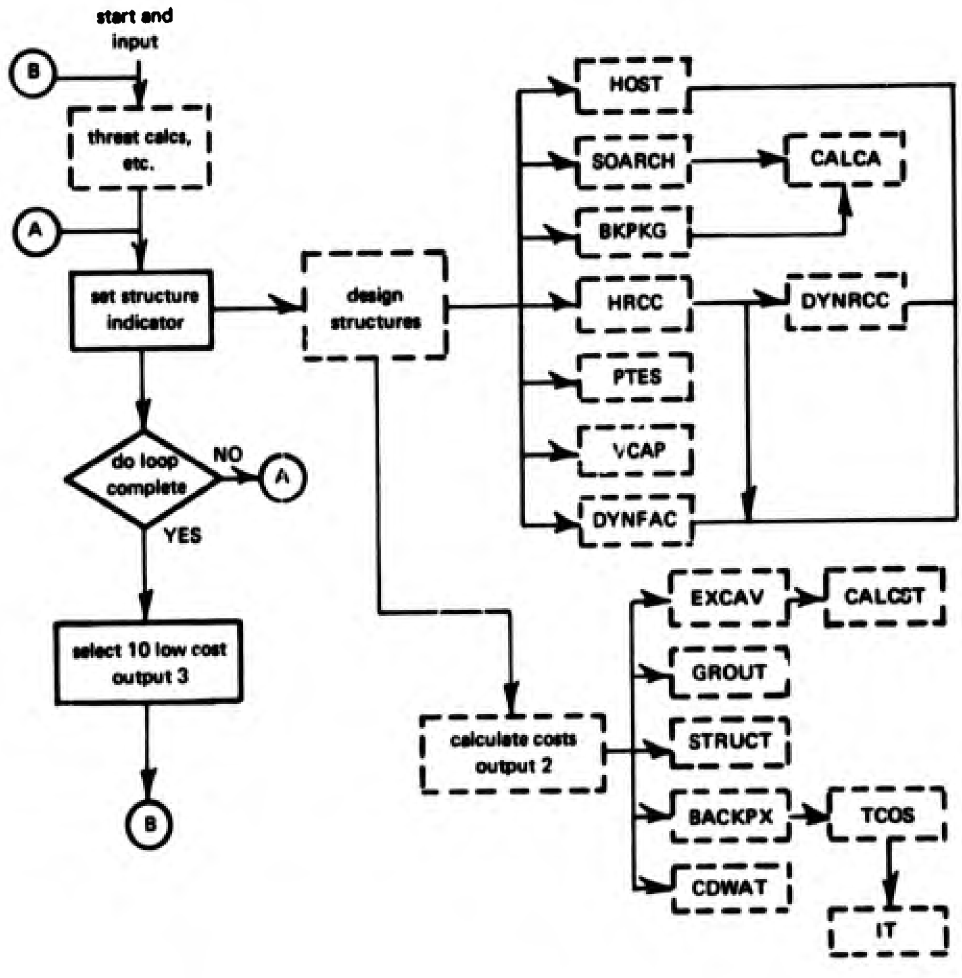

Figure 6.5. Flow diagram for structural design calculations.

6.2.3 Structure Cost Analysis

The total cost of a structure is considered to be the sum of the cost for each construction activity. Cost data are determined separately for different construction techniques, each of which is suboptimized for the best emplacement technique.

6.2.4 Computations and Output

For each structure three different construction methods—steel, reinforced concrete, and composite—are considered. As each structure is qualified and designed, the cost of various items is totaled, and the design parameters and costs are output. Other more detailed information may be output if desired.

Among the benefits of an optimization program is the ability to perform trade-off and sensitivity analyses. Such a program also permits easy determination of system effectiveness.

6.3 REFERENCES

6.1. Classified reference.*

6.2. Classified reference.

* Classified reference list available to qualified requestors.

7.0 SUMMARY

The state of knowledge of soil—structure interaction (S-S-I) as it pertains to facilities providing protection from the effects of nuclear weapons is discussed. It is emphasized that the soil is the component of principal importance, and that for economical designs, proper placement and knowledge of the soil properties are essential.

Considerable confusion has existed in S-S-I technology because of the variety of soil moduli and coefficients that have been employed. Media properties are reviewed and relationships between the various moduli and coefficients are developed. It is proposed that the secant confined compression modulus to the peak overpressure be adopted as the principal soil parameter in design.

Once the soil properties have been established, the next major problem is to determine the load that gets to the structure. Thus, modification of the air-blast-induced stress wave by the soil field, reflection and refraction, and transfer of the stress through and around the inclusion are discussed. This includes the potential occurrence of stress concentration and the determination of the dynamic load factor.

As is well known, the percentage of the surface load which reaches the structure is dependent on the relative stiffness of the structure and the inclusion. Reductions of up to a factor of 10 or more in the interface stress may be achieved by the simple expedient of placing backpacking in the overburden. Relations are given for designing the backpacking and for determining the arching over a buried structure with or without backpacking.

The equations for arching and backpacking are incorporated in a design procedure that is exemplified for horizontally buried cylinders. With suitable, rather obvious modifications, the procedure is applicable to structures of most any configuration. Difficulties do arise for structures with footings because the relative motion of such a structure is governed by the foundation configuration and characteristics. This problem has been treated, and it has been shown that, in general, closed structures (cylinders, spheres, toroids, etc.) are better for resisting high overpressures.

S-S-I aspects of configurations most likely to be of use in protective construction are discussed including the survivability of buried cables and pipes. The principles involved are also shown to be applicable to the design of soil stress gages. Design of an adequate soil stress gage is complicated by conflicting requirements. The gage must be stiff with respect to the host material for the output to be independent of changes in the soil modulus with stress; yet, the gage should have about the same stiffness as the soil to avoid relative displacement and arching around the gage from differential stress wave transmission. Successful operation will depend on the rise time of the stress front.

The state of development of finite element technology for the analysis of S-S-I problems is discussed, and two-dimensional and three-dimensional example solutions are given. It is pointed out that three-dimensional finite element technology is still in its infancy.

Optimization of soil—structure systems is also in its early stages of development. An existing program for converging on a near optimum design is briefly reviewed. There are other areas, such as the behavior of buried structures in fields with a high water table and the attendant possibility of liquefaction, for which information is lacking. Also, little data are available on arching in soils with cohesion and on the behavior of such systems. Likewise, information is lacking on slip and debonding and certain other areas of importance. The major remaining unknowns are those associated with determination of the ground motions.

Not withstanding the indicated unknowns, the basics of soil—structure interaction are now reasonably well understood.

8.0 ACKNOWLEDGMENTS

Material for this report has been drawn from a large number of sources, especially work done at the Waterways Experiment Station. Care has been taken to acknowledge the work of others by appropriate references; any oversight is regretted.

Appreciation is extended to those colleagues who have worked with the author over the years on various aspects of the soil–structure interaction problem. Particular thanks go to Mr. Stanley K. Takahashi, a co-project engineer, who provided the finite element solutions used in the text. Appreciation is also extended to Lt. W. A. Cranston of the Defense Nuclear Agency for providing helpful review comments and to Mr. C. McFarland of DNA who provided an informal summary from which the appendix was developed.

Appendix

CONSTITUTIVE RELATIONS AND PHYSICAL PROPERTIES FROM LABORATORY TESTS

A.1 INTRODUCTION

As has been pointed out in the text, soil is the principal element in most soil–structure systems. It follows that to achieve a good design of such a system, one must know the pertinent physical properties and must have suitable mathematical relationships which define soil behavior. Equations that describe soil behavior can be based on statistical relations from transport mechanics, or they can be based on experimental results. Because of the complex behavior of earth materials, the latter approach is usually employed. Thus, the need arises for determining physical properties that adequately represent material behavior.

The purpose of this appendix is to: (1) indicate how soil properties from laboratory tests relate to elasticity relations, and (2) show how experimentally determined properties enter representative constitutive relations.

A.2 CONSTITUTIVE RELATIONS

A constitutive equation is a relation between stress and strain tensors characterized by two experimentally determined independent parameters, usually the bulk and the shear moduli. These parameters are nonlinear and are sometimes taken as functions of mean stress during loading and unique but different functions of mean stress during unloading.

At stresses less than about 5 kilobars (the region of interest in soil–structure interaction), thermodynamic dependence is negligible; consequently, the material may be considered as an elasto-plastic media. The material is incrementally elastic until some maximum shear stress is achieved, then plastic flow occurs. The limiting shear stress is usually specified by some yield condition based on experimental data.

For convenience, the stress tensor is usually divided into mean and deviatoric components

$$\sigma_{ij} = \frac{\sigma_{kk}}{3}\,\delta_{ij} + \sigma'_{ij} \qquad \text{(A-1)}$$

where σ_{ij} = tensor representing the six independent components of stress

$\sigma_{kk}/3$ = mean stress = $-p$ for hydrostatic conditions

δ_{ij} = Kronecker delta = $\begin{cases} 1 \text{ when } i = j \\ 0 \text{ when } i \neq j \end{cases}$

σ'_{ij} = tensor representing the six deviatoric components of stress

The corresponding strain tensor is

$$\epsilon_{ij} = \frac{e_{kk}}{3}\delta_{ij} + e'_{ij} \tag{A-2}$$

where $e_{kk} = \epsilon_{11} + \epsilon_{22} + \epsilon_{33}$ = bulk strain (A-2a)

and ϵ_{ij} = tensor representing the six independent components of strain

e'_{ij} = tensor representing the six deviatoric components of strain

Assuming linear elasticity, stress and strain are related by Hooke's law

$$\sigma_{ik} = \psi_{iklm}\,\epsilon_{lm} \tag{A-3}$$

where ψ_{iklm} is the tensor of elastic constants. Because of symmetry, the number of independent constants reduces to 21 for the most general form of anisotropy. For an isotropic material the number of independent elastic constants reduces to the two Lame constants, λ and μ.

Useful relations between Lame's constants and the four material constants, E, ν, k, and G are

$$\left.\begin{aligned} \lambda &= \frac{E\nu}{(1+\nu)(1-2\nu)} = \frac{2G\nu}{1-2\nu} = \frac{3k\nu}{1+\nu} \\ \mu &= G = \frac{E}{2(1+\nu)} = \frac{3k(1-2\nu)}{2(1+\nu)} \\ k &= \lambda + \frac{2}{3}\mu = \frac{E}{3(1-2\nu)} \end{aligned}\right\} \tag{A-4}$$

where E = Young's modulus of elasticity

G = shear modulus

ν = Poisson's ratio

k = bulk modulus

For an isotropic elastic material and rectangular Cartesian coordinates, Hooke's law becomes

$$\sigma_{kk} = 3k\,e_{kk} \tag{A-5a}$$

$$\sigma'_{ij} = 2G\,e'_{ij} \tag{A-5b}$$

Substituting Equations A-1 and A-2 into Equation A-5b and making use of Equation A-5a gives the stress–strain relation for linearly elastic isotropic materials as

$$\sigma_{ij} = \left(k - \frac{2}{3}G\right)e_{kk}\,\delta_{ij} + 2G\epsilon_{ij} \tag{A-6}$$

The bases of principal laboratory tests for defining soil parameters are developed from Equation A-6 in the next section.

A.3 BASES OF LABORATORY EXPERIMENTS

A.3.1 Triaxial Compression Test

In a triaxial compression test a cylindrical specimen of soil in a rubber membrane is subjected to constant radial stress and increasing axial stress until failure occurs. The theoretical basis of the triaxial test is established by utilizing the appropriate stress and strain conditions for the test ($\sigma_{22} = \sigma_{33}$; $\epsilon_{22} = \epsilon_{33}$) in Equation A-6. From Equation A-6

$$\sigma_{11} = \left(k - \frac{2}{3}G\right)e_{kk} + 2G\epsilon_{11} \tag{A-7}$$

With $\sigma_{22} = \sigma_{33}$, in Equation A-5a

$$e_{kk} = \frac{\sigma_{11} + 2\sigma_{33}}{3k} \tag{A-8}$$

Substituting the appropriate relations from Equations A-4 and Equation A-8 in Equation A-7 gives

$$E = \frac{\sigma_{11}}{\epsilon_{11}} - 2\nu \frac{\sigma_{33}}{\epsilon_{11}} \tag{A-9}$$

Thus, the modulus corresponding to a given lateral confining stress is determinable by measuring the axial stress and strain and the confining stress. If the lateral strain is measured simultaneously, one can calculate Poisson's ratio. The failure or maximum deviatoric stress defines one point on the yield surface of the material.

When both the axial and lateral stress and strain are measured, it is also possible to determine the shear modulus. From Equation A-1,

$$\sigma'_{ij} = \sigma_{ij} - \frac{\sigma_{kk}}{3} \delta_{ij}$$

Therefore, $$\sigma'_{11} = \sigma_{11} - \frac{\sigma_{11} + 2\sigma_{22}}{3} = \frac{2}{3} (\sigma_{11} - \sigma_{22}) \tag{A-10}$$

Likewise, from Equation A-2

$$e'_{ij} = \epsilon_{ij} - \frac{e_{kk}}{3} \delta_{ij}$$

Therefore, $$e'_{11} = \epsilon_{11} - \frac{\epsilon_{11} + 2\epsilon_{22}}{3} = \frac{2}{3} (\epsilon_{11} - \epsilon_{22}) \tag{A-11}$$

Substituting Equations A-11 and A-1 into Equation A-5b gives

$$2G = \frac{\sigma_{11} - \sigma_{22}}{\epsilon_{11} - \epsilon_{22}}$$

Thus, the shear modulus is determinable from a plot of the stress difference versus the strain difference.

A.3.2 Uniaxial Strain Test

In a uniaxial strain (confined compression) test a layer of soil at a desired initial density is subjected to an applied axial stress.* Lateral strain is prevented by confining the soil in a thick metal cylindrical container. As a consequence,

$$\epsilon_{22} = \epsilon_{33} = 0$$

Hence, $$e_{kk} = e_{11}$$

Substituting these conditions into Equation A-6 gives

$$\sigma_{11} = \left(k - \frac{2}{3} G\right)\epsilon_{11} + 2G\epsilon_{11}$$

or $$\sigma_{11} = \left(k + \frac{4}{3} G\right)\epsilon_{11} \tag{A-12}$$

Thus, the slope of the stress–strain diagram from a uniaxial strain test is $k + (4/3)G = M_s$, called the confined compression modulus. Using appropriate relations from Equations A-4, the relation between Young's modulus of elasticity and the confined compression modulus is

$$E = \frac{(1 - 2\nu)(1 + \nu)}{(1 - \nu)} M_s$$

A.3.3 Proportional Load Test

The proportional load test differs from the triaxial load test only in that servo feedback is used to maintain a constant ratio of radial to axial stress. That is,

$$\sigma_{22} = \sigma_{33} = c_1\sigma_{11} \tag{A-13}$$

where c_1 = constant

Recall that $$e_{kk} = \frac{\sigma_{kk}}{3k} = -\frac{p}{k} \tag{A-14}$$

---

* For reliable results, the axial stress must be applied pneumatically or hydraulically through a flexible diaphragm.

$$p = -\frac{\sigma_{11} + 2\sigma_{22}}{3} \qquad \text{(A-15)}$$

and

$$e_{kk} = \frac{\epsilon_{11} + 2\epsilon_{22}}{3} \qquad \text{(A-16)}$$

Setting Equation A-14 equal to Equation A-16 gives

$$\sigma_{11} = k(1 + 2c_1)\epsilon_{11} \qquad \text{(A-17)}$$

From Equations A-14 and A-17, it is clear that the slope of the volumetric stress–strain or the axial stress–strain diagram should be constant and independent of the stress ratio, σ_{11}/σ_{22}, if the material is isotropic. Tests of earth materials show that the stress–strain diagram from proportional load tests vary with the stress ratio and is seldom perfectly linear at a given stress ratio. Such behavior implies anisotropic behavior and a dependence of specimen properties on loading path.

In placing inclusions in soil, the material is artificially compacted, resulting in a material that is more nearly isotropic than naturally occurring soils. Naturally occurring soils are usually deposited by sedimentation followed by one-dimensional consolidation over long periods of time. Such deposits would be expected to have quite different properties in the vertical and the horizontal directions. It follows that in treating soil–structure interaction, theory based on isotropy will probably provide reasonable results. On the other hand, soil models for ground motion determinations should employ anisotropic relations or use a piece-wise linear approximation over each time increment in conjunction with a suitable flow rule to account for nonlinear and plastic behavior.

A.3.4 Other Tests and Determinations

Among other tests that provide useful information are the direct shear test and the hydrostatic compression test. The direct shear test is sometimes used to determine the shear modulus and failure load; the hydrostatic compression test (as a limit proportional load test) provides an indication of the bulk modulus.

Any of the five cited tests may be used as dynamic tests to provide information on strain rate effects. The uniaxial compression test is the one most often utilized for dynamic tests as it gives information about the strain rate sensitivity of the confined compression modulus. As previously mentioned, the confined compression modulus is the most important soil property for soil—structure system design and analysis. In contrast to the pulse loading used for strain rate effect determinations, oscillatory loading is used in conjunction with hydrostatic loading for determination of compression and shear wave velocities.

Shear waves are induced by electrically excited y-cut crystals, whereas compressional waves are excited with x-cut crystals. Ordinarily, quartz crystals in the form of end caps are utilized to induce the loading. Except at high pressures, such tests give values of sonic velocity which are much higher than field values due to the hysteresis of soils. As a consequence, it is not permissible to directly back calculate moduli from laboratory sonic tests.

In addition to the above-mentioned tests, there are numerous indirect tests, such as the vane shear test and the California CBR test, which provide indirect measures of principal physical constants. Such tests are particularly useful for field control purposes if a valid relationship has been established between the indirect test and a property of concern for the particular soil being used.

The properties and tests discussed above are those directly of interest in the design of soil—structure systems. If one is concerned with the close-in phenomenology of crater formation and ground motions, detailed information on the Hugonio, yielding, and plastic flow must be obtained. Considerations in that realm are beyond the scope of this report.

LIST OF SYMBOLS

A	Arching, cross-sectional area
A_g	Geometry factor
A_{gh}	Geometry factor for horizontal cylinders
A_{gv}	Geometry factor for vertical cylinders
A_o	Maximum active arching
A_r	Projected area of inclusion in direction of stress front
A_s	Area of section at springline; plan area of structure
A_1	Dimensional constant
a_r	Acceleration of the inclusion
a_s	Acceleration of the soil
B	Width of footing
$\tilde{B}$	Factor influencing the effective soil modulus
B_s	Span of arch
b	Distance from center of gravity to center of gravity of liner plate
$\tilde{C}$	Constant that depends on the Poisson's ratio of steel
$\bar{C}$	Constant that depends on the mode of buckling
C_d	Dilatational wave velocity
C_f	Velocity of stress front in an inclusion
C_n	Constants; $n = 1, 2, 3...$
C_s	Velocity of shear wave
c	Distance from midplane to extreme fiber of plate
$\bar{c}$	Coefficient of cohesion
c_o	Ambient sound velocity of air
D	Width of structure, diameter
D_e	Difference in height of overburden on opposite sides of the footing
D_f	Depth of overburden (both sides of footing)
D_L	Deflection lag factor
DLF	Dynamic load factor
D_r	Amplitude of systematic component of displacement
D_{r1}	Peak amplitude of systematic component attributable to air blast
D_{r2}	Peak downward amplitude of the systematic component attributable to the direct induced motion
D_1	Systematic component of displacement from air blast
D_2	Systematic component of displacement from direct induced wave
$\bar{d}$	Depth from surface to top of footings
d_e	Depth from top of structure to the plane of equal settlement
d_o	Depth of cover over the crown
d_r	Relative density
d'	Distance from bottom face to stress front
E	Young's modulus of elasticity
E'	Modulus of soil reaction
EI	Stiffness
E_s	Modulus of elasticity of soil
e	Naperian constant; modulus of passive pressure on the side fill material
$\bar{e}$	Void ratio
e'_{ij}	Deviatoric strain tensor
e_{kk}	Change of volume per unit volume
e_{max}	Maximum void ratio
e_{min}	Minimum void ratio
e_o	Initial void ratio
e_w	Water content
F	Factor in cylinder deflection equation
F.S.	Factor of safety
$f(...)$	Function of several variables
f_{min}	Minimum stress (maximum compression) in element
f_r	Radial stress in element
f'_t	Tensile failure stress
f_z	Vertical stress in element
G	Shear modulus
g	Acceleration of gravity
H	Height of inclusion
H'	Height of vertical cylinder
h	Total depth of element
I	Moment of inertia, impulse
I_t	Impulse to the time that the wave reflected from the basement rock reaches the cable
J'_1	First invariant of the Cauchy deviatoric stress tensor

XXXXXXXXXXXXXXXXXXXX
See the following pages
for greater detail.
XXXXXXXXXXXXXXXXXXXX

J_2'	Second invariant of the Cauchy deviatoric stress tensor
K	Measure of lateral strain
$\bar{K}$	Bedding coefficient
K_a	Coefficient of active earth pressure
K_o	At-rest coefficient of lateral earth pressure
K_p	Coefficient of passive earth pressure
k	Bulk modulus
$\hat{k}$	Stiffness of soil field
k_c	Shape factor for component of resistance manifested by soil cohesion
k_f	Foundation modulus
k_s	Modulus of elastic support
k_z	Coefficient of soil reaction
k_γ	Shape factor for component of resistance attributable to soil weight
k_1	Material constant
L	Length, depth to water table or to bedrock
L_r	Length of random component
L_s	Length of systematic component; length of soil block
$L_{s_{min}}$	Minimum possible length of the systematic component
L_w	Parameter in attenuation equation
M	Moment (usually maximum moment)
M_ℓ	Loading modulus
M_r	Reloading modulus

158.1

M_s	Effective secant confined compression modulus at a stress equal to the applied load
$M_{s_{eff}}$	Effective value of confined compression modulus
M_t	Tangent modulus
M_u	Unloading modulus
m	Mass of silo
m_i	Mass of inclusion
m_s	Mass of displaced soil
N	Thrust (usually maximum thrust)
N_c, N_γ, N_q	Bearing capacity factors
N_{cr}	Thrust at the crown
N_{sp}	Thrust at springline
$\bar{N}_{sp}$	Thrust at springline under dynamic load conditions
n	Experimentally determined constant, modular ratio
p	Surface pressure
$\hat{P}, \hat{G}, D_q', k_n'$	Factors in foot bearing capacity equation
P_s	Stress at which the value of M_s is required
$\bar{P}_a$	Ambient air pressure
P_{cr}	Critical buckling load
P_o	Stress in free field at midheight of the inclusion
P_i	Interface pressure
P_{ir}	Reflected interface pressure
$P_{(tcr)}$	Transitional buckling stress

158.2

P_{so}	Peak surface overpressure
P_u	Limit stress at the elevation of the plane of equal settlement
P_v	Vertical stress at the elevation of the crown
P_y	Soil stress to produce yielding
P_z	Peak stress at depth
q	Bearing capacity
q_{ult}	Unit bearing capacity at failure
R	Range from ground zero, radius
R_s	Shock radius of blast at time t
r	Radius of culvert
r_f	Foundation reaction
S	Perimeter of structure; section modulus
s	Shear strength
t	Time
t_d	Effective duration of the applied overpressure
t_e	Equivalent thickness of culvert; equivalent flat plate thickness
t_L	Thickness of backpacking
t_p	Plate thickness
t_r	Rise time of blast overpressure
t_1	Equivalent triangular duration of load
t_{50}	Time corresponding to the intercept on the time axis of a straight line drawn from the peak pressure through the point on the overpressure curve at which the pressure is 50% of its maximum value
Δt	Increment of time

158.3

XXXXXXXXXXXXXXXXXXXX
See the following pages
for greater detail.
XXXXXXXXXXXXXXXXXXXX

J_2'	Second invariant of the Cauchy deviatoric stress tensor
K	Measure of lateral strain
$\bar{K}$	Bedding coefficient
K_a	Coefficient of active earth pressure
K_o	At-rest coefficient of lateral earth pressure
K_p	Coefficient of passive earth pressure
k	Bulk modulus
$\hat{k}$	Stiffness of soil field
k_c	Shape factor for component of resistance manifested by soil cohesion
k_f	Foundation modulus
k_s	Modulus of elastic support
k_z	Coefficient of soil reaction
k_γ	Shape factor for component of resistance attributable to soil weight
k_1	Material constant
L	Length; depth to water table or to bedrock
L_r	Length of random component
L_s	Length of systematic component; length of soil block
$L_{s_{min}}$	Minimum possible length of the systematic component
L_w	Parameter in attenuation equation
M	Moment (usually maximum moment)
M_ℓ	Loading modulus
M_r	Reloading modulus

158.1

M_s	Effective secant confined compression modulus at a stress equal to the applied load
$M_{s_{eff}}$	Effective value of confined compression modulus
M_t	Tangent modulus
M_u	Unloading modulus
m	Mass of silo
m_r	Mass of inclusion
m_s	Mass of displaced soil
N	Thrust (usually maximum thrust)
N_c, N_γ, N_q	Bearing capacity factors
N_{cr}	Thrust at the crown
N_{sp}	Thrust at springline
$\bar{N}_{sp}$	Thrust at springline under dynamic load conditions
n	Experimentally determined constant; modular ratio
p	Surface pressure
$\hat{p}$, $\hat{G}$, D_e', k_n'	Factors in foot bearing capacity equation
p_a	Stress at which the value of M_s is required
$\bar{p}_a$	Ambient air pressure
p_{cr}	Critical buckling load
p_e	Stress in free field at midheight of the inclusion
p_i	Interface pressure
p_{ir}	Reflected interface pressure
$p_{i(cr)}$	Transitional buckling stress

158.2

Effective secant confined compression modulus at a stress equal to the applied load

Effective value of confined compression modulus

Tangent modulus

Unloading modulus

Mass of silo

Mass of inclusion

Mass of displaced soil

Thrust (usually maximum thrust)

N_q Bearing capacity factors

Thrust at the crown

Thrust at springline

Thrust at springline under dynamic load conditions

Experimentally determined constant; modular ratio

Surface pressure

, k'_n Factors in foot bearing capacity equation

Stress at which the value of M_s is required

Ambient air pressure

Critical buckling load

Stress in free field at midheight of the inclusion

Interface pressure

Reflected interface pressure

Transitional buckling stress

p_o	Peak surface overpressure
p_u	Limit stress at the elevation of the plane of equal settlement
p_v	Vertical stress at the elevation of the crown
p_y	Soil stress to produce yielding
p_z	Peak stress at depth
q	Bearing capacity
q_{ult}	Unit bearing capacity at failure
R	Range from ground zero; radius
R_s	Shock radius of blast at time t
r	Radius of culvert
r_f	Foundation reaction
S	Perimeter of structure; section modulus
s	Shear strength
t	Time
t_d	Effective duration of the applied overpressure
t_e	Equivalent thickness of culvert; equivalent flat plate thickness
t_L	Thickness of backpacking
t_p	Plate thickness
t_r	Rise time of blast overpressure
t_1	Equivalent triangular duration of load
t_{50}	Time corresponding to the intercept on the time axis of a straight line drawn from the peak pressure through the point on the overpressure curve at which the pressure is 50% of its maximum value
Δt	Increment of time

LIST OF SYMBOLS

A	Arching; cross-sectional area
A_g	Geometry factor
A_{gh}	Geometry factor for horizontal cylinders
A_{gv}	Geometry factor for vertical cylinders
A_o	Maximum active arching
A_r	Projected area of inclusion in direction of stress front
A_s	Area of section at springline; plan area of structure
A_1	Dimensional constant
a_r	Acceleration of the inclusion
a_s	Acceleration of the soil
B	Width of footing
$\tilde{B}$	Factor influencing the effective soil modulus
B_s	Span of arch
b	Distance from center of gravity to center of gravity of liner plate
$\tilde{C}$	Constant that depends on the Poisson's ratio of steel
$\bar{C}$	Constant that depends on the mode of buckling
C_d	Dilatational wave velocity
C_f	Velocity of stress front in an inclusion
C_n	Constants; $n = 1, 2, 3...$
C_s	Velocity of shear wave
c	Distance from midplane to extreme fiber of plate
$\bar{c}$	Coefficient of cohesion
c_o	Ambient sound velocity of air
D	Width of structure; diameter
D_e	Difference in height of overburden sides of the footing
D_f	Depth of overburden (both sides of
D_L	Deflection lag factor
DLF	Dynamic load factor
D_r	Amplitude of systematic componen displacement
D_{r1}	Peak amplitude of systematic compo attributable to air blast
D_{r2}	Peak downward amplitude of the sy component attributable to the direc motion
D_1	Systematic component of displacem air blast
D_2	Systematic component of displacem direct-induced wave
$\bar{d}$	Depth from surface to top of footin
d_e	Depth from top of structure to the p settlement
d_o	Depth of cover over the crown
d_r	Relative density
d''	Distance from bottom face to stress f
E	Young's modulus of elasticity
E'	Modulus of soil reaction
EI	Stiffness
E_s	Modulus of elasticity of soil

$\bar{c}$ Coefficient of cohesion

c_o Ambient sound velocity of air

D Width of structure; diameter

D_e Difference in height of overburden on opposite sides of the footing

D_f Depth of overburden (both sides of footing)

D_L Deflection lag factor

DLF Dynamic load factor

D_r Amplitude of systematic component of displacement

D_{r1} Peak amplitude of systematic component attributable to air blast

D_{r2} Peak downward amplitude of the systematic component attributable to the direct induced motion

D_1 Systematic component of displacement from air blast

D_2 Systematic component of displacement from direct-induced wave

$\bar{d}$ Depth from surface to top of footings

d_e Depth from top of structure to the plane of equal settlement

d_o Depth of cover over the crown

d_r Relative density

d'' Distance from bottom face to stress front

E Young's modulus of elasticity

E' Modulus of soil reaction

EI Stiffness

E_s Modulus of elasticity of soil

e Naperian constant; modulus of passive pressure on the side fill material

$\bar{e}$ Void ratio

e'_{ij} Deviatoric strain tensor

e_{kk} Change of volume per unit volume

e_{max} Maximum void ratio

e_{min} Minimum void ratio

e_o Initial void ratio

e_w Water content

F Factor in cylinder deflection equation

F.S. Factor of safety

f(...) Function of several variables

f_{min} Minimum stress (maximum compression) in element

f_r Radial stress in element

f'_t Tensile failure stress

f_z Vertical stress in element

G Shear modulus

g Acceleration of gravity

H Height of inclusion

H' Height of vertical cylinder

h Total depth of element

I Moment of inertia; impulse

I_t Impulse to the time that the wave reflected from the basement rock reaches the cable

J'_1 First invariant of the Cauchy deviatoric stress tensor

1572

U	Velocity of shock front in air; unit step function
u	Pore pressure
u_i	Initial pore pressure
Δu_{cw}	Excess pore pressure developed during shear at constant water content
Δu_{dis}	Excess pore water pressure negated by consolidation during loading
V	Total volume
V_v	Volume of voids
ΔV	Change in volume
v	Particle velocity
W	Weapon yield
W_c	Load on pipe per unit of length
W_e	Equivalent yield
W_s	Weight of solids
W_w	Weight of water
w	Fundamental compression mode frequency
x	Distance
Δx	Horizontal diametral extension
y	Radial deflection of the crown; deflection
y_r	Relative displacement of the silo with respect to the soil
Δy	Vertical diametral deformation
z	Vertical distance below surface
α	Experimental constant; material constant
α_z	Attenuation factor
β	Angle of stress front with the surface
γ	Unit weight of soil
δ	Deflection at point of interest
δ_{ij}	Kronecker delta
δ_m	Downward deflection of a point near the surface
δ_r	Peak amplitude of direct-induced displacement
δ_u	Ultimate deflection
ϵ	Unit strain; unit strain in outer fiber due to bending
ϵ_c	Average strain over height of inclusion
ϵ_{hL}	Hardening strain of backpacking material
ϵ_{ij}	Tensor representing the six independent components of strain
ϵ_s	Unit strain or average unit strain in the soil over loaded depth
ζ	Coordinate of position
η	Factor depending on Poisson's ratio
$\bar{\eta}$	Stress concentration factor
η_1	Factor depending on the acoustical impedances of the soil and the inclusion
θ	Angle measured clockwise from a horizontal diameter; rotation
θ_r	Rotation attributable to random component
θ_s	Rotation attributable to systematic component
λ	Wave length of random component of displacement; Lamé's constant
Δ_λ	Amplitude of random displacement

μ	Coefficient of friction; Lamé's constant
ν	Poisson's ratio
ν_c	Poisson's ratio of cylinder
ν_h	Poisson's ratio of host material
ν_s	Poisson's ratio of steel; Poisson's ratio of the soil
ξ	Damping coefficient; relative displacement
ξ_I	Relative displacement between the inclusion and the soil attributable to direct loading
ξ_s	Relative displacement attributable to the stress wave
π_n	Pi term; n = 1, 2, 3...
ρ	Mass density; deformed radius of curvature
ρ_I	Effective mass density of the inclusion
ρ_s	Mass density of the soil
(ρC)	Acoustic impedance
σ	Total stress normal to the plane
$\bar{\sigma}$	Peak stress
σ_{allow}	Allowable stress
σ_{ij}	Tensor representing the six independent components of stress
σ'_{ij}	Deviator stress tensor
σ_{kk}	3 times the mean normal stress
σ_r	Average stress on inclusion
$\sigma_s = p_v$	Stress in soil at elevation of crown (or top)
σ_y	Yield stress
σ_{yL}	Yield stress of backpacking
σ_z	Stress after first reflection from bottom of slab, etc.
$\sigma_{z_{max}}$	Maximum value of σ_z
τ	Positive phase duration
τ_{cr}	Critical time that will result in spalling
τ_e	Interface shear on the extrados
φ	Friction angle at constant volume on effective stress basis
ψ_{iklm}	Tensor of elastic constants
Ω	Factor in arching equation
Ω_m	Maximum value of factor Ω
ω	Exponent in arching equation